Investigation of Proteins Involved in the Biosynthesis and Utilization of 2,3-Dihydroxybenzoic Acid, an Intermediate of *E. coli* Enterobactin Biosynthesis

Ian Jaworski

A Thesis in

The Department Of

Chemistry and Biochemistry

Presented in Partial Fulfillment of the Requirements

for the Degree of Master of Science (Chemistry) at

Concordia University

Montreal, Quebec, Canada

Summer 2012

CONCORDIA UNIVERSITY

School of Graduate Studies

This is to certify that the thesis prepared

By: Ian Jaworski

Entitled: Investigation of Proteins Involved in the Biosynthesis and Utilization of 2,3-Dihydroxybenzoic acid, an Intermediate of *E. coli* Enterobactin Biosynthesis

and submitted in partial fulfillment of the requirements for the degree of

Master of Science (Chemistry)

complies with the regulations of the University and meets the accepted standards with respect to originality and quality.

Signed by the final examining committee:

_____ Chair

Dr. Judith Kornblatt

_____ Examiner

Dr. Joanne Turnbull

_____ Examiner

Dr. Justin Powlowski

_____ Supervisor

Dr. Peter Pawelek

Approved by _____

Chair of Department or Graduate Program Director

_____ _____

Date Dean of Faculty

Abstract

Investigation of Proteins Involved in the Biosynthesis and Utilization of 2,3-Dihydroxybenzoic acid, an Intermediate of *E. coli* Enterobactin Biosynthesis

Ian Jaworski

Siderophores are small-molecule iron chelators that have very high affinity for iron(III). Many bacteria synthesize siderophores to obtain scarce iron(III) from the extracellular environment. Under iron stress, *E. coli* synthesizes and secretes the catecholate siderophore enterobactin. The enterobactin biosynthetic pathway is composed two functional modules: (1) the dihydroxybenzoate (DHB) biosynthesis module contains the enzymes EntC, EntB (ICL domain) and EntA, and (2) the non-ribosomal peptide synthesis (NRPS) module contains the activities of EntE, EntD, EntB (ArCP domain), and EntF. Protein-protein interactions (PPI) necessary for enterobactin biosynthesis have been reported among the NRPS proteins, but not among the DHB biosynthetic proteins. A goal of this project was to investigate the existence of a possible EntC-EntB protein interaction that could facilitate direct channeling of metabolic intermediates. A second goal was to better understand how a PPI between EntA and EntE facilitates a direct metabolic link between the DHB and NRPS modules.

EntC, the first enzyme in the DHB module, was overexpressed and purified to homogeneity with an in-frame C-terminal hexahistidine tag. Far-UV circular dichroism spectroscopy confirmed that the secondary structure content of recombinant EntC was consistent with the published EntC crystal structure. Isothermal titration calorimetry (ITC) was used to measure the affinity of recombinant EntC for chorismic acid. The K_D for

chorismic acid was determined to be 336.7 μM and was found to bind to EntC with a stoichiometry of 1.11. The steady-state kinetic parameters of EntC were determined using a coupled enzyme assay. The K'_m and k'_{cat}/K'_m were found to be 40.5 μM and 0.026 μM^{-1} s^{-1} respectively at pH 7.5 and 37 ^{o}C. Preliminary evidence of a protein interaction involving EntC was provided by a pull-down assay using EntC as bait and *E. coli* BW25113 WT soluble cell lysates as prey. The pull-down assay identified a band corresponding to *E. coli* EntB. Further demonstrating a PPI between EntC and EntB, chemical crosslinking has revealed bands with MWs corresponding to EntC-EntB complexes.

A PPI has been previously demonstrated in our lab between EntA of the DHB module and EntE of the NRPS module. Growth phenotype assays of bacterial strains carrying mutations to EntA residues (Q64A, and Q64A/A68Q) of the predicted interaction interface showed poor growth in low iron. Far-UV circular dichroism demonstrated that all variants had similar secondary structure and melting temperature to that of WT. Thus the amino acid substitutions did not cause any structural change to the proteins. The steady-state kinetic parameters of wild-type and variant EntA proteins were determined using a coupled enzyme assay. The K_m' and k'_{cat}/ K'_m of EntA WT was found to be 1280 μM and 6.09E-04 $\mu M^{-1}s^{-1}$, respectively. All variants were found to have similar K_m' and k'_{cat}/ K'_m values confirming that the amino acid substitutions to the interaction interface did not significantly alter enzyme activity. The poor *in vivo* growth of the variants (Q64A, and Q64A/A68Q) under iron limiting conditions is likely due to the disruption of the PPI between EntA and EntE.

A docking a model was produced using AutoDock 4.2 and the crystal structures of EntE and EntA. The interface of the protein-protein interaction predicted by docking predicts a common interaction interface on EntE for EntE-EntB binding as well as EntE-EntA binding.

Acknowledgements

I would like to thank my supervisor, Dr. Peter D. Pawelek, for his support, excellent advice, patience and guidance throughout my Master studies.

I would also like to thank my committee members Dr. Joanne Turnbull and Dr. Justin Powlowski for their time and excellent advice.

I would like to thank all the members of the Pawelek Lab: Michael Lowden, Daniel Foshag, Paknoosh Pakarian, Vasken Parshekian and Sofia Khalil. I would also like to thank Francis McManus.

I would like to thank my parents William and Lois Jaworski for their unwavering support in all aspects of my life. Everything I accomplish is thanks to them and their infinite love. I would also like to thank my sisters Lois-Ann and Lisa for their love and support. I would especially like to thank my brother Kenneth for quite simply being the best possible brother anyone could ask for.

I could have never accomplished what I have in the last few years have it not been for my girlfriend Lydia. Her love, moral and emotional support as well as her endless patience I am forever grateful for. I am so anxious to begin our life together.

Table of Contents

LIST OF FIGURES

LIST OF TABLES

ABBREVIATIONS

2,3-DHB	2,3-Dihydroxybenzoate
ACS	Acetyl-CoA Synthetase
AMP	Adenosine monophosphate
APS	Ammonium Persulfate
Å	Angstrom Unit
ArCP	Aryl carrier Protein
ATP	Adenosine Triphosphate
AUC	Analytical Ultracentrifuge
BSA	Bovine serum albumin
CoA	Coenzyme A
CD	Circular Dichroism
Da	Dalton
DMSO	Dimethylsulfoxide
DNA	Deoxyribonucleic Acid
EntA	2,3-Dihydro-2,3-Dihydroxybenzoate Dehydrogenase
EntB	Isochorismate lyase/Aryl Carrier Protein
EntC	Isochorismate Synthase
EntD	Phosphopantetheinyl Transferase
EntE	2,3-Dihydroxybenzoate AMP Ligase
EntF	Enterobactin Synthetase Component F
EntH	Hot dog-fold thioesterase
EDTA	Ethylenediamine Tetra-Acetic Acid

FRET	Fluorescence Resonance Energy Transfer
FUR	Ferric Uptake Regulator
FPLC	Fast Protein Liquid Chromatography
HEPES	4-(2-Hydroxyethyl)-1-Piperazineethanesulfonic Acid
ICL	Isochorismate Lyase
IMAC	Immobilized Metal Affinity Chromatography
ITC	Isothermal Titration Calorimetry
IPTG	Isopropyl-β-D-Thiogalactopyranoside
k_{cat}	Turnover Number
k'_{cat}	Apparent Turnover Number
K_D	Dissociation Constant
K_m	Michaelis Constant
K'_m	Apparent Michaelis Constant
LB	Luria Broth
MS	Mass Spectrometry
MW	Molecular Weight
MWCO	Molecular Weight Cut-off
NRPS	Non-Ribosomal Peptide Synthesis
OTG	n-Octyl β-D-Thioglucopyranoside
PBS	Phosphate Buffered Saline
PCP	Peptidyl Carrier Protein
PCR	Polymerase Chain Reaction
PDB	Protein Data Bank
PMSF	Phenylmethylsulfonyl Fluoride

RMSD	Root-mean-square-deviation
RNA	Ribonucleic Acid
RT	Room Temperature
SDS	Sodium Dodecyl Sulfate
SDS-PAGE	Sodium Dodecyl Sulfate Polyacrylamide Gel Electrophoresis
SIP	Siderophore Interacting Protein
SMPT	4-Succinimidyloxycarbonyl-alpha-methyl-alpha(2-pyridyldithio)toluene
Sulfo-LC-SPDP	Sulfosuccinimidyl 6-[3'-(2-pyridyldithio)propionamido]hexanoate
TCA	Tricarboxylic Acid Cycle
TCEP	TRIS(2-Carboxyethyl)Phosphine
TE	Thioesterase
TEMED	Tetramethylethylenediamine
TLC	Thin Layer Chromatography
Tris	TRIS(hydroxymethyl)Aminomethane
UV	Ultraviolet
WT	Wild-type

Amino-Acids

Ala (A)	Alanine	Glu (E)	Glutamate
Arg (R)	Arginine	His (H)	Histidine
Phe (F)	Phenylalanine	Tyr (Y)	Tyrosine
Gln (Q)	Glutamine	Trp (W)	Tryptophan

1. Introduction

1.1. General Introduction

The ever-evolving resistance of pathogenic bacteria to antibiotics is of great concern due to its implications in human health (French 2010). Recently, a strain of *Neisseria gonorrhoeae* has been shown to be resistant to most antibiotics historically used to treat infections (Katz et al. 2012). Researchers are thus trying to discover new antibiotics that may be used to treat bacterial infections that have developed resistance to commonly used antibiotics. The work that will be discussed in this thesis focuses on the process by which *E. coli* acquire iron from the host environment. It has been proposed that inhibition of bacterial iron acquisition systems may lead to new classes of antibiotics (Ballouche et al. 2009).

1.2. Bacterial Iron Requirement

Iron is a required micronutrient for the vast majority of living organisms. The dependence on iron is attributed to the many biological roles it plays in both eukaryotes as well as prokaryotes. In *E. coli*, iron is required for processes such as electron transport, DNA synthesis and amino acid biosynthesis. Proteins utilizing iron are divided into three categories: (i) heme-containing, (ii) iron-sulfur and (iii) non-heme/non-iron-sulfur containing. An example of a heme-containing protein is Cytochrome c oxidase. Cytochrome c oxidase is the last enzyme in the electron

transport chain and it catalyzes the conversion of molecular oxygen to water (Earhart 2004). The second class of iron-utilizing proteins encompasses iron-sulfur proteins. Glutamate synthase is an example of an iron-sulfur protein that participates in amino acid biosynthesis by catalyzing the reaction of α-ketoglutarate and glutamine to form glutamate (Miller & Stadtman 1972). Another example of an iron-sulfur protein is aconitase, which participates in the TCA cycle (reviewed in Kiley & Beinert 2003). Finally, a third example of iron-sulfur protein is nitrogenase. Nitrogenase catalyzes the conversion of nitrogen gas to ammonia NH_3 (Dean et al. 1993). The last group of iron-utilizing proteins does not contain heme or an iron-sulfur cluster. Ribonucleotide reductase is an example of non-heme/non-iron-sulfur containing protein that is required in DNA synthesis (Atkin et al. 1973). To sustain these essential process and microbial growth, sufficient levels of intracellular iron must be maintained. The minimum cellular iron requirement for bacteria is 10^{-6} M (Miethke & Marahiel 2007).

1.3. Iron Bioavailability

Iron exists in two states: iron(II) (ferrous) and iron(III) (ferric). Iron(II) is freely soluble at physiological pH and can be imported by Gram-negative bacteria through the outer membrane by divalent-cation importers such as SitABCD and MntH (Ballouche et al. 2009; Cartron et al. 2006). However under aerobic conditions iron(II) is oxidized to form iron(III). At physiological pH ferric iron forms ferric hydroxide polymers that are insoluble, having a solubility constant lower than 10^{-38}

M (Bagg & Neilands 1987). Due to the insolubility of ferric hydroxide, the free ferric iron concentration in aqueous solutions is 10^{-18} M (Miethke & Marahiel 2007). Furthermore, in a host environment, the majority of ferric iron is bound by proteins such as transferrin and lactoferrin. The intracellular iron storage protein, ferritin, binds the majority of the remaining free iron. Tight iron regulation of available iron is required because, in a host environment free iron(III) will lead to the formation of harmful free radicals by the Fenton reaction (Touati 2000). To protect itself against damage from free radicals, the host employs the iron-binding proteins transferrin and lactoferrin to bind the circulating pool of iron(III). The free, soluble iron(III) concentration in human serum is approximately 10^{-24}M (Raymond et al. 2003). With the free iron concentration well below the required levels for survival, bacteria have evolved to uptake iron(III) by a number of different methods.

1.4. Bacterial Iron Uptake

Bacteria have evolved to have several complementary iron uptake systems, further demonstrating the importance of iron acquisition for survival. There are two general strategies of importing iron from the extracellular environment either by direct or indirect import. Direct import involves importing the entire iron source, such as scavenging iron from ferric-lactoferrin or ferric-transferrin. In *Neisseria*, import of iron from ferric-human transferrin is mediated by TbpA, an integral outer-membrane protein, and TbpB a lipid anchored transferrin binding protein (Noinaj et

al. 2012). TbpA is a TonB-dependent transporter that transports iron(III) removed from transferrin into the cell (Sandy & Butler 2009). TbpB is a transferrin-binding protein that increases the efficiency of transferrin binding and thus iron import (Noto & Cornelissen 2008).

The disadvantage of direct import is that a single unique receptor is required for each iron source. Indirect import is a more efficient method because it can obtain iron(III) from multiple sources and likely is the reason it is the most common method by which bacteria import iron (Miethke & Marahiel 2007). Examples of indirect iron import include the HasA/HasR system, and siderophore-mediated iron uptake pathways. As heme is bound to the majority of iron in a host cell it would make sense that bacteria evolve a method of obtaining iron from heme. Bacteria employ two main proteins for heme import: HasA and HasR (Izadi-Pruneyre et al. 2006). HasR is a TonB-dependent outer-membrane receptor that can import heme directly if the heme concentration is above 10^{-6} M. However, HasR also has the ability of binding to HasA, a soluble protein that has high affinity for heme, and of importing the heme bound to HasA (Sandy & Butler 2009). Another example of indirect iron import is siderophore-mediated iron uptake, which is the focus of this thesis.

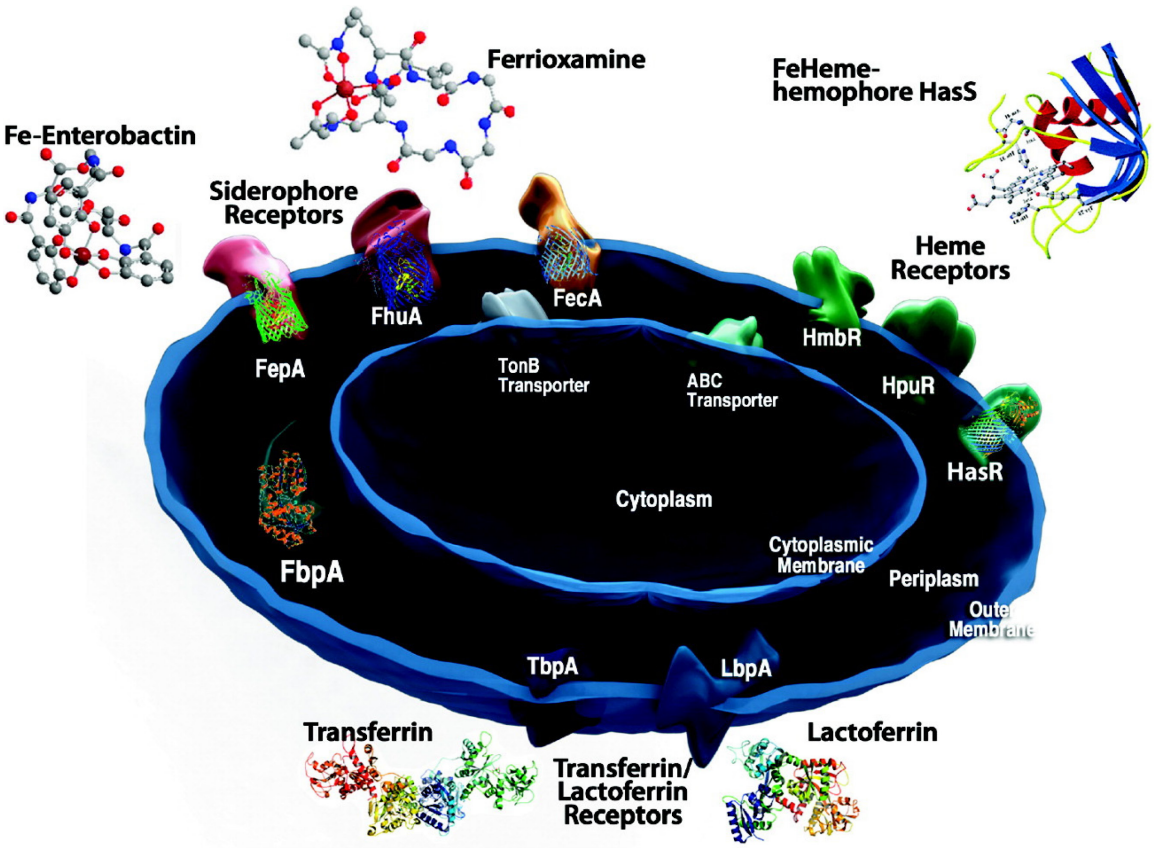

Figure 1 - Iron Uptake by Microorganisms - (Sandy & Butler 2009)

1.5. Siderophore Mediated Iron Uptake

Siderophores are low-molecular weight compounds that have very high affinity for iron (III). This affinity is required to compete with the host's iron-binding proteins in order to obtain iron from sources such as transferrin and lactoferrin. Bacteria synthesize siderophores in the cytoplasm and secrete them to the extracellular environment. After secretion, the ferric-siderophore is then imported to the periplasm by a TonB-dependent outer membrane receptor. The ferric-siderophore is then shuttled across the inner membrane by an ABC-type transporter.

Since siderophore mediated iron uptake is the predominant means by which Gram-negative bacteria uptake iron, it is not surprising that there is a very large number (over 500) of chemically-distinct siderophores that have so far been identified. Siderophores are generally divided into five groups based on the chemistry of their functional, coordinating groups: (i) catecholate, (ii) phenolate, (iii) hydroxamate, (iv) carboxylate and (v) mixed type. The catecholate-type siderophore is composed of catechol coordinating ligands. The best-studied example of a catechol siderophore is enterobactin from *Escherichia coli* (Raymond et al. 2003), which is the subject of this thesis. Phenolate siderophores have phenol functional groups as the iron-coordinating ligands. An example of a phenolate siderophore is yersiniabactin. Yersiniabactin is synthesized by *Yersinia* bacterium, most notably the pathogenic bacteria *Yersina pestis,* the pathogen associated with the plague (Gehring et al. 1998). The hydroxamate-type siderophore is defined as having coordinating groups composed of a carbonyl and a hydroxylamine called hydroxamic acid. An example of a hydroxamate siderophore is alcaligin, which is produced by *Bordetella purtussis* and *Bordetella bronchiseptica,* the pathogens responsible for whooping cough and bronchitis (Moore et al. 1995). Desferrioxamine B is another siderophore that belongs to the hydroxamate family. Desferrioxamine B (Desferal) is used as a treatment to treat iron overload, a symptom of beta thalassemia major patients (Daar & Pathare 2006; Miethke & Marahiel 2007). Carboxylate siderophores are defined by having carboxylic acid groups as the coordinating ligand. Staphyloferrin A is a carboxylate-type siderophore that is produced by the bacterium

Staphylococcus hyicus (Meiwes 1990). There is also a number a mixed-type siderophores that have different compositions of coordinating ligands from the four major classes. One example of a mixed-type siderophores is Mycobactin T from *Mycobacterium tuberculosis* (Quadri et al. 1998).

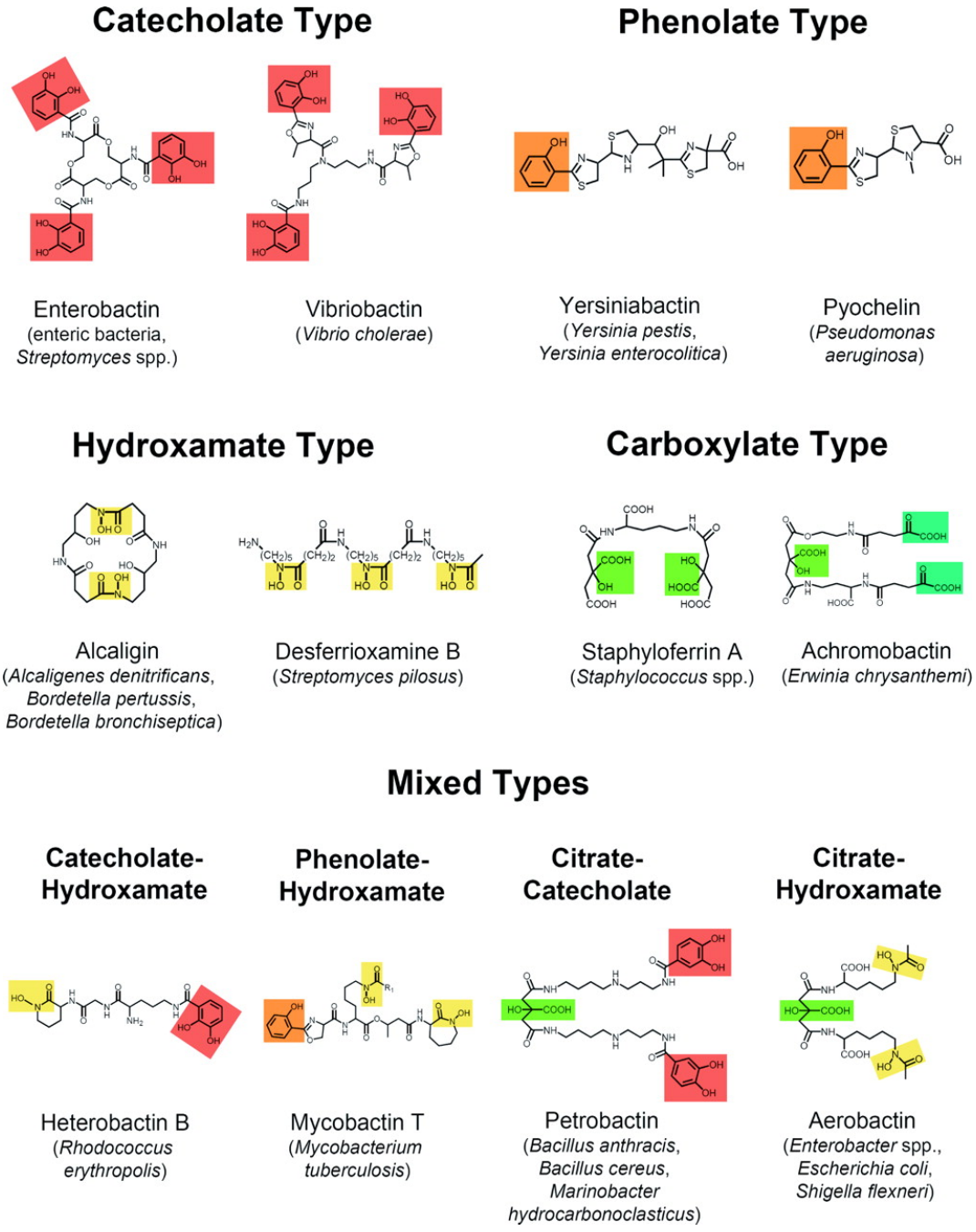

Figure 2 - Classes of Siderophores (Miethke & Marahiel 2007)

1.6. Enterobactin

E. coli synthesizes and secretes two siderophores aerobactin and enterobactin (Caza et al. 2011). Enterobactin, a triscatecholate siderophore, was first isolated from *Escherichia coli* and *Salmonella typhimurium* in 1970 by two independent groups (O'Brien & Gibson 1970; Pollack &Neilands 1970). Enterobactin, depicted in Figure 3A, is composed of three molecules of 2,3-dihydroxybenzoic acid and three molecules of L-serine to form a trilactone ring. Enterobactin has very high affinity for iron(III) with a K_D at physiological pH of $10^{-35.5}$ M. (Crosa et al. 2004). Upon iron binding, the 2,3-DHB moieties fold to one side of the trilactone ring in a manner to coordinate iron(III) in a hexadentate orientation, as in Figure 3B.

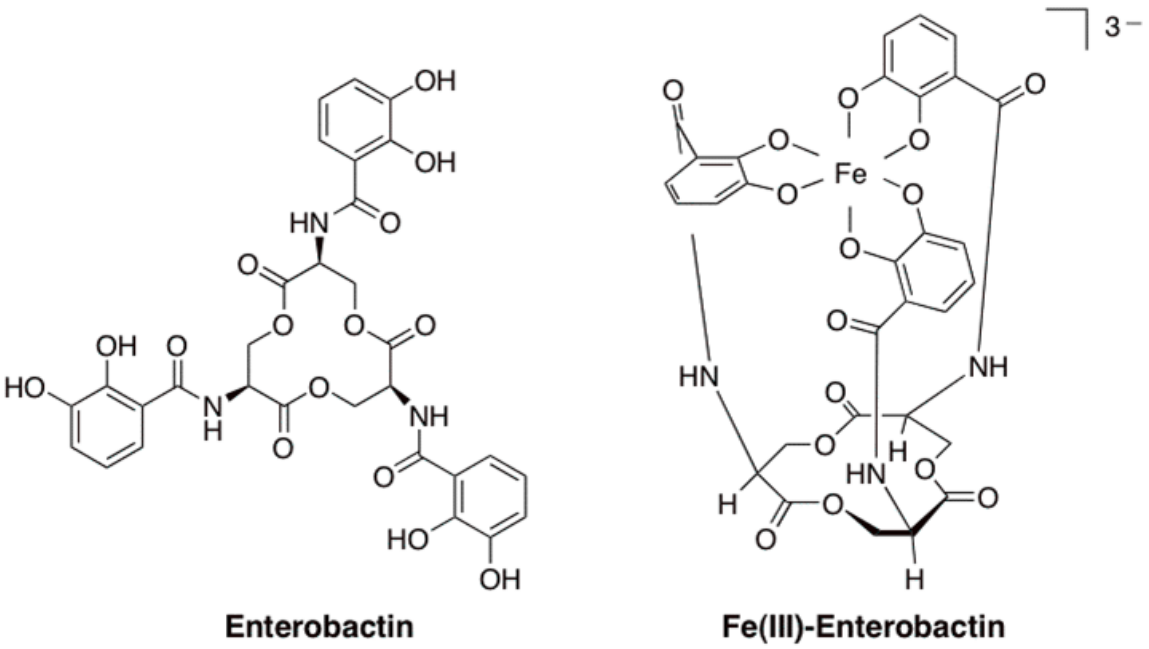

Figure 3 - Enterobactin Structure (Harris et al. 1979) A) The left panel shows the structure of enterobactin. B) The right panel show enterobactin bound to iron(III)

1.7. Enterobactin Biosynthesis

Enterobactin biosynthesis utilizes the activities of the *E. coli* cytoplasmic enzymes EntA-EntF. The activities are subdivided into two functional modules, the dihydroxybenzoate (DHB) module and the non-ribosomal peptide synthesis (NRPS) module. The DHB module utilizes chorismate, which is derived from the shikimate pathway, as the initial substrate. The DHB module produces 2,3-dihydroxybenzoic acid, a subunit of enterobactin, using the enzyme activities of EntC, EntB and EntA (Raymond et al. 2003). The first enzyme in the biosynthetic pathway of enterobactin biosynthesis, EntC, is an isochorismate synthase that catalyzes the isomerization of chorismate to isochorismate in both the forward and reverse directions. EntB, an isochorismatase, catalyzes the hydrolysis of isochorismate to produce 2,3-dihydro-2,3-dihydroxybenzoic acid. The reaction catalyzed by EntB releases a by-product, pyruvate. EntB is considered to be the first committed step in

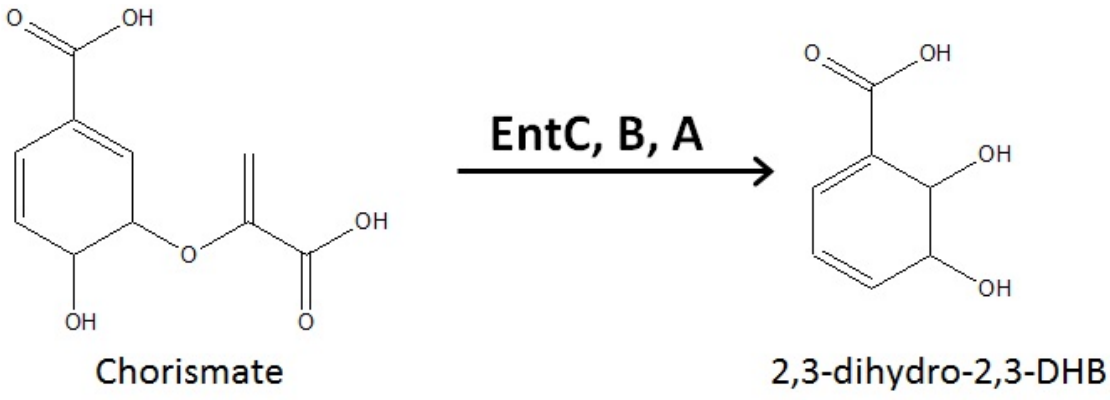

Figure 4 - DHB Module of Enterobactin Biosynthesis

enterobactin biosynthesis because the conversion of chorismate to isochorismate by EntC is reversible (Liu et al. 1990). The last enzyme in the DHB module, EntA, converts the product of EntB to 2,3-dihydroxybenzoic acid using the reduction potential of NAD^+.

The NRPS module contains four biosynthetic enzymes EntD, EntE, EntF and the ArCP domain of EntB. EntD activates EntE and EntF by transferring a phosphopantetheine group to the respective substrates. EntE then adenylates the product of EntA, 2,3-DHB, and subsequently transfers it to the phosphopantetheine group of the ArCP domain of holo-EntB, which results in 2,3-DHB-S-EntB (*i.e.*, acyl-holo-EntB). EntF is a multidomain enzyme that acts as the final scaffold for enterobactin biosynthesis. EntF is composed of the Condensation domain (C), the Adenylation domain (A), the Peptidyl Carrier Protein domain (PCP) and the Thioesterase domain (TE). The adenylation domain is responsible for the adenylation of L-serine and its transfer to the PCP domain. The condensation domain catalyzes the amide bond formation between L-serine on the PCP domain of EntF and the 2,3-DHB on the ArCP domain of EntB. The 2,3-DHB-Serine is then transferred from the PCP domain to the TE domain to allow two more rounds of condensation before enterobactin can be formed (Gehring et al. 1997).

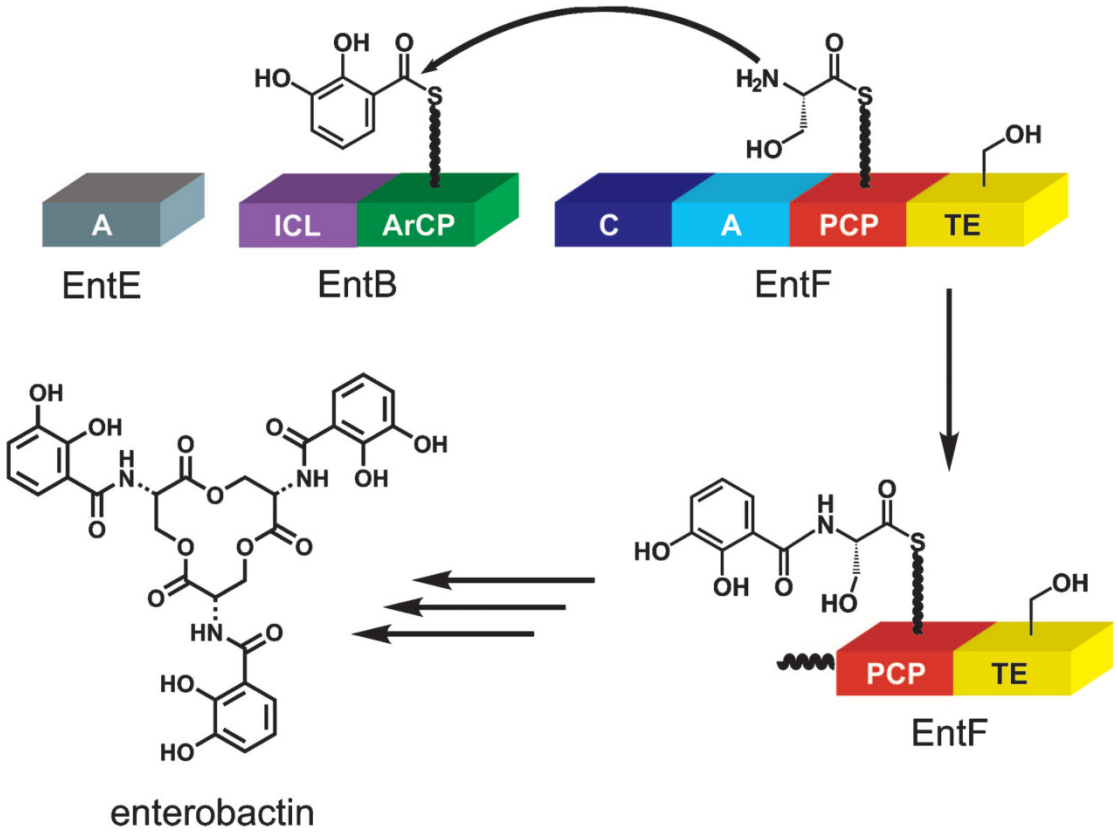

Figure 5 - NRPS Module of Enterobactin Biosynthesis (Lai et al. 2006)

1.8. Enterobactin Secretion and Ferric-Enterobactin Uptake

The export of enterobactin to the extracellular environment from the cytoplasm is not yet fully understood, but what is known is shown in Figure 6. EntS, a cytoplasmic membrane protein and member of the Major Facilitator Superfamily, is responsible for the shuttling of enterobactin from the cytoplasm to the periplasm (Furrer et al. 2002). It is also thought that the outer membrane protein TolC is involved in exporting of enterobactin through the outer-membrane to the extra cellular environment (Bleuel et al. 2005).

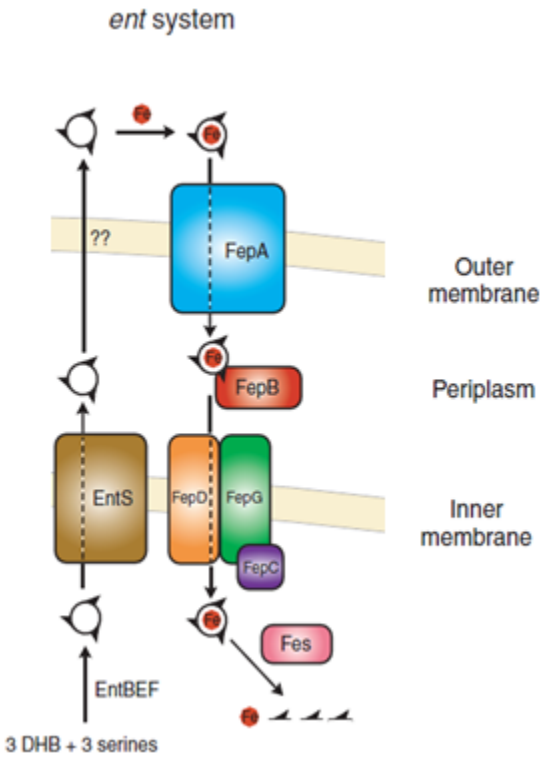

Figure 6 - Enterobactin Secretion Pathway (Fischbach et al. 2006)

Ferric-enterobactin import is much better understood than enterobactin export. Ferric-enterobactin is transported across the outer-membrane, to the periplasm, by FepA. FepA, a TonB-dependent transport protein, obtains energy from the TonB-ExbB-ExbD energy transduction system (Garénaux et al. 2011). After transport to the periplasm by FepA, FepB shuttles the ferric-enterobactin to the surface of the inner-membrane. At the surface of the inner-membrane the ferric-enterobactin is transported across the membrane by the trans-membrane ATP-dependent FepDGC complex (Chenault & Earhart 1992). Once in the bacterial cytoplasm ferric iron is released from enterobactin following the degradation of the

trilactone ring by Fes esterase (Abergel et al. 2009). Many bacteria also have siderophore-interacting proteins (SIPs) that act as ferric reductases by binding siderophores and reducing the bound iron(III) to iron(II) leading to the release of iron(II) from the siderophore (Fontecave et al. 1994). In *E. coli.* the SIP YqjH binds ferric-enterobactin and uses the cofactor NADPH to reduce the bound iron, resulting in its subsequent release and the recycling of enterobactin (Miethke et al. 2011).

1.9. Enterobactin as a Virulence Factor

Enterobactin biosynthesis, secretion and uptake allows for bacteria to very efficiently scavenge for iron, especially in a host environment. However, the mammalian innate immune system has been shown to produce the protein siderocalin in response to bacterial infection (Abergel et al. 2008). Siderocalin has the ability to bind ferric- and apo-enterobactin thus making the siderophore with its iron payload unavailable to the bacterial cell (Abergel et al. 2006).

In response to the limitation introduced by the mammalian innate immune system, pathogenic bacteria have evolved a means to modify enterobactin and evade siderocalin binding. Pathogenic bacteria carry a five-gene cluster, called iroA, that is complementary to the genes involved in enterobactin biosynthesis (Bäumler et al. 1996). The iroA cluster is composed of five enzymes IroB-E and IroN. IroB is the first enzyme of this cluster and is directly responsible for the glycosylation of enterobactin on its C5 carbon. IroB can produce mono-, di-, and tri-glycosylated

enterobactin but the most prominent is di-glycosylated (Fischbach et al. 2006). The di-glycosylated enterobactin, salmochelin, is no longer recognized by siderocalin. IroC is responsible for transporting di- and tri-glycosylated enterobactin across the inner membrane where it is assumed to be then exported, like enterobactin, by TolC. Mono-glycosylated enterobactin may be exported and imported similarly to enterobactin by EntS and FepA. Ferric-salmochelin is then imported by the cell surface receptor IroN. Ferric-salmochelin is then thought to be imported across the inner-membrane to the cytoplasm by the same FepDGC ABC-transporter as enterobactin. IroD and IroE, the two remaining enzymes, are esterases specific for salmochelin (Zhu et al. 2005). IroE is an esterase associated with the outer membrane that is responsible for the linearization of apo-salmochelin before export. IroD, also an esterase, is located in the cytoplasm and is responsible for the degradation of ferric-salmochelin to glycosylated-serine-2,3-DHB (Lin et al. 2005).

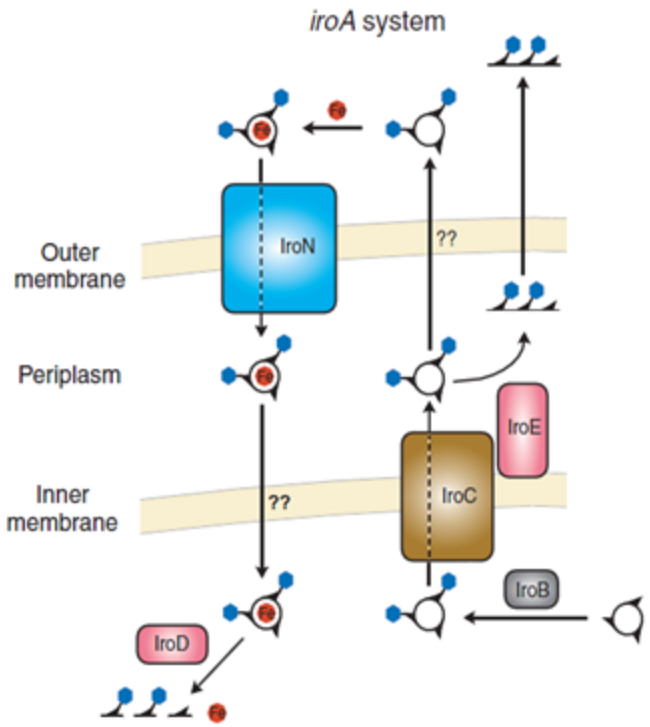

Figure 7 - Proteins Expressed by the iroA Cluster (M. a Fischbach et al. 2006)

1.10. Regulation of Enterobactin Biosynthesis

The *ent* and *fep* genes are regulated at the transcriptional level by the Ferric Uptake Regulator protein (Fur) (Walsh et al. 1990). Fur is a DNA-binding protein that binds to a 19 base-pair sequence upstream of *ent* and *fep* genes called the Fur Box (reviewed in Miethke & Marahiel 2007). The Fur box overlaps with the binding site of RNA polymerase. When iron is abundant and the Fur protein is bound to iron(II) it has high affinity for the Fur box and thus competes for binding with RNA polymerase. When Fur is bound, RNA polymerase cannot bind to the promoter region and transcription is down-regulated. However, when iron(II) concentration in the cell is low Fur does not bind to DNA, allowing for the expression of the *ent* and

fep genes. The Fur box is located in several positions among the enterobactin gene cluster as can be observed by the brackets above the genes in Figure 8.

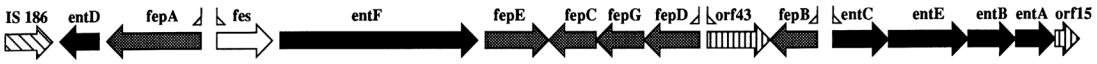

Figure 8 – The *ent* and *fep* Gene Cluster. Fur box sequences are shown in this figure with brackets (◿ ◺).(Charles F Earhart 2004)

1.11. Isochorismate Synthase: EntC

EntC (EC 5.4.4.2) is a 42 kDa protein that is the first enzyme of the DHB module in enterobactin biosynthesis. EntC is an isochorismate synthase that catalyzes the reaction of chorismate, derived from the shikimate metabolic pathway, to isochorismate by a SN2 displacement reaction (Liu et al. 1990)**.** It is a member of a larger class of chorismate-utilizing enzymes that includes: (i) MenF, (ii) Irp9, (iii) TrpE. MenF is involved in menaquinone biosynthesis and converts chorismate to isochorismate (Daruwala et al. 1997). Irp9 is an isochorismate synthase pyruvate lyase that converts isochorismate to salicylate in salicylate biosynthesis (Kerbarh et al. 2005). TrpE is a chorismate-utilizing enzyme involved in anthranilate biosynthesis, a precursor to tryptophan (Kozlowski et al. 1995; Sridharan et al. 2010). EntC can also efficiently convert isochorismate to chorismate and the K_{eq} of the reaction was reported to be 0.56 with chorismate being slightly more stable than isochorismate

(Liu et al. 1990). The K_m and k_{cat} of the reaction in the forward direction have been reported to be 14 μM and 173 min^{-1}, respectively. The K_m and k_{cat} of the reaction in the reverse direction, isochorismate to chorismate, were reported to be 5 μM and 108 min^{-1}, respectively (Liu et al. 1990).

The crystal structure of EntC has recently been solved in the presence of isochorismate and two magnesium ions (Sridharan et al. 2010). The crystal structure is shown in Figure 9, with isochorismate highlighted in green and a helix of interest, α2a, highlighted in red. EntC adopts the overall α+β fold that is similar to other chorismate-utilizing enzymes, most notably the *E. coli* menaquinone biosynthetic enzyme MenF. Residues situated in the EntC active site that are thought to be involved in catalysis are K147 and E197. K147 is thought to act as a catalytic base in both EntC and MenF (K190) by activating a water molecule that forms a hydrogen bond with the substrate (Sridharan et al. 2010). Likewise, E197 is thought to act as a general acid donating its hydrogen to stabilize the loss of a hydroxyl group at C4 of the substrate.

A structural alignment of EntC with other members of the chorismate utilizing enzyme family has been reported (Dahm et al. 1998). The cores of the proteins were all very similar since they have conserved residues in the catalytic region. However, there were differences in structure at the surfaces of the proteins, most notably near the N-terminus of all enzymes.

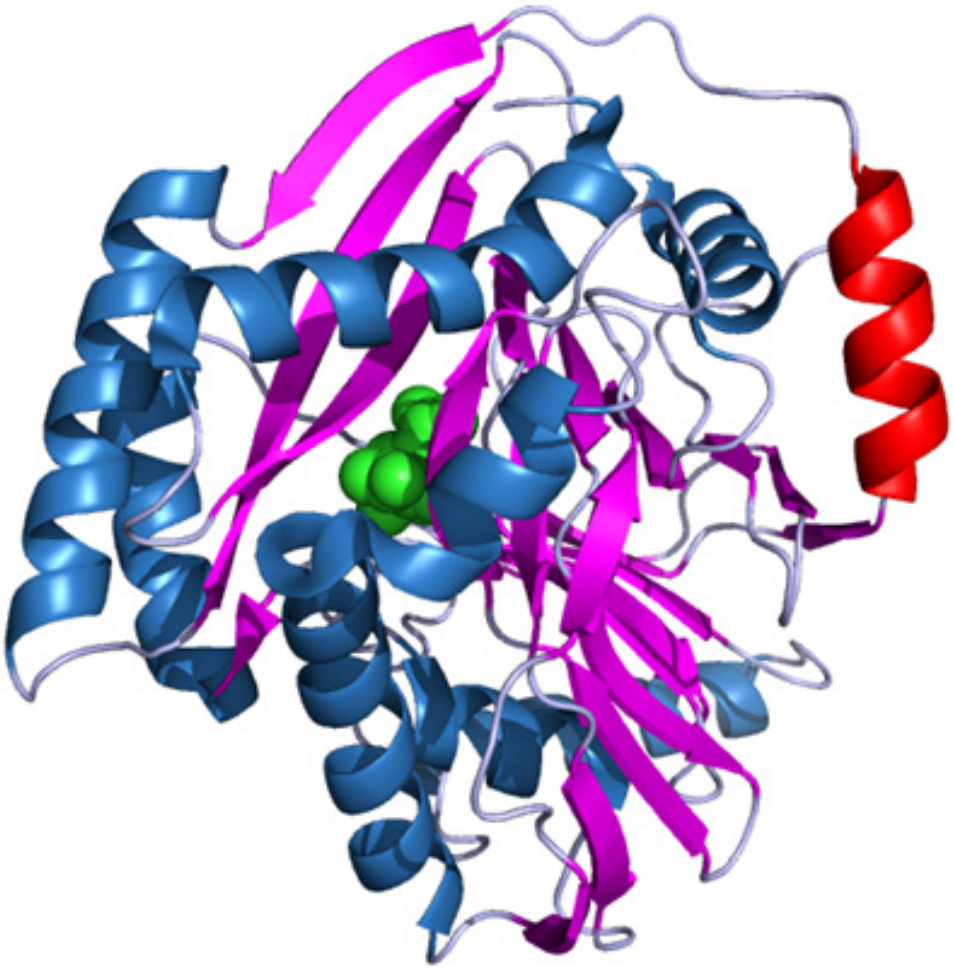

Figure 9 - Crystal Structure of monomeric EntC PDB: 3HWO. The protein is colored as follows: (α-helix : Blue, β-sheet : Purple, α2a helix : Red and isochorismate : Green).

MenF, which catalyzes the same reaction as EntC but in menaquinone biosynthesis, has additional secondary structure between amino acids 1-40, as well as 118-154, as do other chorismate utilizing enzymes. EntC differs from all other enzymes in its family by the helix labeled α2a (Sridharan et al. 2010). The role of this helix in the activity or regulation of EntC has not yet been elucidated.

1.12. Isochorismatase: EntB

EntB (EC 3.3.2.1) is a 32.5 kDa protein that exists as a dimer and is a member of the cysteine hydrolase and phosphopantetheine-binding superfamilies. EntB is composed of two domains. The N-terminal domain of EntB participates in the DHB module of enterobactin biosynthesis, highlighted in blue in Figure 10, and the C-terminal domain participates in the NRPS module of enterobactin biosynthesis, highlighted in green in Figure 10. The N-terminal domain is an isochorismate lyase domain (ICL) and it catalyzes the conversion of isochorismate to 2,3-dihydro-2,3-dihydroxybenzoic acid, releasing pyruvate as a by-product. The C-terminal domain acts as the aryl carrier protein (ArCP) in the NRPS module by accepting a phosphopantetheine group from EntD and then accepting the 2,3-DHB from EntE.

The crystal structure of EntB has been solved (Drake et al. 2006). EntB was crystallized as a dimer with the dimerization interface identified to be between the ICL domains. The ICL domain is composed of a parallel β-sheet with three α-helices on one side of the β-sheet forming the dimerization interface. On the other side of the β-sheet is a long α-helix.

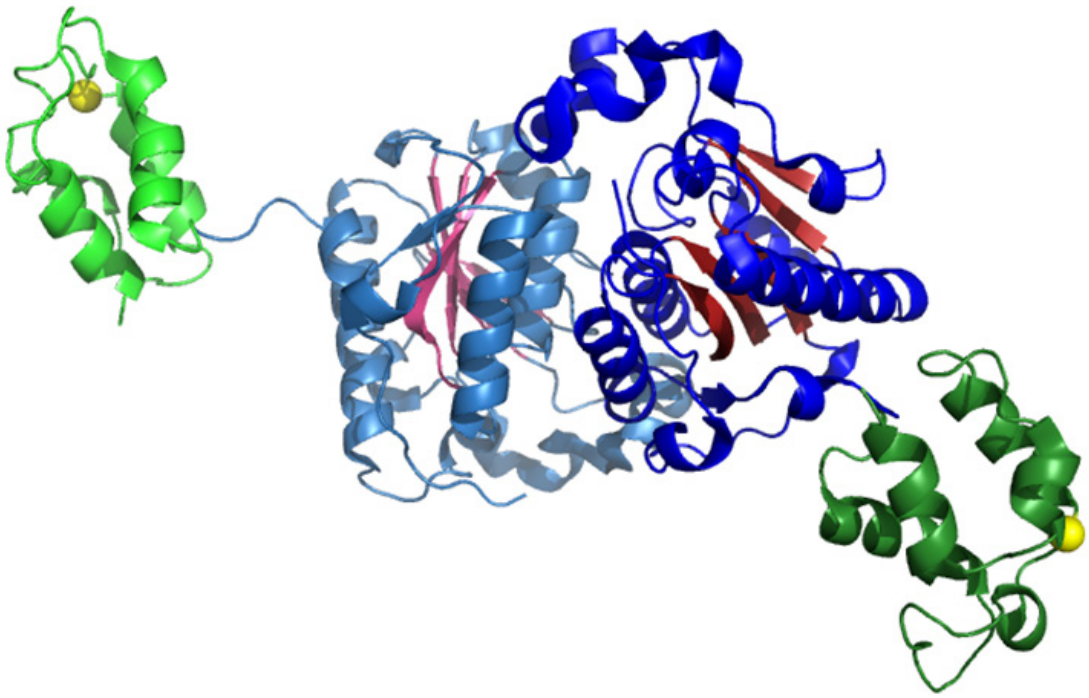

Figure 10 - Crystal Structure of EntB PDB:2FQ1. The ICL domain of EntB is colored in blue(α-helix) and red(β-sheet). The ArCP domain of EntB is colored in green. The residue that participates in the NRPS module Ser 245 is colored in yellow. The dimer is shown with the second chain being colored in different shades.

The ArCP domain is a standard ArCP fold that is composed of four α-helices. The active site residue of the ArCP domain is Ser 245 and is found at the start of the second α-helix on the face of the ArCP domain that faces away from the ICL domain. The position of this residue makes it accessible to the other NRPS proteins EntD, EntE, and EntF (Drake et al. 2006).

1.13. 2,3-Dihydroxy-2,3-Dihydroxybenzoate Dehydrogenase: EntA

EntA (EC 1.3.1.28) is a 26 kDa protein that exists in a concentration-dependent equilibrium between dimeric and tetrameric states (Khalil & Pawelek 2011). It is the last enzyme in the DHB module of enterobactin biosynthesis and belongs to the short-chain oxidoreductase superfamily. EntA catalyzes the reaction of 2,3-dihydro-2,3-dihydroxybenzoic acid to 2,3-DHB via reduction of NAD^+. The X-ray crystal structure of EntA has been solved to a resolution of 2.0 angstroms (Sundlov et al. 2006).

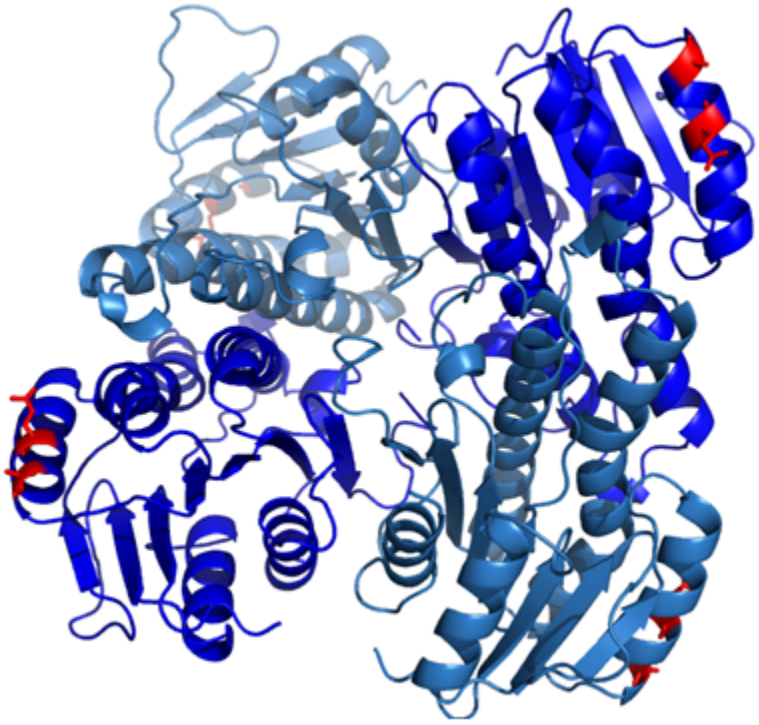

Figure 11 - Crystal Structure of EntA PDB:2FWM. EntA is colored in two shades of blue highlighting the four chains. Residues 64 and 68, proposed to be involved in the PPI between EntA and EntE, are highlighted in red.

EntA was crystalized as tetramer that is classified as a dimer of dimers. Each monomer is composed of a Rossmann fold with a central parallel β-sheet. In total there are five α-helices: three on one side of the β-sheet and two on the other. The dimer interface is formed of α-helices α5 and α6. The major secondary structure elements that participate in tetramer formation are α7 and β7.

1.14. 2,3-DHB-AMP Ligase: EntE

EntE (EC 2.7.7.58) is a 59 kDa protein that exists as a monomer (Rusnak et al. 1989). EntE is a 2,3-DHB-AMP ligase that catalyzes a two-step adenylation-ligation reaction. First it uses ATP to catalyze the adenylation of 2,3-DHB, from the DHB module, to form 2,3-DHB-AMP. Then it catalyzes the ligation of 2,3-DHB, and the release of AMP, to the phosphopantetheine group of the ArCP domain of EntB. The crystal structure of EntE has not yet been solved. However, a chimeric protein comprising a fusion between EntE and the ArCP domain of EntB has been crystallized (Sundlov et al. 2012). The EntE fold in the chimeric protein is composed of two domains: an N-terminal domain and a C-terminal domain. The C-terminal domain is composed of five β-strands and three α-helices. The C-terminal domain is connected to the N-terminal domain by a small loop in which a lysine residue acts as a hinge to allow the C-terminal domain to rotate (J. A. Sundlov et al. 2012). The lysine acts as the hinge by undergoing main chain torsion angle rotation (Gulick 2009). EntE is hypothesized to exist in two conformations. One conformation is preferential for the catalysis of the adenylation of 2,3-DHB, and the second conformation optimizes the

catalysis of the thioester bond formation (*i.e.*, ligation) between the 2,3-DHB and the phosphopantetheine group of EntB. The structure of EntE in the chimeric protein exists in the conformation for optimal ligase activity. The structure of an EntE homologue, DhbE, involved in bacillibactin synthesis in *Bacillus subtilis* has been solved in the presence and absence of substrates (May et al. 2002). DhbE, in the presence of 2,3-DHB bound in its active site, shows a conformational change in the C-terminal domain when aligned to EntE in the ligase conformational state. However, no large conformational change is observed in the crystal structures of DhbE in the absence of substrate, or when bound to 2,3-DHB-AMP or to 2,3-DHB and AMP.

1.15. Protein-Protein Interactions Involved in Enterobactin Biosynthesis

Protein-protein interactions play an essential role in the NRPS synthesis of the catecholate siderophore enterobactin in *E. coli*. Within the NRPS module there have been obligate protein interactions identified between apo-EntB-EntD, holo-EntB-EntE, acyl-holo-EntB-EntF, and holo-EntB-EntH. The interaction between the ArCP domain of apo-EntB and the phosphopantetheinyl transferase EntD is required to activate Ser 245 on apo-EntB so as to receive the adenylated 2,3-DHB molecule from EntA.(Lai et al. 2006) The EntE-holo-EntB interaction is required for the proper transfer and ligation of 2,3-DHB from EntE to the holo-EntB phosphopantetheine group. Recently, it was observed that upon 2,3-DHB binding EntB undergoes a conformational change that promotes an interaction with EntE (Khalil & Pawelek

2009). Furthermore, as discussed above, a chimeric protein of EntE and the ArCP domain of EntB has been crystallized and the interaction interface has been extensively studied (Sundlov et al. 2012).

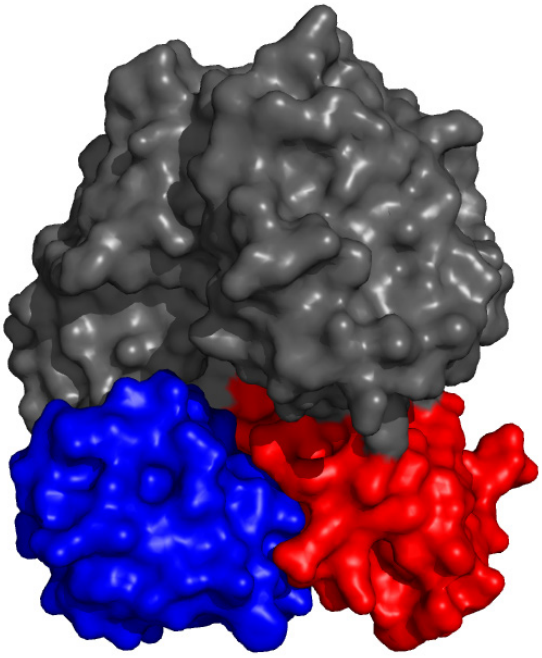

Figure 12 – A Surface Representation of an Interaction between EntB (Blue) and EntE (N-Terminal domain: Grey, C-Terminal domain: Red)

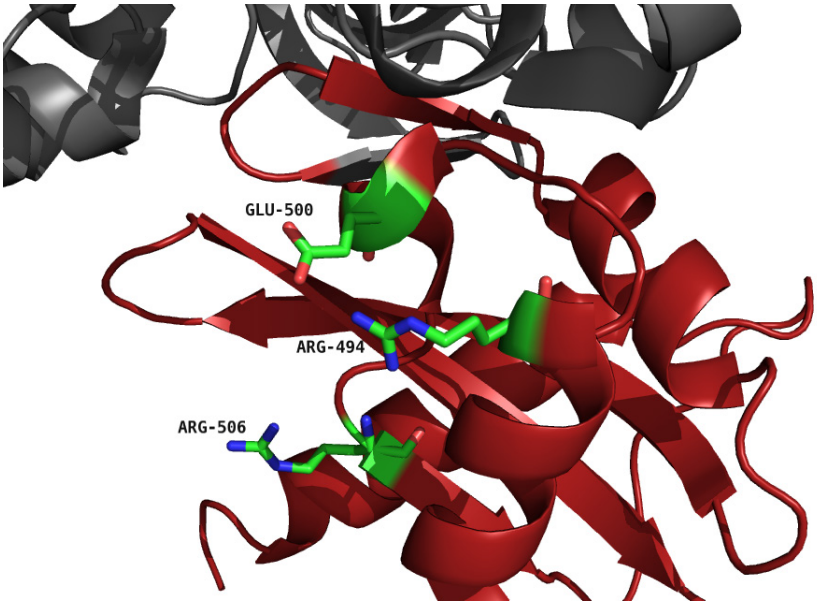

Figure 13 – Representation of the Key Residues on the Surface of the C-terminal Domain of EntE (Red) that are required for the EntE-EntB Interaction. The residues E500, R494 and R506 are highlighted in green.

The chimeric protein was crystallized as a dimer with the ArCP domain of EntB from one chain interacting with EntE from the next chain. The structure elucidates two binding sites on the ArCP domain of EntB for EntE. One of the binding sites on EntB corresponds to Loop 1 of the ArCP domain and the second binding site is formed by helix 2, also of the ArCP domain. Loop 1 residue D557 was found to form a salt bridge with both R490 and R506 of the C-terminal domain of EntE. An ionic interaction is also apparent between D570 of the ArCP domain and R494 of EntE. The second binding site of ArCP formed by Helix 2 contacts EntE in both the C-terminal and N-terminal domains. The residue R577 of the ArCP domain interacts with D467 of the EntE C-terminal domain. A hydrophobic pocket is formed by the EntE residues Leu469, Met470 and Leu285 to accommodate Valine 576 of the ArCP domain. Helix 2 also interacts with the N-terminal domain of EntE by hydrophobic and ionic interactions.

The interaction between EntF and acyl-holo-EntB is required for the transfer of 2,3-DHB from acyl-holo-EntB to the PCP domain of EntF. Alanine scanning of EntB identified Met 249, Phe 264 and Ala 268 as forming an interaction interface with EntF (Lai et al. 2006). Surprisingly, these mutations did not disrupt the interaction between EntE and EntB indicating that EntB has distinct interaction interfaces for both EntE and EntF (Lai et al. 2006). Finally the last interaction among members of the NRPS module is between EntB and EntH, the hotdog thioesterase. The specific interaction between EntB and the hotdog thioesterase EntH is required for EntH to

perform its proofreading of acyl-holo-EntB, correcting misacylation events (Leduc et al. 2007).

The reported and hypothesized protein-protein interactions involved in enterobactin biosynthesis are summarized in Figure 14. We hypothesize that the enterobactin biosynthetic machinery operates as a metabolon, a multi-enzyme complex of enzymes that catalyze sequential reactions in a biochemical pathway that enables substrate channeling, increasing the metabolic efficiency of the pathway (reviewed in Williamson & Sutcliffe 2010). A metabolon has been reported in the TCA cycle of *Bacillus subtilis* involving five enzymes with sequential activities (Meyer et al. 2011). The six enzymes involved in purine biosynthesis in mammalian cells have also been reported to form a metabolon based on fluorescence microscopy of whole HeLa cells (An et al. 2010). The protein-protein interactions that exist among the NRPS module enzymes are necessary for substrate channeling. Likewise, the hypothesized protein-protein interactions within the DHB module are thought to increase the efficiency of enterobactin biosynthesis by substrate channeling.

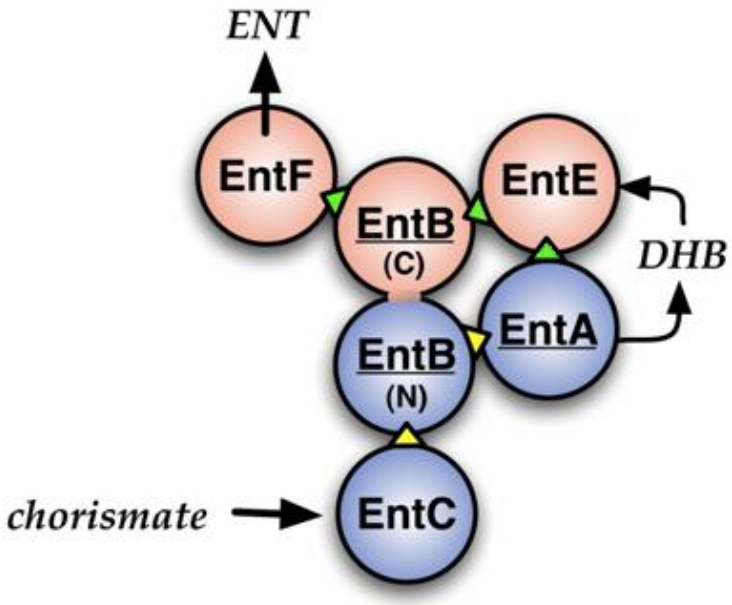

Figure 14 - Protein Interaction Network in Enterobactin Biosynthesis. Proteins in the DHB module are highlighted in blue and proteins in the NRPS module are highlighted in pink.

1.16. EntA – EntE Protein-Protein Interaction

Until recently all protein-protein interactions reported to be involved in enterobactin biosynthesis were between enzymes of the NRPS module. Khalil and Pawelek (Khalil & Pawelek 2011) were the first to report a protein-protein interaction between EntA and EntE. Initial evidence of a protein-protein interaction between EntA and EntE was obtained from a pull-down assay using EntA and EntE as bait (Khalil & Pawelek 2011). EntE pulled down proteins that correspond to EntA and EntB. EntA pulled down a protein that corresponds to EntE. The authors also demonstrated the protein-protein interaction between EntE and EntA disrupts the FRET signal between EntE and its substrate 2,3-DHB, presumably due to

conformational remodelling of the EntE active site upon complex formation. The authors used this property to develop a fluorescence-based equilibrium-binding assay to measure the EntA-EntE interaction. It was determined that the $K_{0.5}$ of EntA binding was 1.94 μM. Furthermore, the protein-protein interaction was measured directly by isothermal titration calorimetry (ITC).

To probe the interaction interface between EntA and EntE phage display was used with EntE as bait. The phage display experiment revealed peptides that align with EntA helix 4 (Khalil, PhD Thesis 2010). Residues Q64 and A68 were selected for mutagenesis and three mutants were produced, Q64A, A68Q and the double mutant Q64A/A68Q. The ability of these mutants to interact with EntE was tested by near-UV circular dichroism (CD) difference spectra. It was found that upon mixing the mutant EntA Q64A and Q64A/A68Q with EntE there was no change to the CD spectra whereas there was in the presence of WT EntA and A68Q. Furthermore, a growth phenotype assay was performed to test the ability of variant EntA proteins to recover WT activity *in vivo*. *E. coli entA*-knockout cells were transformed with expression constructs encoding WT EntA or EntA variants. It was found that upon growth of these transformants under iron-limiting conditions, Q64A and the double mutant Q64A/A68Q grew poorly when compared to WT and A68Q (Khalil, PhD Thesis 2010). The conclusion of these experiments was that the mutations Q64A and the double mutant Q64A/A68Q were likely disrupting the protein-protein interaction between EntA and EntE thus leading to the loss of substrate channeling and efficient

production of enterobactin *in vivo*. However, the effects of EntA mutagenesis on fold integrity had not been investigated.

1.17. Research Objectives

The first goal of this study was to express and purify EntC, thoroughly characterize its ligand-binding properties using available biophysical techniques, and to identify possible protein-protein interactions that occur within the DHB module of enterobactin biosynthesis. The secondary structure of purified recombinant EntC was studied using far-UV CD, and the binding of the EntC cofactor, Mg^{2+}, was studied by near-UV CD. The oligomeric state of EntC was studied using AUC to determine if it is a monomer or dimer *in vitro*. Furthermore, two enzyme concentrations of EntC were studied to determine if the quaternary structure is dependent on enzyme concentration. We hoped to identify a protein-protein interaction within the DHB module by using a pull-down assay as well as chemical crosslinking.

The second goal of this study was to express and purify EntA WT and variants and to characterize the effect of the introduced mutations on secondary structure, thermal stability and quaternary structure. The secondary structure of the variants were studied by far-UV CD to ensure the mutants fold properly during protein expression. To ensure the varriants were equally as stable as WT, thermal denaturation experiments followed by the far-UV CD signal at 222 nm were used to determine the T_ms of WT and variants. The quaternary structure of WT and variants were also

studied to ensure the mutations do not change the quaternary structure of EntA. The steady-state enzyme kinetics of the mutants were studied to confirm that the mutations to the surface of EntA do not disturb its *in vitro* activity. Finally, a model of the protein-protein interaction between EntE and EntA was proposed to better understand the protein-protein interaction interface.

2. Material and Methods

2.1. Strains, Growth Media, and Buffers

All of the *ent* genes in this study were expressed from pCA24N expression vectors obtained from the ASKA repository (Kitagawa et al. 2005). The *entC* gene was PCR-amplified from the pCA24N-*entC* construct and subcloned into a pET24B vector between the *Not*I and *Bam*H1 cut sites. All other expression vectors were used as-is. Mutations on *entA* were previously carried out by Sofia Khalil using site-directed mutagenesis. All growth media and buffers used in this study are listed below. All chemicals and reagents were obtained from BioShop Canada or Sigma-Aldrich unless otherwise indicated. All solutions indicated below were prepared as per Sambrook and colleagues, unless otherwise stated (Sambrook & Russel 2001).

Growth Media:

Luria broth (LB) :

- 10 g Tryptone
- 5 g Yeast Extract
- 10 g NaCl
- Dilute to 1 L in dH_20

2xYT :

- 16 g Tryptone
- 10 g Yeast Extract
- 5 g NaCl
- Dilute to 1 L in dH_20

M63 Minimal Media:

10X M63:

- 30 g KH_2PO_4
- 70 g K_2HPO_4
- 20 g $(NH_4)_2SO_4$

1X M63:

- 100 mL of 10X M63 100 mL
- 5 mL of 1 mg/mL $FeSO_4$-$7H_2O$ 5 mL
- 10 mL of 20% SDS
- 0.4 mL of 50 mg/mL Thiamine
- 1 mL $MgSO_4$
- Dilute to 1 L in ddH_2O

10X-SDS-PAGE Running Buffer:

- 30.30 g TRIS
- 144.5 g Glycine
- 50 mL of 20% SDS
- Dilute to 1 L in dH_20

5X-SDS PAGE Loading Buffer:

- 2.5 mL 1 M TRIS-HCl pH 6.8
- 180 μL 14.3 M β-mercaptoethanol
- 1.25 mL 2% Bromophenol Blue
- 2.5 mL 20% SDS
- 1.07 mL dH_20
- 2.5 mL 100% glycerol

Blue-Silver Stain:

Prepared as described by Candiano and colleagues (Candiano et al. 2004).

TAE:

- 40 mM TRIS-acetate
- 1 mM EDTA

PBS:

- 1 M Sodium Phosphate
- 150 mM NaCl
- pH 7.2

Antibiotics:

30 mg/mL Chloramphenicol in Ethanol

30 mg/mL Kanamycin in dH_2O, filter sterilized

50 mg/mL Ampicillin in dH_2O, filter sterilized

IPTG Stock Solution

1 M IPTG in dH_2O, filter sterilized

5X Activity Assay Buffer

- 250 mM TRIS pH 7.5
- 250 mM NaCl
- 25 mM $MgCl_2$

2.2. Preparation of *E. coli* AG-1, DH5-α and BL21 (DE3) Competent Cells

Competent *E. coli* AG-1, DH5-α and BL21(DE3) cells were prepared using a common protocol (Sambrook & Russel 2001). Cells were streaked onto antibiotic-free LB agar plates and incubated overnight at 37 °C. Streaked plates were removed from the incubator after 16 hours and placed at 4 ^{o}C. An overnight culture was prepared by inoculating 5 mL of LB with a single colony. The o/n culture was grown for 16 hours at 37^{o}C with agitation of 225 rpm. A 50 mL culture was inoculated with 1 % of the overnight culture and grown at 37 ^{o}C with agitation of 225 rpm until an OD_{600} of 0.6 was reached. The cultures were then centrifuged at 1000 g for 15 minutes. The supernatant was decanted and 10 mL of 0.1 M $CaCl_2$ was used to resuspend the cell pellet. The resuspended pellet was incubated on ice for 15 minutes. The culture was again centrifuged at 1000 g for 15 minutes and the supernatant was decanted. The final pellet was resuspended in 2 mL of 0.1 M $CaCl_2$ with 15 % glycerol. The competent cells were aliquoted into 100 µL fractions in microfuge tubes and immediately stored at -80 ^{o}C.

2.3. *E. coli* Transformation

The transformation protocol was adapted from the NEB protocol (NEB 2012). To 50 µL of competent *E. coli* cells 5 ng of plasmid DNA was added. The mixture was incubated on ice for 30 minutes. The cells were then incubated at 42 °C for 30 seconds. Cells were allowed to recover on ice for 5 minutes. The cells were then

diluted with 950 μL of LB and grown at 37 ^{o}C and 225 rpm for 1 hour. An aliquot of 100 μL of the cultures was then plated on LB agar plates, with appropriate antibiotics, and grown overnight at 37 °C.

2.4. Agarose Gel Electrophoresis

Agarose gels were prepared to a final concentration of 1% agarose in 1X TAE buffer. The mixture was heated in a microwave just until the agarose was fully dissolved. Once the agarose solution cooled sufficiently, SYBRSAFE DNA stain from Invitrogen was added to a final concentration of 1X from a 10000X stock. DNA samples were prepared by the addition of 6X DNA loading dye. The gel was run at 100 volts for approximately 35 minutes and 1kb DNA ladder was used as a standard.

2.5. Plasmid DNA Extraction

Plasmid DNA was extracted from DH5-α cells using the EZ-10 Spin Column Plasmid DNA MiniPrep Kit (BioBasic Inc). The protocol was adapted from the manual obtained with the kit. A 10 mL volume of LB was inoculated with *E. coli* DH5-α cells containing the vector of interest and incubated overnight at 37 ^{o}C with agitation and the appropriate antibiotic (kanamycin for pET24b and chloramphenicol for pCA24N). The culture was centrifuged at 14,000 g for 2 minutes. The supernatant was discarded and the pellet was resuspended in 200 μL of Solution I. The solution was

mixed by inverting at least 10 times and incubated at RT for 1 minute. Then 400 μL of Solution II was added and mixed by inverting and the solution was allowed to incubate at RT for 1 minute. Finally, 700 μL of Solution III was gently mixed in and the entire solution was again allowed to incubate at RT for 1 minute. The mixture was then centrifuged at 14,000 g and half of the supernatant was transferred to the EZ-10 column and allowed to incubate for 2 minutes. The column was then centrifuged at 10,000 X g and the flow-through was discarded. The second half of the supernatant was loaded, and incubated with the EZ-10 column for 2 minutes before being centrifuged at 10,000 g. The column was then washed twice with 750 μL of Wash Solution. The column was then centrifuged without any solution to remove any remaining ethanol. To elute the bound DNA 50 μL of Milli-Q water was added to the column and allowed to incubate at RT for 30 minutes. The 50 μL was then eluted and the DNA concentration was measured on an Implen Nanospectrophotometer using a LabelGuard Microliter Cell located in the Center for Structural and Functional Genomics (CSFG).

2.6. Sodium Dodecyl sulfate – Polyacrylamide Gel Electrophoresis (SDS-PAGE)

SDS-PAGE was used to estimate the size and purity of purified proteins. Unless otherwise mentioned all SDS-PAGE gels consisted of a 10 % acrylamide separating gel and a 5 % acrylamide stacking gel. The recipes used were adapted from the protocol described by Sambrook and Russel (Sambrook & Russel 2001). The

gels were cast using the BioRad Mini-Protean Tetra Cell Casting Module for 0.75 mm thick gels. The plates were washed in ethanol and dried immediately prior to use. The plates were assembled and placed in the casting module. The resolving gel consisted of 2.35 mL of dH_2O, 1.25 mL of 40 % 29:1 acrylamide/bisacrylamide (BioBasic), 1.25 mL 1.5 M TRIS pH 8.8, 50 μL of 10 % SDS, 50 μL of 10 % APS and 2 μL of TEMED. Once the resolving gel was poured between the plates, 2-propanol was added on top of the gel to give an extremely flat and level surface between resolving and stacking gels. The stacking gel was made from 1.45 mL of dH_2O, 250 μL of 40 % 29:1 acrylamide/bisacrylamide (BioBasic), 250 μL 1 M TRIS pH 6.8, 20 μL of 10 % SDS, 20 μL of 10 % APS and 2 μL of TEMED and the comb was inserted immediately. Protein samples were prepared using the 5X loading buffer (250 mM TRIS-HCl pH 6.8, 257.4 mM β-mercaptoethanol, 0.25 % Bromophenol Blue, 5 % SDS, 25% glycerol) and heated at $95^{o}C$ for 10 minutes then centrifuged briefly. The gels were run at 100 V until the dye front reached the resolving gel. Once in the resolving gel the voltage was increased to 150 V. Electrophoresis was stopped when a prestained marker corresponding to a similar weight as the protein of interest had traveled into the middle of the gel. The gel was washed 3 times in dH_20 for a total time of 20 minutes to remove all SDS and then stained in the colloidal Blue Silver Stain (Candiano et al. 2004) overnight. The gels were destained in water for several hours. When appropriate, some gels were stained using the SilverQuest Silver Staining Kit from Invitrogen.

2.7. Protein Expression

2.7.1. Expression of Isochorismate Synthase, EntC

E. coli BL21(DE3) cells carrying the pET24B-*entC* plasmid were streaked onto LB + kanamycin (30 µg/mL) plates and incubated overnight at 37 °C. A single colony was selected and inoculated into 50 ml 2xYT + kanamycin and incubated overnight at 37 °C with shaking at 225 rpm. Ten mL of the overnight culture was used to inoculate 1 L of fresh 2xYT. The cells were grown between 3 and 4 hours, at 37 ^{o}C with shaking at 225 rpm, until an OD_{600} of 0.75 was reached. Protein expression was induced with the addition of 0.4 mM IPTG and induced cell cultures were incubated at 20 ^{o}C overnight. Cells were harvested by centrifugation in 500 mL centrifuge bottles at 5,000 g and 4 ^{o}C. The pellet was then frozen at -20 ^{o}C until purification.

2.7.2. Expression of EntB

E. coli AG-1 cells carrying the pCA24N-*entB* plasmid were streaked on a LB + chloramphenicol (30 µg/mL) plate and incubated overnight at 37 °C. A single colony was selected and inoculated into 50 ml 2xYT + chloramphenicol and incubated overnight at 37 °C with shaking at 225 rpm. Ten mL of the overnight culture was used to inoculate 1L of fresh 2xYT. The cells were grown between 3 and 4 hours, at 37^{o}C with shaking at 225 rpm, until an OD_{600} of 0.6 was reached. Protein expression was induced with 0.4 mM IPTG and incubated overnight at 25 ^{o}C. Cells were harvested by centrifugation in 500 mL centrifuge bottles at 5,000 g and 4 ^{o}C. The pellet was then frozen at -20 ^{o}C until purification.

2.7.3. Expression of EntA

E. coli AG-1 cells carrying the pCA24N-*entA* plasmid were streaked on a LB + chloramphenicol (30 µg/mL) plate and incubated overnight at 37 °C. A single colony was selected and inoculated into 50 ml 2xYT + chloramphenicol and incubated overnight at 37 °C with shaking at 225 rpm. Ten mL of the overnight culture was used to inoculate 1 L of fresh 2xYT. The cells were grown between 3 and 4 hours, at 37 ^{o}C with shaking at 225 rpm, until an OD_{600} of 0.6 was reached. Protein expression was induced with 1 mM IPTG and incubated for 3 hours at 37 ^{o}C. Cells were harvested by centrifugation in 500 mL centrifuge bottles at 5,000 g and 4 ^{o}C. The pellet was then frozen at -20 ^{o}C until purification.

2.8. Cell Lysis

2.8.1. Cell Lysis of BL21(DE3) Cells Harbouring EntC

Frozen pellets, from a 1 L culture, containing overexpressed H6-EntC were resuspended in 20 mL 50 mM TRIS (pH 8.0) containing 30 µg/mL lysozyme and 3 µg/mL DNAase using a tissue homogenizer. The resuspended pellet was passed through a French Press operating at 1,000 PSI. The lysate was then centrifuged using a Beckman JA-20 operating at 40,000 g for 30 minutes at 4 ^{o}C. After centrifugation, and before applying to the FPLC, the supernatant was filtered through a 0.45 µm filter.

2.8.2. Cell Lysis of AG1 Cells Harbouring EntB and EntA

Frozen pellets, from a 1 L culture, containing either H6-EntB or H6-EntA were resuspended in 20 mL 50 mM TRIS (pH 8.0), 1% n-Octyl β-D-Thioglucopyranoside (OTG), 3 μg/mL for DNAse and RNAse I, and 30 μg/mL of lysozyme. The cells were homogenized using a tissue homogenizer. The resuspended cell pellet was allowed to incubate on a mixing platform at RT for 30 minutes. After the incubation step protease inhibitor cocktail (BioShop) and 1 mM PMSF were added. The cell lysate was then centrifuged at 40,000 g in a JA-20 rotor at 10 ^{o}C for 30 minutes. The supernatant was then filtered through a 0.45 μm syringe filter before being loaded onto the FPLC.

2.9. Purification of Hexahistidine Tagged Proteins by IMAC Chromatography

2.9.1. Purification EntC

Hexahistidine-tagged EntC (H6-EntC) was purified using Profinity IMAC Resin (BioRad) in combination with a BioRad Biologic DuoFlow FPLC. A 10 mL column was freshly packed with new resin and equilibrated with 10 column volumes of EntC Loading Buffer (50 mM TRIS (pH 8.0), 50 mM NaCl, 5 mM imidazole) at 5 mL/min. Clarified lysate containing soluble H6-EntC was loaded onto the 10 mL column at a flow rate of 2 mL/min. The resin and bound EntC were then washed with 10 column volumes of EntC Loading Buffer to bring the A_{280} back down to baseline. The protein was then eluted in a stepwise manner using the EntC Elution Buffer (50 mM TRIS (pH 8.0), 50 mM NaCl, 250 mM imidazole). Fractions of the elution were collected in 2.5

mL windows and pooled fractions were analyzed by SDS-PAGE and then dialyzed into EntC Storage Buffer (50 mM TRIS (pH 8.0), 50 mM NaCl, 0.5 mM TCEP, 15 % glycerol).

2.9.2. Purification of EntA and EntB

H6-EntB and H6-EntA were also purified using the Profinity IMAC Resin (BioRad) and a BioRad Biologic DuoFlow FPLC. The resin was equilibrated with 10 column volumes of EntB/EntA Loading Buffer (50 mM HEPES (pH 8.0), 100 mM KCl, 20 mM imidazole, 0.5 mM TCEP) at 5 mL/min. Clarified lysate containing soluble H6-EntB/H6-EntA was loaded onto the 10 mL column at a flow rate of 2 mL/min. The resin and bound EntB/EntA were then washed with 5 column volumes of EntB/EntA Loading Buffer, 10 column volumes of EntB/EntA Salt Wash Buffer (50 mM HEPES (pH 8.0), 500 mM KCl, 20 mM imidazole, 0.5 mM TCEP) and 5 column volumes of EntB/EntA Loading Buffer. The protein was then eluted with a linear imidazole gradient (20 mM to 250 mM) in the presence of 50 mM HEPES (pH 8.0), 100 mM KCl, and 0.5 mM TCEP. Fractions of the elution (2.5 ml) were collected, and pooled fractions were analyzed by SDS-PAGE and then dialyzed into EntB/EntA Storage Buffer (50 mM HEPES (pH 8.0), 100 mM KCl, 0.5 mM TCEP, 15 % glycerol).

2.10. Measurement of Protein Concentration

Protein concentrations were estimated using two different methods: (i) dye-binding assay using Coomassie G-250 (Bio-Rad Protein Assay Kit), and (ii) absorbance

of aromatic chromophores at 280 nm. For the dye-binding assay, protein samples were diluted in water to a final volume of 800 μL and then 200 μL of 5X Bio-Rad dye concentrate was added. The mixture was incubated for 15 minutes at RT, and then the absorbances at 595 nm were measured. To accurately measure protein concentration, a standard curve was created with the following concentrations of BSA: 1.5, 2.5, 5, 7.5 and 10 μg/mL. The linear regression resulted in the following equation: [Protein] = $(A_{595}-0.073)/0.0466$. For the spectrophotometric assay, protein absorbance at 280 nm was measured in a Genesys 10 Spectrophotometer (Thermo). Unless explicitly mentioned all protein concentrations reported were determined using molar extinction coefficients predicted from primary amino acid sequences, as listed in Table 1.

	Molar Extinction Coefficient $M^{-1}cm^{-1}$
EntA	20970
EntB	51910
EntC	31970
EntE	57300

Table 1 - Molar Extinction Coefficients: all extinction coefficients were predicted from the Expasy site (http://au.expasy.org/tools/protparam) using the ProtParam application.

2.11. Dialysis

After purification and prior to certain experiments proteins were buffer exchanged by dialysis. Spectra/Por Molecularporous Membrane Tubing was

obtained from VWR in two formats 20.4 mm diameter and 6.4 mm diameter. Both had molecular weight cut-offs of 12,000 to 14,000 Da. In both cases, for large and small sample volumes, the proteins were dialyzed against 1 L of the required buffer overnight in a beaker with constant stirring. The above steps were repeated in fresh buffer two times before dialysis was completed.

2.12. Buffer Exchange on Desalting Columns.

To perform buffer exchange on small volumes the Econo-Pac 10DG Desalting Columns from Bio-Rad were employed. The columns were equilibrated with 25 mL of the buffer to be exchanged into. The protein sample to be exchanged was diluted until at least 0.5 mL and added to the column. After the protein sample had completely entered the column 2.5 mL of buffer was added. The protein sample was then eluted by adding an additional 0.5 mL of buffer. The protein concentration was determined and if necessary proteins were concentrated using Nanosep centrifugal devices with a MWCO of 3 kDa (Pall Life Sciences).

2.13. Pull Down Assay

Pull-down assays using H6-EntC and H6-EntB as bait were performed using the ProFound Pull-Down PolyHis Protein:Protein Interaction Kit (Pierce). Cobalt chelate slurry (50 μL) was pipetted into a Handy Spin Column and equilibrated with 2000 μL of washing solution (1:1 dilution of 25 mM TRIS-HCl, 0.5 M NaCl, 5 mM

Imidazole in ProFound Lysis Buffer (provided with kit)). Purified H6-EntB and H6-EntC bait proteins were incubated in separate columns with the cobalt chelate resin for 1 hour at 4 ^{o}C on a rotating platform. Unbound bait was eluted and the columns were washed another five times with washing solution. Potential protein interaction partners were introduced by adding cell lysate from *E. coli* BW25113 cells, grown 37 ^{o}C in iron-free M63 minimal media in the presence of 75 μM 2,2'-dipyridyl, to each column. The cell lysates were added to the spin columns in the presence or absence of 100 μM 2,3-DHB and then incubated at 4 °C on a rotating platform for 2 hours. Unbound prey proteins from the lysate were eluted upon washing five times with washing solution. The proteins that form complexes with either EntB or EntC were eluted with the elution buffer (1:1 dilution of 25 mM TRIS-HCl, 0.5 M NaCl, 600 mM Imidazole in ProFound Lysis Buffer). All eluted samples were prepared with 5X SDS Loading Buffer and heated at 95 ^{o}C for 10 minutes. The prepared samples were run on a 10 % SDS-polyacrylamide gel. The gel was then stained with SilverQuest Silver Staining kit (Invitrogen).

2.14. Sulfo-SMCC Protein-Protein Crosslinking

To study the protein complexation of EntC and EntB, the hetero-bifunctional crosslinker sulfosuccinimidyl 4-[N-maleimidomethyl]cyclohexane-1-carboxylate (Sulfo-SMCC) was used. Sulfo-SMCC was dissolved in 20 μL of dimethylsulfoxide (DMSO) to a concentration of 100 mg/mL and then diluted in PBS (0.1 M sodium phosphate, 0.15 M NaCl, pH 7.2) to 10 mg/mL with a DMSO concentration of 10%.

The crosslinker was used to maleimide-activate EntC and EntB in separate crosslinking reactions. The EntC activation reaction contained 20 μM EntC and 50-fold molar excess of Sulfo-SMCC. The EntB activation reaction contained 10 μM EntB and 50-fold molar excess of the crosslinker. Both reactions were allowed to proceed for 30 minutes at RT. The final DMSO concentration in the reaction mixture was 0.5 %. The EntC-SMCC and EntB-SMCC were then desalted to remove unreacted crosslinker using BioRad desalting columns. The maleimide-activated proteins were concentrated to approximately 40 μM (EntC) or 20 μM (EntB). Activated proteins EntC-SMCC and EntB-SMCC were mixed with pure EntB and EntC, respectively. The proteins were mixed in a 1:1 molar ratio to a final concentration of 10 μM and incubated for 1 h at RT. The reactions were then loaded on to a 10 % SDS-polyacrylamide gel and visualized using the Blue Silver stain described above.

2.15. Thin-Layer Chromatography

To qualitatively assess the production of 2,3-DHB by EntC, EntB and EntA using chorismate and NAD^+, thin layer chromatography (TLC) was used to identify 2,3-DHB. A previous study detected the presence of 2,3-DHB in *Brucella abortus* using TLC and the following method was adapted from the authors' protocol (López-Goñi et al. 1992a). The stationary phase consisted of silica plates and the mobile phases consisted of butanol:acetic acid:water in the following ratios 12:3:5. The samples (10 μL) were spotted three times on a line drawn 1 cm from the bottom of the plate and allowed to dry extensively. The TLC plate was then placed in a beaker

containing the mobile phase described above ensuring that the mobile phase was below the 1 cm line. The TLC plate was removed from the mobile phase chamber when the mobile phase reached 1 cm from the top of the plate. The plate was allowed to air dry and the 2,3-DHB was visualized by briefly immersing it in a 0.1 M solution of iron chloride.

2.16. Biophysical Experiments

2.16.1. Isothermal Titration Calorimetry

Isothermal titration calorimetry (ITC) experiments were performed on a VP-ITC MicroCalorimeter (MicroCal, Inc.). EntC was dialyzed into buffer containing 50 mM TRIS pH 8.0, 50 mM NaCl, 0.5 mM TCEP and 15 % glycerol. The EntC was diluted to a final concentration of 310 μM. Chorismate was dissolved in the dialysate of the EntC dialysis and diluted to a final concentration of 8400 μM. The concentration of EntC and chorismate were measured by OD_{280} and OD_{275} (chorismate ε = 2632 $M^{-1}cm^{-1}$) respectively. Both protein and substrate samples were degassed and equilibrated at 18 ^{o}C for 15 minutes. The experiment consisted of one 3 μL injection and thirty-nine 7 μL injections, separated by 240 s. The temperature and stirring rate of the cell were 20 ^{o}C and 300 rpm respectively. The heats of injection generated by chorismate injection into EntC were measured and then corrected by subtracting heats of dilution obtained by injection of chorismate into buffer. The corrected data, with the exception of the first 3 μL injection, were fitted to a single-

site binding model using Origin 5.0 (MicroCal, Inc.). The values for stoichiometry, enthalpy, entropy and K_D were determined by the software.

2.16.2. Far-UV Circular Dichroism

Far-UV CD spectra of EntC were recorded over the range of 190 to 260 nm in 0.2-cm path-length cell on Jasco J-815 CD spectrophotometer. Prior to data collection, purified EntC was buffer-exchanged using a BioRad Desalting column into 50 mM phosphate buffer at pH 8.0. The final concentration of EntC was adjusted to 2 mg/mL. The far-UV CD spectra of EntA and EntA variants were recorded over the range of 200 to 260 nm in 0.2-cm path-length cell. The proteins samples were buffer exchanged by dialysis into 50 mM TRIS (pH 8.0, adjusted using H_2SO_4), 0.5 mM TCEP, 100 mM NaF, and 15% glycerol. The final concentration of the samples were adjusted to 5 µM by dilution with the dialysis buffer. The spectra for all proteins investigated were recorded at 20 °C by averaging 5 wavelength scans (1 nm bandwidth) in 0.2-nm steps at a rate of 100 nm/min, and 0.25 sec response.

2.16.3. Near-UV Circular Dichroism

Near-UV circular dichroism experiments were performed on a Jasco J-715 CD spectrophotometer connected to a circulating water bath set at 20 ^{o}C. EntC was buffer exchanged using a Bio-Rad Econo-Pac 10DG Desalting Column into 50 mM TRIS pH 8.0 and 50 mM NaCl. The spectra of 2 mg/mL EntC was collected in the

presence and absence of 10 mM $MgCl_2$ using a 1 cm pathlength. The wavelength range was from 250 nm to 340 nm and the scan rate used was 20 nm/min with 0.2 nm steps. The near-UV spectra presented is an average of three scans with the buffer spectrum being subtracted from the raw spectrum of EntC with or without $MgCl_2$.

2.16.4. Temperature Denaturation Monitored by Circular Dichroism.

Thermal stability experiments on EntA wild-type and variants were performed by monitoring ellipticities at 222 nm starting at 20 ^{o}C and increasing at a rate of 15 ^{o}C/min to a final temperature of 65 ^{o}C using a Jasco J-815 CD spectrophotometer with a water-cooled Peltier cell. The samples were dialyzed into 50 mM TRIS (pH 8.0, adjusted using H_2SO_4), 0.5 mM TCEP, 100 mM NaF, 15% glycerol. The following instrument parameters were used for these experiments: data pitch 0.2 °C, sensitivity standard (100 mdeg), response time 8 s, band width 1 nm. The melting point for each protein was determined by determining the temperature corresponding to the maximum peak of the first derivative function. The data were plotted as Fraction Folded vs. Temperature by using the following conversion:

$$Fraction\ Folded\ = \frac{(\ Ellipticity\ -\ Ellipticity\ at\ 65^{o}C)}{(Ellipticity\ at\ 20^{o}C\ -\ Ellipticity\ at\ 65^{o}C\ )}$$

2.16.5. Fluorescence Anisotropy

Fluorescence anisotropy measurements were used to determine DHB binding to DHB module enzymes EntA, EntC and EntB. Anisotropy experiments were performed on a Varian Cary Eclipse fluorimeter with the excitation and emission wavelengths for 2,3-DHB at 320 nm and 440 nm respectively and both excitation and emission slit widths were adjusted to 5 nm. All samples contained 15 μM 2,3-DHB in 50 mM HEPES (pH 8.0), 100 mM KCl, and 0.5 mM TCEP. Anisotropy was measured for the addition of 15 μM of EntA, EntB or EntC in the presence and absence of $MgCl_2$ (10 mM). Anisotropy (*r*) values were calculated using the following equation:

$$r = \frac{I_{\parallel} - I_{\perp}}{I_{\parallel} - 2I_{\perp}}$$

where $I_{//}$ is the fluorescence emission with the polarizers positioned in a parallel orientation and $I_{\perp}$ is the fluorescence emission intensity with polarizers in a perpendicular orientation (Lakowicz 2006).

2.16.6. Analytical Ultracentrifugation

A Beckman XLI analytical ultracentrifuge with an An-60Ti rotor was used to determine the oligomeric state of EntC as well as EntA WT and variants by sedimentation velocity experiments. Prior to AUC analysis an EntC sample was diluted to 20 μM and dialyzed extensively in 50 mM TRIS pH 8.0, 50 mM NaCl, 0.5 mM TCEP and then diluted after dialysis to 5.5 μM and 11 μM. EntA WT and variants

were extensively dialyzed in 50 mM HEPES pH 8.0, 150 mM NaCl, 0.5 mM TCEP and diluted to a final concentration of 6 μM in the same buffer. The samples were centrifuged at 40,000 rpm at 20 ^{o}C and 225 (or 250) absorbance scans were collected. The data were fit to a c(S) distribution using SEDFIT to determine the sedimentation coefficients.(P Schuck 2000) The buffer density and viscosity as well as protein partial specific volumes were calculated using SEDNETERP.(Hayes, Laue, , and Philo 1995)

2.17. Coupled Enzyme Assays

2.17.1. EntC Activity Assay

EntC activity was monitored by means of a coupled colorimetric enzyme assay utilizing the activities of the DHB module enzymes EntB and EntA. The reaction mixture (total volume 0.5 mL) contained 10 μM EntA, 10 μM EntB, 1 μM EntC, 50 mM TRIS (pH 7.5), 50 mM NaCl, 10 mM $MgCl_2$, 2.5 mM NAD^+ and varying amounts of chorismate between 0 and 300 μM. The progress of the reaction was monitored by the reduction of NAD^+ to NADH by EntA. All of the enzyme reactions were initiated by the introduction of chorismate to the reaction mixture pre-equilibrated at 37 ^{o}C. The initial rates were measured at 37 ^{o}C over a two-minute interval. All assays were performed in triplicate with the averages being plotted with standard deviations as error bars. Two control reactions in the absence of chorismate or EntC showed no increase in absorbance at 340 nm.

2.17.2. EntA Activity Assay

The steady-state kinetics of EntA wild-type and variants were assayed in the presence of excess EntB and EntC, which enzymatically converts chorismate to the EntA substrate 2,3-dihydro-2,3-dihydroxybenzoate. EntA activity was monitored by following the production of NADH at 340 nm. The final reaction mixtures (total volume 1 mL) contained 1 µM EntA, 10 µM EntC, 10 µM EntB, 50 mM TRIS (pH 7.5), 50 mM NaCl, 10 mM $MgCl_2$, 300 µM chorismate and varying concentrations of NAD^+. All of the reactions were initiated by adding chorismate to the reaction mixture pre-equilibrated at 37 ^oC. The initial rates were monitored at 37 ^oC over a two-minute interval. The rate at each NAD^+ concentration was converted from A340/min into [NADH]/min using the molar extinction coefficient for NADH at 340 nm (6,220 M^{-1} cm^{-1}). Initial rates were plotted against NAD^+ concentration to determine steady-state kinetic parameters. All initial rate measurements were performed at least three times and the average and standard deviations are plotted. No increase in A_{340} was detected in control reactions lacking EntA or EntB.

2.18. Automated Docking of EntE to EntA

The atomic coordinates of the EntA X-ray structure were obtained from the PDB entry 2FWM and the atomic coordinates of the EntE structure were extracted from the PDB entry 3RG2, a chimera of EntE and the ArCP domain of EntB. Due to the size of the systems being docked the smaller protein EntE, was docked to the

larger assembly of tetrameric EntA. AutoDockTools was used to prepare the pdbqt (a modified pdb file containing atomic coordinates, partial charges and AutoDock 4 atom types) files for AutoDock 4.2 (Sanner 1999; Morris et al. 2010). Surface residues on EntA (Asp 55, Gln 58, Gln 61, Gln 64, Arg 65 and Glu 69) located on helix 4, shown experimentally to interact with EntE, were made flexible. EntE obtained from the chimera in 3RG2 was used as a rigid ligand. The grid corresponding to the docking simulation was the largest possible at 126 Å x 126 Å x 126 Å. Due to size limitations the grid box was positioned such that only one face of the EntA tetramer was available for docking. The docking was run using the Lamarckian genetic algorithm with an initial population of 300 random orientations and 25,000,000 energy evaluations per run. A single model with flexible residues was produced. The atomic coordinates of EntE after the flexible docking were used in a second docking experiment in which both proteins were docked as rigid bodies. The rigid body docking generated ten models that all aligned to within an RMSD of 0.5 Å. All figures presented within were generated using PyMOL (Schrodinger LLC 2010).

3. Results

3.1. Characterization of EntC

3.1.1. Over-Expression and Purification of EntC

The *entC* gene was previously PCR-amplified from the pCA24N-*entC* construct, obtained from the ASKA collection (Kitagawa et al. 2005). The PCR product was subcloned into the pET24b expression vector between the *Not*I and *Bam*HI cut sites following restriction digestion. The pET24b expression construct is under control of a T7 lac promoter and encodes an in-frame T7 epitope tag as well as an in-frame hexahistidine (H6) affinity tag. To maximize the yield of H6-EntC, the expression conditions were optimized according to OD_{600} at induction as well as induction medium and induction conditions (IPTG concentration and length of induction). The first parameter optimized was the culture cell density (OD_{600}) at which induction was initiated. Samples of 1 mL were removed from a 50 mL culture (inoculated with 1 % of o/n culture) at OD_{600} of 0.35, 0.55, 0.75, 0.95, 1.10, 1.5, 1.7, 1.9, 2.2 and 2.5 and induced with 1 mM IPTG for 3 hours at 37 ^{o}C. The non-induced samples (-) and the induced samples (+) were run on a 10% SDS-polyacrylamide, shown in Figure 15. The optimum OD_{600} at induction was chosen to be 0.75 because the band corresponding to EntC is very abundant with the bands representing other proteins found in the cell lysate relatively low.

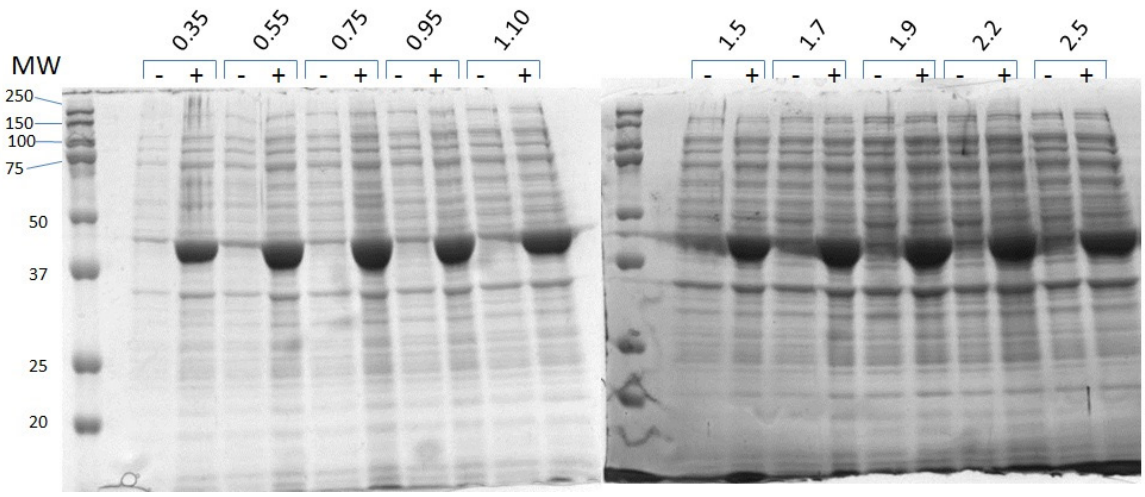

Figure 15 - Optimization of OD_{600} at Induction. A 10 % SDS-polyacrylamide gel showing the whole cell lysate of sampes with OD_{600} from 0.35 to 2.5. non-Induced (-), Induced (+).

To test if the expressed protein was soluble, a small culture was again inoculated with an o/n culture and grown to an OD_{600} of 0.75 before being induced with 1 mM IPTG for 3 hours. The culture was centrifuged and the pellet was lysed as per section 2.8.2. The expressed protein was found to be localized to insoluble inclusion bodies (data not shown). To limit the extent of which EntC would be expressed to inclusion bodies, the induction conditions were switched to 0.4 mM IPTG at 20 ^{o}C overnight.

The last parameter to be optimized was the growth medium used for overexpression. Three growth media used in our lab were tested: (*i*) an auto-induction medium (Studier 2006), (*ii*) 2xYT and (*iii*) LB. Lysates recovered from cells grown in each medium were tested for total protein (T), as well as proteins found in soluble (S) and insoluble fractions (IB); the results are reported in Figure 16. Cells that were grown in the auto-induction media over-expressed EntC being targeted to

inclusion bodies. The results obtained using 2xYT growth media and LB were similar but cells grown in 2xYT appeared to produce more EntC. Thus 2xYT was used for the expression and purification of EntC.

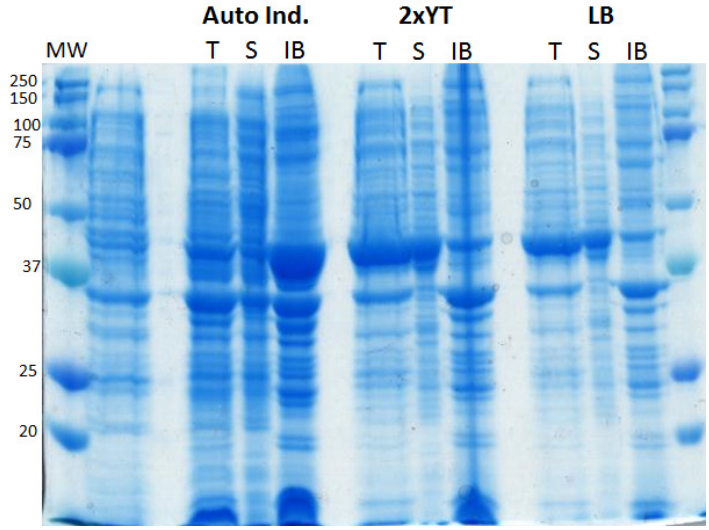

Figure 16 – Selection of Growth Media for Expression of EntC. The three media used from left to right is Auto Induction, 2xYT and LB. Each media has three lanes corresponding to Total protein (T), soluble protein (S) and insoluble protein (IB).

Cells harbouring H6-EntC were lysed by French press and loaded onto IMAC Profinity resin using a BioRad DuoFlow FPLC. EntC was eluted with EntC Elution buffer containing 250 mM imidazole.

The outcome of H6-EntC purification by IMAC chromatography is shown in Figure 17 (OD_{280} in blue, conductivity in red). Proteins from the collected fractions were separated on a denaturing gel and the fractions containing the largest amounts of H6-EntC as estimated by OD_{280} were pooled and dialyzed. The final purity of H6-EntC is compared to the flow through and wash of the purification in Figure 18.

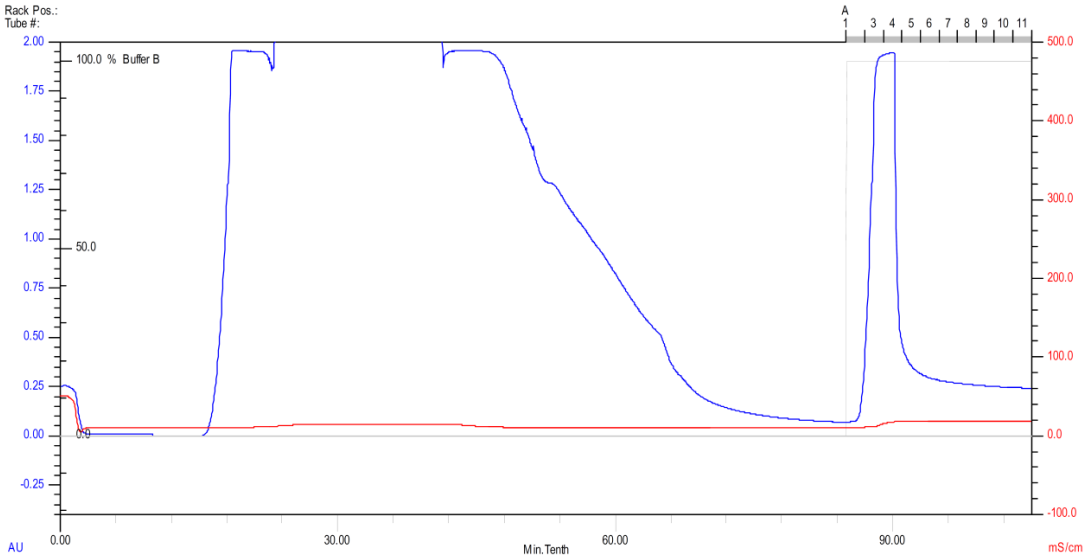

Figure 17 - Representative Chromatogram of EntC Purification. Blue line represents OD280 and red line represents conductivity.

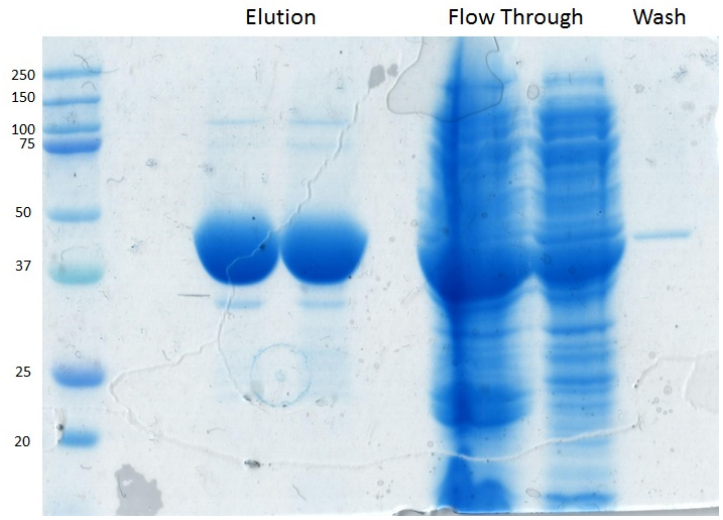

Figure 18 - Fractions of an H6-EntC Purification Run on a 10 % SDS-polyacrylamide gel.

3.1.2. Far-UV Circular Dichroism.

Far-UV circular dichroism was used to gain qualitative information regarding the secondary structure of recombinant H6-EntC. Far-UV CD spectra of protein can be used to determine relative amounts of α-helical, β-sheet and random coil secondary structure elements in a given protein sample (Kelly et al. 2005). The far-UV CD spectrum of H6-EntC was recorded over the range 190-260 nm in a 0.2 cm cuvette at 20 ^{o}C. EntC protein stock was thawed on ice and exchanged against the buffer described in section 2.16.2.

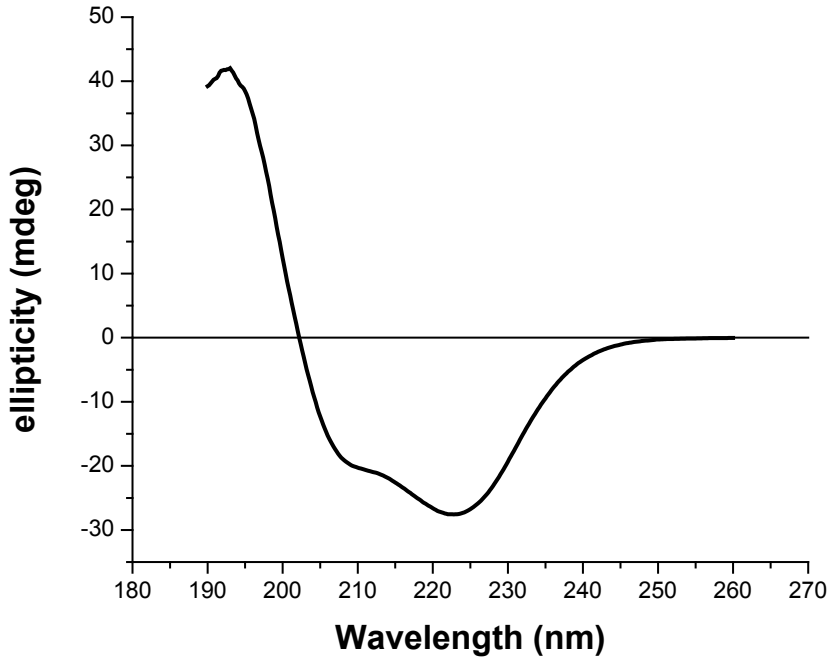

Figure 19 - Far-UV CD spectrum of EntC

After dialysis the EntC was diluted in dialysate to a final concentration of 2 mg/mL. The smoothed spectrum presented in Figure 19 is the average of five collections and corrected for buffer contribution. The far-UV CD spectrum collected for EntC at 2 mg/mL demonstrates a major minimum at 222 nm and a second less intense minimum at 208 nm. The double minima at 208 and 222 nm along with a strong positive signal at 200 nm are indicative of strong α-helical content (Kelly et al. 2005). The far-UV CD analysis of H6-EntC reveals secondary structure content that agrees with the reported X-ray crystal structure (Sridharan et al. 2010).

3.1.3. Cofactor Binding of Mg^{2+} to EntC Observed by Near-UV CD

Near-UV CD spectra were collected for H6-EntC in the presence and absence of 10 mM magnesium chloride, since magnesium is a cofactor that is important for EntC catalysis. Near-UV CD spectroscopy was used to observe possible changes in the local environment of the protein aromatic chromophores (Phe, Tyr, and Trp) due to magnesium binding. The resulting spectra are shown in Figure 20. Changes in peak intensity were observed for peaks at 288 nm and 295 nm upon mixing with Mg^{2+}. Furthermore, a new peak at 267 nm was observed to appear only in the presence of Mg^{2+}.

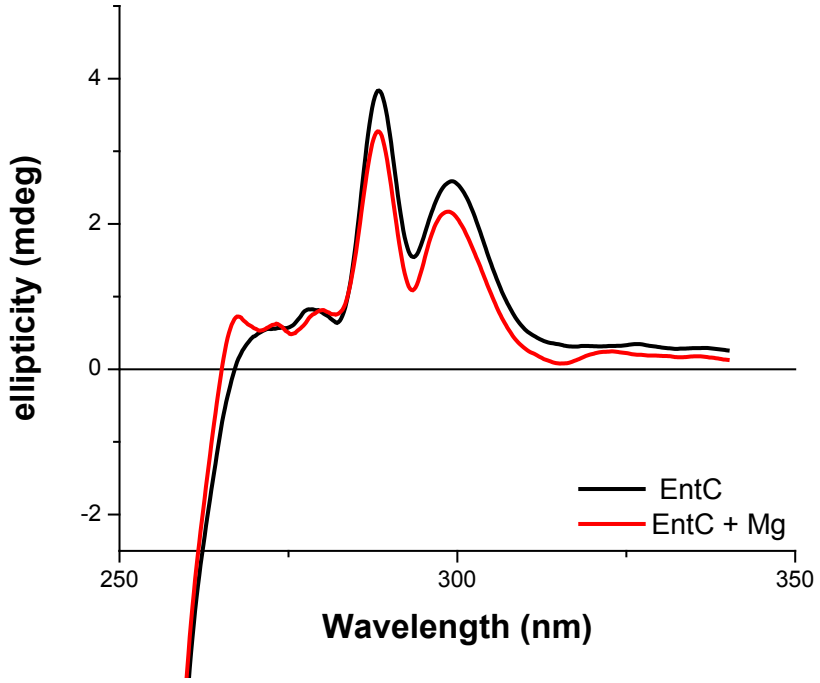

Figure 20 - Near-UV CD of EntC in the Presence and Absence of Mg^{2+}. The spectra of EntC (2mg/mL) were collected in the presence (Red) and absence (Black) of Mg^{2+} (10 mM) in a 1 cm pathlength cell.

3.1.4. Determination of EntC Oligomeric State by AUC

To probe the quaternary structure of recombinant H6-EntC, sedimentation velocity analytical ultracentrifugation (AUC) was used. AUC allows for the measurement of the sedimentation distribution of protein concentration along the length of a cell during centrifugation at very high g-forces. In a sedimentation velocity experiment AUC measures the rate of migration of the protein concentration when a centrifugal force is being applied (Balbo & Schuck 2005). The sedimentation velocity behaviour of a protein sample can determine its approximate

molecular weight and shape. Furthermore, if the subunit molecular weight of a protein is known, AUC can be used to determine protein quaternary structure.

The oligomeric state of H6-EntC has previously been reported to be monomeric. However, a closed related homologue MenF exists as a dimer (Daruwala et al. 1997). To determine if our purified recombinant H6-EntC exists in solution as a monomer, sedimentation velocity AUC experiments were performed at two concentrations: 0.25 mg/mL and 0.5 mg/mL (5.5 μM and 11 μM respectively) in 50 mM HEPES pH 8.0, 150 mM NaCl, 0.5 mM TCEP. The raw AUC data from every 25th scan of EntC at 0.25 mg/mL is shown in Figure 21. The AUC analysis was performed using SEDFIT (Schuck 2000).

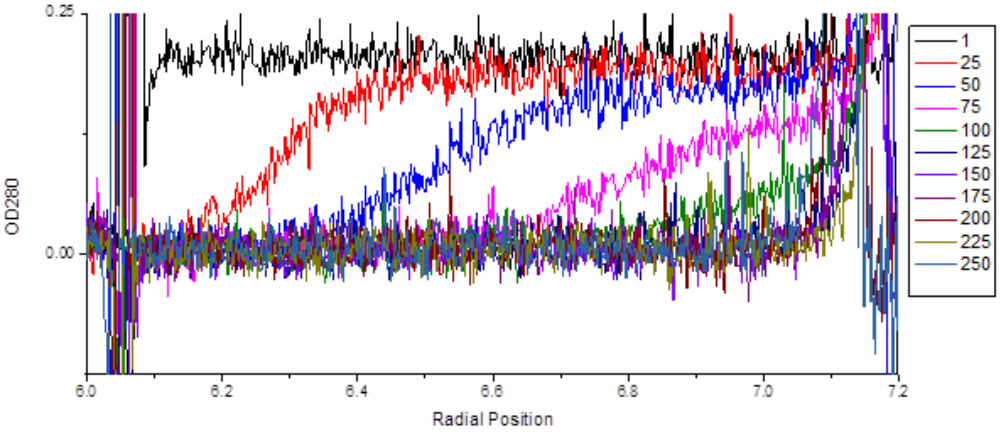

Figure 21 – Raw AUC Data of EntC at 0.25 mg/mL. Every 25th scan is observed in this figure.

The raw data were fit to a c(S) continuous distribution model and the resulting plot is shown in Figure 22. The sedimentation coefficients, MW and quaternary structures of H6-EntC at both concentrations are listed in Table 2.

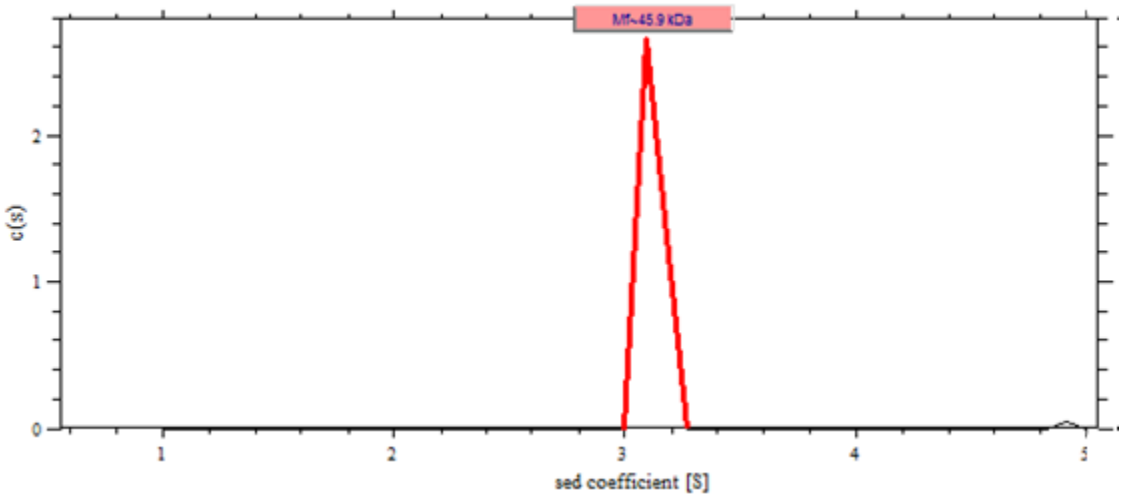

Figure 22 – c(S) Distribution of 0.25 mg/mL EntC.

[EntC] μM	$S_{20,w}$	MW kDa	Quaternary Structure
5.5	3.30	48.0	Monomer
11.0	3.28	45.9	Monomer

Table 2 - AUC Analysis of EntC at Two Concentrations 0.25 mg/mL and 0.5 mg/mL.

3.1.5. Fluorescence Anisotropy

Fluorescence anisotropy was used to probe the possible binding of 2,3-DHB, an intrinsic fluorophore, to H6-EntC. Although 2,3-DHB is neither a substrate nor a

product of EntC, it is the final product of the DHB module, and thus a possible feedback regulator of EntC activity. We therefore investigated 2,3-DHB binding to H6-EntC, as well as the other DHB module proteins (H6-EntB, H6-EntA) using a fluorescence-based equilibrium-binding assay. Fluorescence anisotropy measures fluorescence in two directions perpendicular to one another. A small fluorophore such as 2,3-DHB will have fast rotational diffusion and thus have equal fluorescence emission in both the parallel and perpendicular orientation. However, if the fluorophore is bound by a protein, the large protein will slow the rotational diffusion of the fluorophore leading to unequal emission and an increase in anisotropy signal.

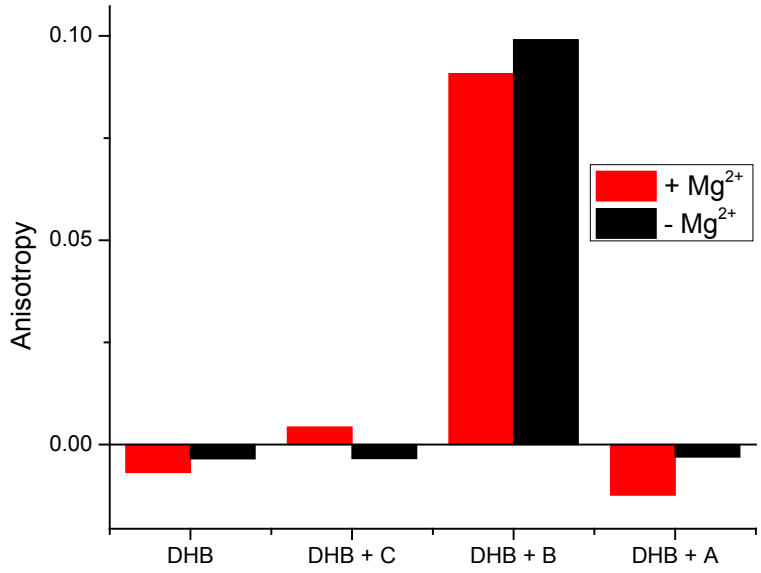

Figure 23 – Fluorescence Anisotropy of 2,3-DHB (15 μM) in the Presence of EntA, EntB and EntC (all at 15 μM). The fluorescence anisotropy of each sample was measured in the presence (Red) and absence (Black) of Mg^{2+}(10 mM).

A DHB concentration of 15 μM was used and all enzyme concentrations were 15 μM. Resulting fluorescence anisotropies in the presence and absence of magnesium are shown in Figure 23. No increase in anisotropy of DHB was observed in the presence of EntA or EntC. There is, however, an increase in anisotropy in the presence of EntB indicating that EntB binds 2,3-DHB, consistent with what has been previously reported (Khalil & Pawelek 2009). Furthermore, addition of 10 mM Mg^{2+} was found to have no effect on the binding of 2,3-DHB to EntC.

3.1.6. EntC Binding to Chorismate by ITC

Having overexpressed and purified H6-EntC, it was important to determine that the protein was properly folded and thus able to bind chorismate, its natural substrate. Equilibrium-binding information (*i.e.*, K_D) is also complementary to steady-state kinetic parameters *(i.e.*, K_m) in elucidating enzyme function. Isothermal titration calorimetry (ITC) was used to measure the stoichiometry n, entropy ΔS, enthalpy ΔH, and the dissociation constant K_D of chorismate binding to EntC. The ITC experiment was performed in 50 mM TRIS pH 8, 50 mM NaCl, 0.5 mM TCEP and 15% glycerol and consisted of titrating chorismate into EntC. The experiment consisted of 40 injections, each of 7 μL. The raw injection data are shown in Figure 24a. The MicroCal Origin software package was used to integrate the individual heats of injection after correction for baseline and heats of dilution. The integrated heats of injection were plotted against molar ratio of ligand to protein. The data were then fit to a one-binding site model. The resulting binding isotherm is shown in Figure 24b.

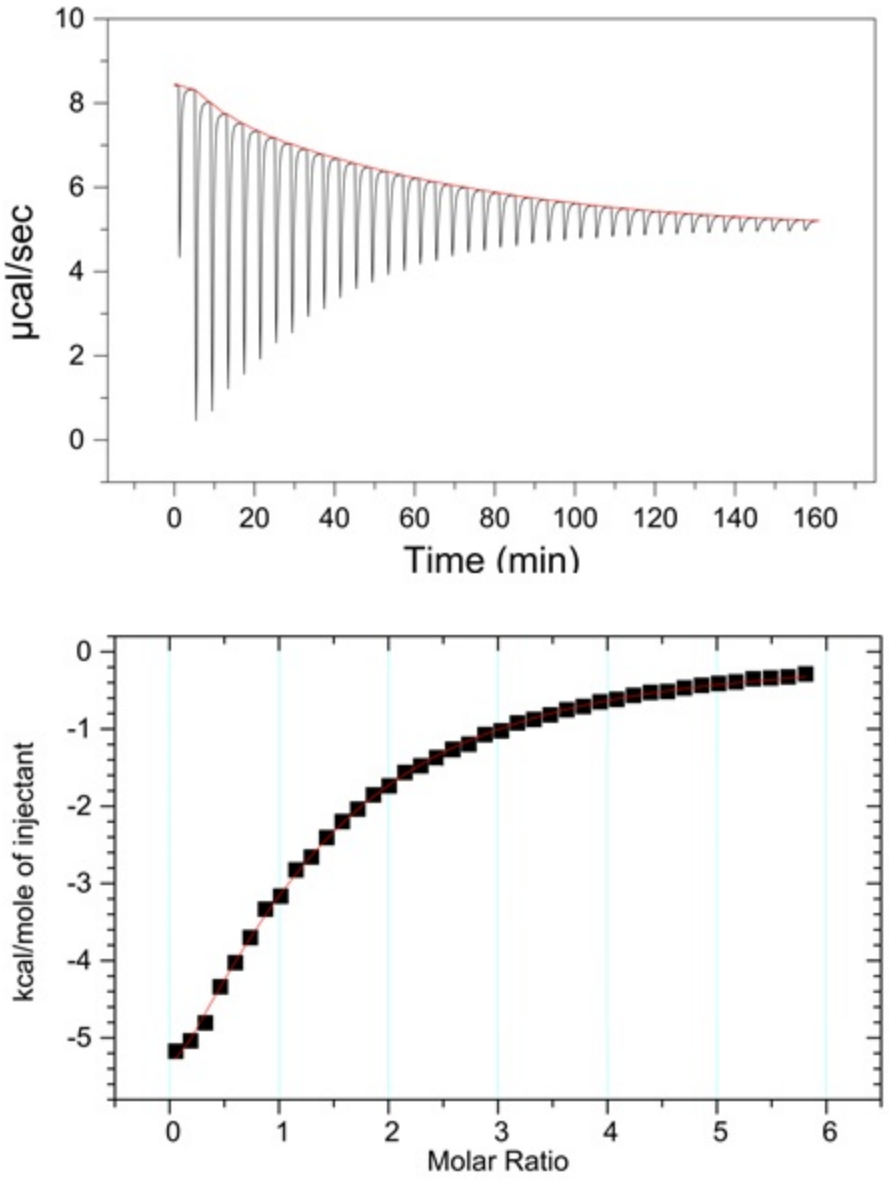

Figure 24 – Chorismate Binding to EntC Measured by ITC. A) The top panel shows the heats of injection for injection chorismate into EntC. B) The bottom panel shows the Chorismate-EntC binding isotherm of the integrated heats of injection.

The results of the fitting are summarized in Table 3. The stoichiometry of binding was determined to be 1.11:1 and the K_D was found to be 336.7 µM. The enthalpy and entropy were found to be -1.056 x 10^4 cal*mol^{-1} and -20.1 cal*$K^{-1}mol^{-1}$, indicating that chorismate binding to H6-EntC is enthalpy-driven. ITC results are summarized in Table 3.

ITC Data Table	
Chi-squared	**1288.82**
N	**1.11 ± 0.025**
ΔH	**-1.056 x 10^4 ± 292.6 cal*mol^{-1}**
ΔS	**-20.1 cal*$K^{-1}mol^{-1}$**
K_D	**336.7 ± 10.1 μM**

Table 3 – Summary of Data Obtained from ITC experiment studying Chorismate binding to EntC

3.1.7. Initial Determination of DHB Module Activity by TLC

To test the activity of all our recombinant purified DHB module enzymes (H6-EntC, H6-EntB and H6-EntA), a TLC-based single end-point assay was first employed. The production 2,3-DHB was detected by separation on a TLC plate and visualization using ferric chloride (due to the ability of 2,3-DHB to bind iron) as previously described (López-Goñi et al. 1992b). Lane 1 contains pure 2,3-DHB obtained from Sigma. Lanes 2 (-EntC) and 4 (-chorismate) are the negative controls in this assay. Lane 3 represents the lane in which the three enzymes of the DHB module are all present along with the required cofactors and substrate. The TLC plate stained with $FeCl_3$ is shown in Figure 25.

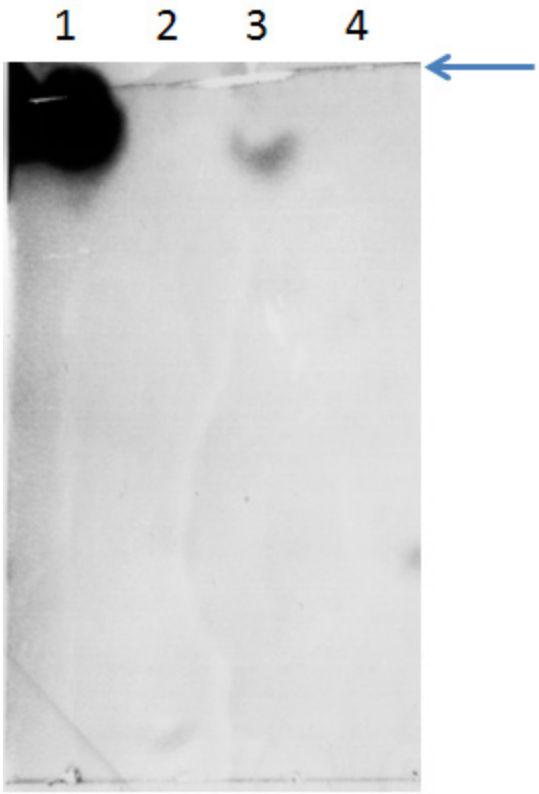

Figure 25 - TLC Detection of Enzymatically produced 2,3-DHB.The solvent front is indicated by the arrow above. Lane 1 contains pure 2,3-DHB. Lane 2 and 4 contain the reaction mixture in the absence of EntC and chorismate, respectively. Lane 3 contains all three proteins of the DHB module and all necessary cofactors.

A spot having an R_f value similar to the pure 2,3-DHB control was observed in lane 3. The results reveal the production of 2,3-DHB, indicating that all the recombinant hexahistidine-tagged proteins of the DHB module produced in our lab are active.

3.1.8. Steady-State EntC Kinetic Parameters: Coupled Enzyme Assay

After demonstrating that the purified, recombinant enzymes of the DHB module produced for this study were all active, it was necessary to develop an assay to measure the activity of each individual enzyme. In order to measure the kinetic

parameters of H6-EntC, we coupled H6-EntC activity to the activities of H6-EntB and H6-EntA. The assay was designed such that the coupled enzymes were in ten-fold molar excess over the concentration of EntC used in the assay. The progress of the reaction was followed spectrophotometrically by monitoring EntA-produced NADH at 340 nm. The reaction conditions were 1 μM EntC, 10 μM EntB and EntA, 5 mM NAD^+ in a 50 mM TRIS pH 7.5, 50 mM NaCl, 5 mM $MgCl_2$, with chorismate concentrations varying from 0 to 300 μM. The scheme of the coupled enzyme assay is demonstrated in Figure 26.

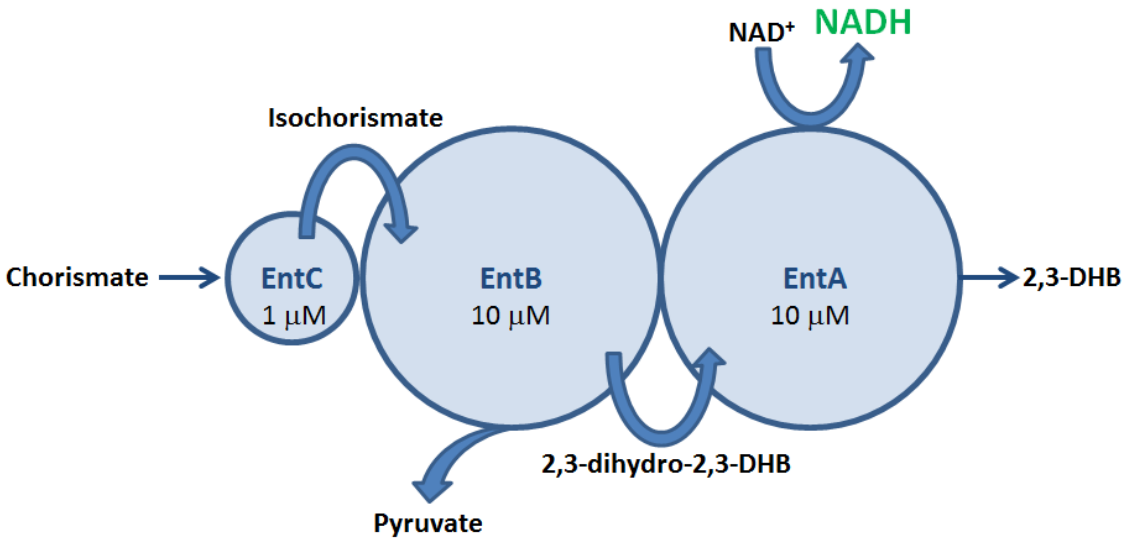

Figure 26 - Coupled Enzyme Assay Used to Determine EntC Steady-state Parameters.

To ensure that the assay was valid for measuring the steady-state kinetic parameters of EntC, it was necessary to demonstrate that EntC was the limiting component of the activity measured. The rate of NADH production was therefore measured as a function of EntC concentration, keeping the remaining components

of the reaction consistent. The rate of NADH production was determined at the following H6-EntC concentrations: 0.5 μM, 1.5 μM and 2.0 μM EntC (Figure 27).

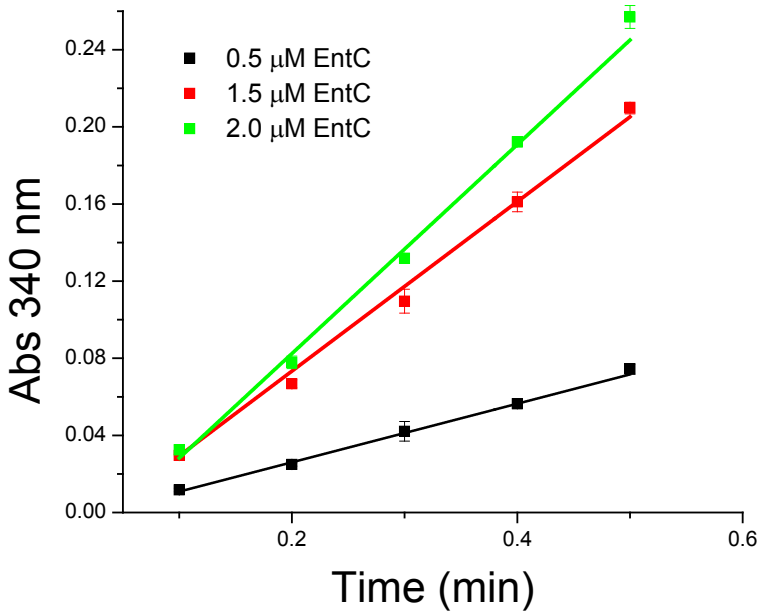

Figure 27 – Validation of EntC Assay. Rates of NADH production at three concentrations of EntC 0.5 μM (Black), 1.5 μM (Red) and 2.0 μM (Green)

The initial rates determined from the data shown in Figure 27 were then plotted as a function of H6-EntC concentration (Figure 28). The resulting plot demonstrated that the rate of NADH production responded linearly with respect to EntC concentration. This indicates that under the conditions of the coupled assay employed, H6-EntC was the limiting activity. We therefore had confidence that apparent steady-state kinetic parameters determined from our coupled assay under these conditions truly reflected H6-EntC activity and not a combination of the coupled enzyme activities.

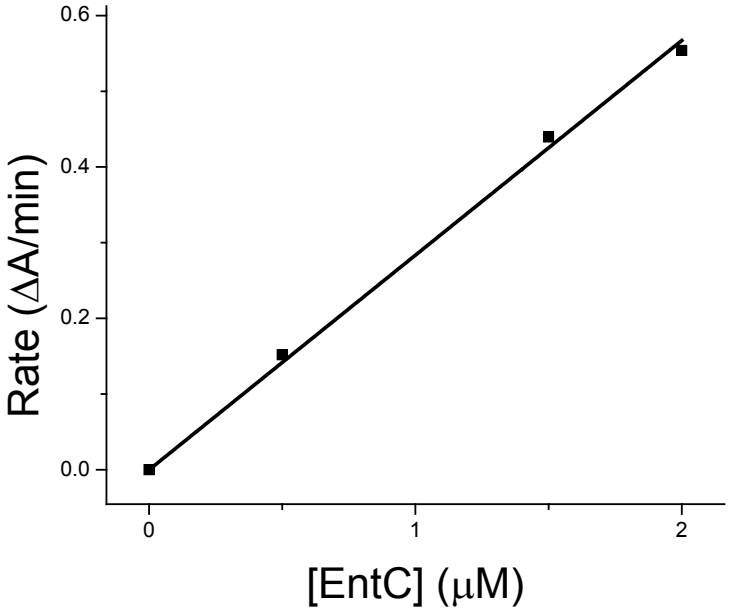

Figure 28 - Validation of EntC Activity Assay. Plot of rates determined for three concentrations of EntC vs. EntC concentration

The steady-state kinetic parameters for EntC were measured using our validated coupled enzyme assay. The K_m and k_{cat} values of EntC were previously reported to be 14 μM and 0.096 $\mu M^{-1}s^{-1}$ respectively (Liu et al. 1990; Sridharan et al. 2010). For this reason the initial concentration range for chorismate was 0 to 50 μM. However, upon analysis of preliminary data, our measured K_m fell outside of this range of chorismate concentration. The assay was thus repeated with the following concentrations of chorismate: 25 μM, 50 μM, 100 μM, 200 μM and 300 μM. Initial rates for each chorismate concentration were measured in triplicate and the averages were plotted, Figure 29. The error bars in this figure represent the

standard deviations of the means. The data were fit to a positive cooperativity model (Hill Plot) using OriginPro 8.6 and the equation used for this fit is

$$y = V_{max} \frac{x^n}{k^n x^n}$$

This specific fit was used because it was observed to give a lower error of fit compared to that obtained using the Michaelis-Menten equation. The apparent kinetic parameters K'_m and K'_m/k'_{cat} were found to be 40.48 μM and 0.026 $\mu M^{-1}s^{-1}$, respectively. The steady state kinetic parameters of EntC are summarized in Table 4.

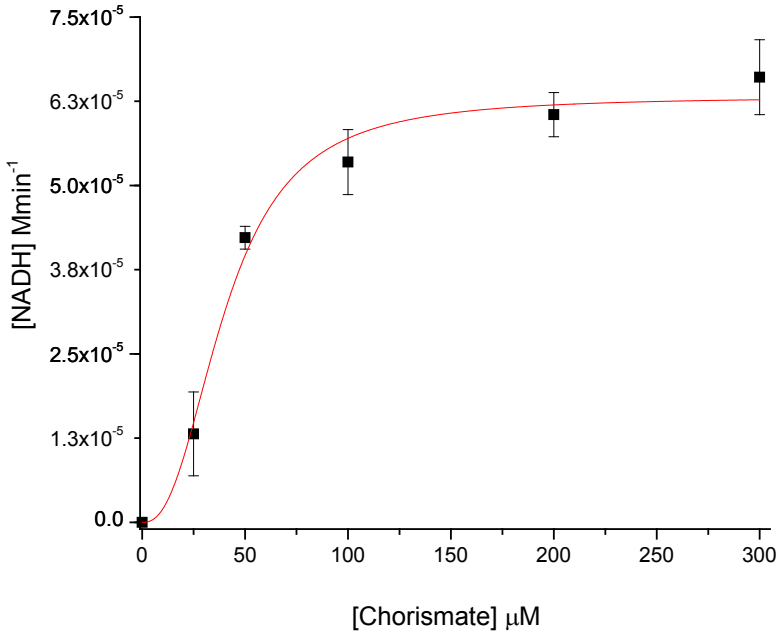

Figure 29 - Steady-State Kinetics Plot of Rate NADH Production vs. Chorismate Concentration

K'_m μM	k'_{cat} s^{-1}	k'_{cat}/K'_m s^{-1} μM^{-1}
40.48 ± 2.77	1.05 ± 0.04	0.026

Table 4 –Steady-State Kinetic Constants for EntC and Chorismate determined at pH 7.5 at 37 °C.

3.1.9. Novel Evidence of an EntC-EntB Protein-Protein Interaction

To probe the possible protein-protein interactions involving EntC a commercial pull-down assay (Pierce) was used. We hypothesized that EntC interacts with EntB because it is the next sequential enzyme in the DHB module of enterobactin biosynthesis, and this interaction could facilitate metabolite flux towards 2,3-DHB by 'pulling' isochorismate away from EntC, which could potentially convert the isochorismate product back to chorismate in an efficient reverse reaction (Liu et al. 1990). In our pull-down experiments, we used both H6-EntC and H6-EntB as bait in separate columns. Furthermore, because 2,3-DHB has been shown to induce a conformational rearrangement in EntB (Khalil & Pawelek 2009), the samples were incubated in the absence and presence of exogenous 2,3-DHB. The prey used in each experiment was whole-cell lysate prepared from *E. coli* BW25113 cells grown under iron-limiting conditions to induce expression of the *ent* genes following Fur derepression. Protein complexes were eluted with high imidazole following extensive washing, and recovered proteins were separated by SDS-PAGE (Figure 30). Lanes 1 and 2 contain proteins pulled down using H6-EntC as bait in the absence (Lane 1) and presence (Lane 2) of 2,3-DHB. Lanes 3 and 4 contain proteins pulled down using H6-EntB as bait in the absence (Lane 3) and presence (lane 4) of 2,3-DHB. Lane 5 represents proteins pulled down by non-specific interactions with the column (*i.e.*, no bait added). Lane 6 and 7 contain purified recombinant H6-EntC and H6-EntB, respectively.

Upon closer examination of the gel, the no-bait control pulls down a protein that is migrating at approximately the same position as EntC. This band in the no-bait control hampers our ability to examine whether or not EntB pulls down EntC. However, if we examine the proteins pulled down by EntC there is a clear band that migrates at the same distance as EntB which does not appear in either the no bait control or purified EntC. This section of the gel is highlighted by a red rectangle in Figure 30. The ability of EntC to pull down the band running at the same position of EntB is independent of exogenously added 2,3-DHB. This pull-down assay demonstrates initial evidence of a protein-protein interaction involving EntC and EntB.

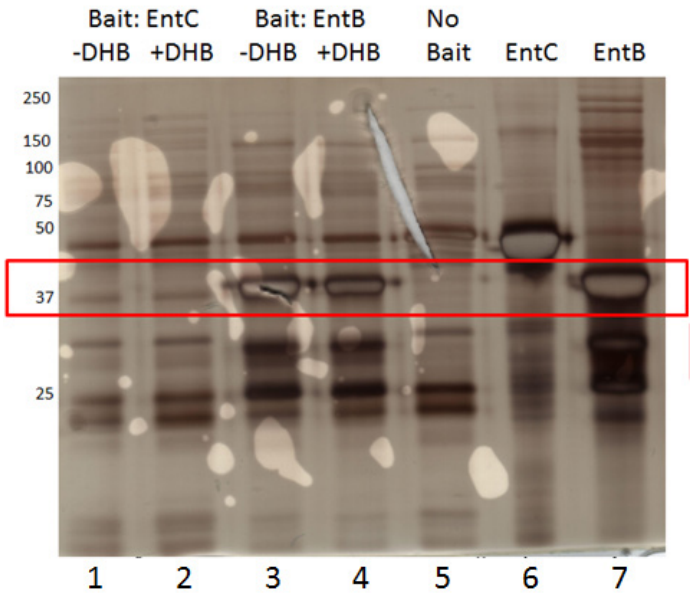

Figure 30 - Initial Evidence of a Protein-Protein Interaction Between EntC and EntB by Pull-Down Assay. Lanes 1 and 2 used EntC as bait in the absence and presence of 2,3-DHB, respectively. Lanes 3 and 4 used EntB as bait in the absence and presence of 2,3-DHB, respectively. Lane 5 contains proteins pulleddown by no specific interactions with the resin as it contained no bait proteins. Lane 6 and 7 contain purified EntC and EntB respectively. The red rectangle highlights the region of interest where a band in lane 1 and 2 is migrating at the same height as EntB.

3.1.10. Evidence of an EntB-EntC Protein-Protein Interaction by Crosslinking

Chemical crosslinking of proteins is a common technique to investigate protein-protein interactions (Sinz 2006). The hetero-bifunctional crosslinker sulfo-SMCC was reacted with H6-EntC and H6-EntB in separate reactions in order to create maleimide-activated forms of the proteins. Maleimide-activated H6-EntC and H6-EntB were then each mixed in a 1:1 ratio with the purified unactivated H6-EntB and H6-EntC, respectively. Mixtures were incubated for 1 h at room temperature and then run on a 10 % SDS-polyacrylamide gel, shown in Figure 31. The crosslinking reaction containing activated H6-EntC is presented on the left side of the figure. Lanes C1, C2 and C3 contain purified H6-EntC, maleimide-activated H6-EntC and the crosslinking reaction between activated H6-EntC and unactivated H6-EntB, respectively. The crosslinking reaction containing maleimide-activated H6-EntB is presented on the right side of the figure. Lanes B1, B2 and B3 contain purified H6-EntB, activated H6-EntB and the crosslinking reaction between activated H6-EntB and unactivated H6-EntC. When comparing the lanes containing the reactions with the lanes of activated protein and purified protein alone it is evident that bands appear. Using activated EntC a band appears in lane C3 at a migration distance between the 100 kDa and 75 kDa standards.

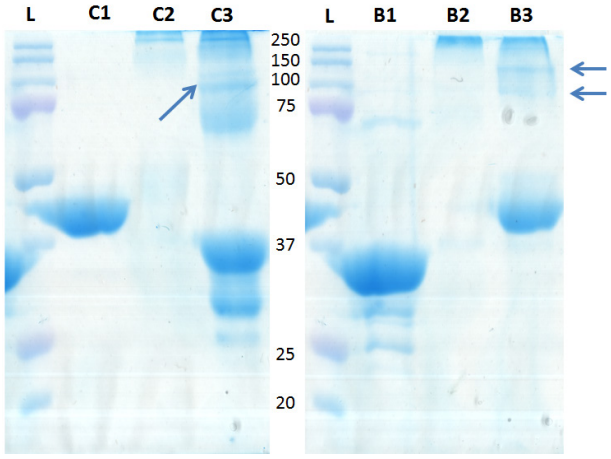

Figure 31 – 10% SDS-Polyacrylamide Gel of Sulfo-SMCC Crosslinking of EntC and EntB stained with Blue-Silver Stain. On the left of the figure is crosslinking reactions set up with maleimide-activated-EntC. The lanes contain unactivated EntC (C1), activated-EntC (C2) and a mixture of activated-EntC and unactivated EntB. On the right of the figure is crosslinking reactions set up with maleimide-activated-EntB. The lane contain unactivated EntB (C1), activated-EntB (C2) and a mixture of activated-EntB with unactivated EntC.

This band may represent crosslinking between EntC monomer (42 kDa) and one monomer subunit of EntB (32.5 kDa). In the reaction containing activated EntB a band appears at a migration position between the 150 kDa and 100 kDa standards. This band may represent crosslinking between EntB dimer (65 kDa) and two EntC monomers (84 kDa). A fainter secondary band can also be observed in Lane B3 that corresponds to the dominant band in Lane C3. Migration positions likely do not correspond to direct summations of theoretical subunit molecular weights due to maleimide activation of surface lysine residues. Although qualitative, these preliminary crosslinking experiments suggest crosslinking between EntC and EntB, supporting our pull-down data that suggest formation of a specific EntC-EntB complex *in vitro*.

3.2. Characterization of Wild-Type EntA and Variants

3.2.1. Purification of EntA WT and Variants

The wild-type *entA* gene was obtained from the ASKA collection in the form of a pCA24N-*entA* expression construct (Kitagawa et al. 2005). The EntA variants Q64A, A68Q, and Q64A/A68Q were produced previously by site-directed mutagenesis (Khalil, PhD Thesis 2010). Cells harbouring the wild-type and variant proteins were resuspended in lysis buffer as described in section 2.8.2. The clarified lysate was loaded onto IMAC Profinity resin using a BioRad DuoFlow FPLC. EntA WT and variants were eluted by a linear gradient of 20 mM imidazole to 250 mM imidazole. A representative chromatogram of EntA WT is shown in Figure 32.

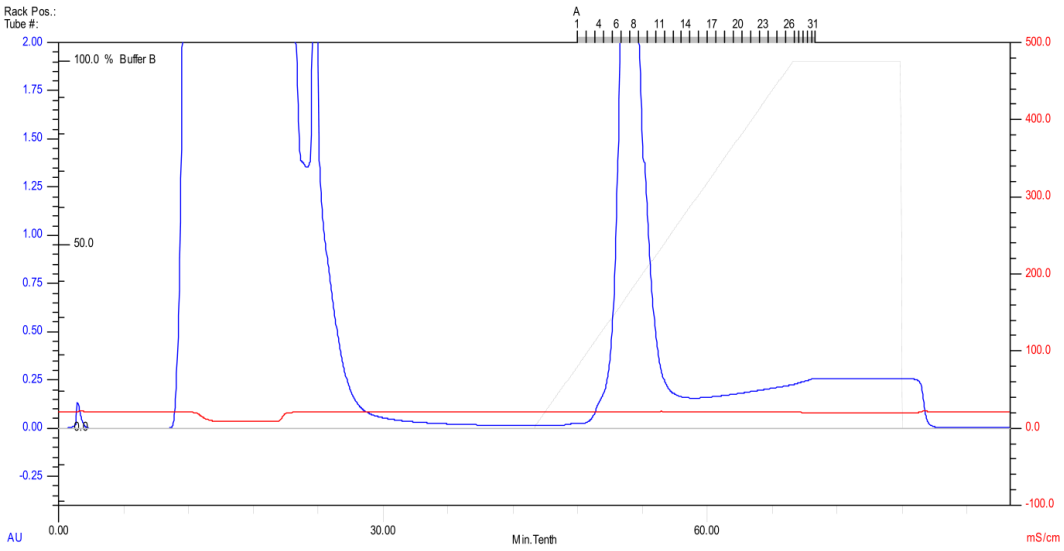

Figure 32 - Representative Chromatogram of EntA WT Purification.

The protein was collected in 2.5 mL fractions. The fractions containing H6-EntA WT or variant were pooled and dialyzed as per section 2.12 in 50 mM HEPES pH

8.0, 100 mM KCl, 0.5 mM TCEP, 15 % glycerol. The purified samples of EntA WT and variants were then separated on a 10 % SDS-polyacrylamide gel and stained with Blue Silver stain (Candiano et al. 2004). The resulting gel, Figure 33, demonstrates that the purity of EntA WT and variants is greater than 90 %.

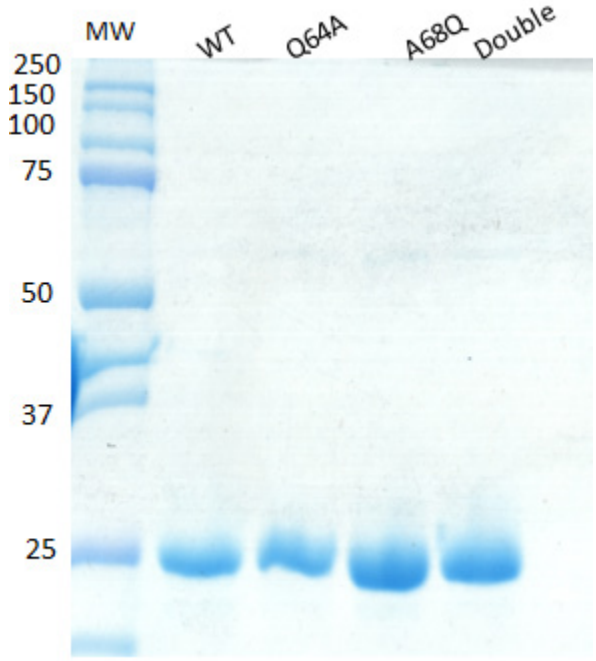

Figure 33 - SDS-Polyacrylamide Gel Demonstrating the Final Purity of EntA WT and Variants.

3.2.2. Secondary Structure Comparison of EntA WT and Variants

The secondary structure content of WT H6-EntA was compared to H6-EntA variants by collecting far-UV CD spectra of each protein in solution. The spectra of WT and variant EntA were collected between 200 and 260 nm in a 50 mM TRIS (pH 8.0 with H_2SO_4), 0.5 mM TCEP , 100 mM NaF. The far-UV CD spectra of EntA WT and

variant proteins that are presented below, Figure 34, have been corrected for buffer contribution and smoothed. The spectra show similar secondary structure content for all protein samples with typical double minima at 222 nm and 208 nm characteristic of strong α-helical content.

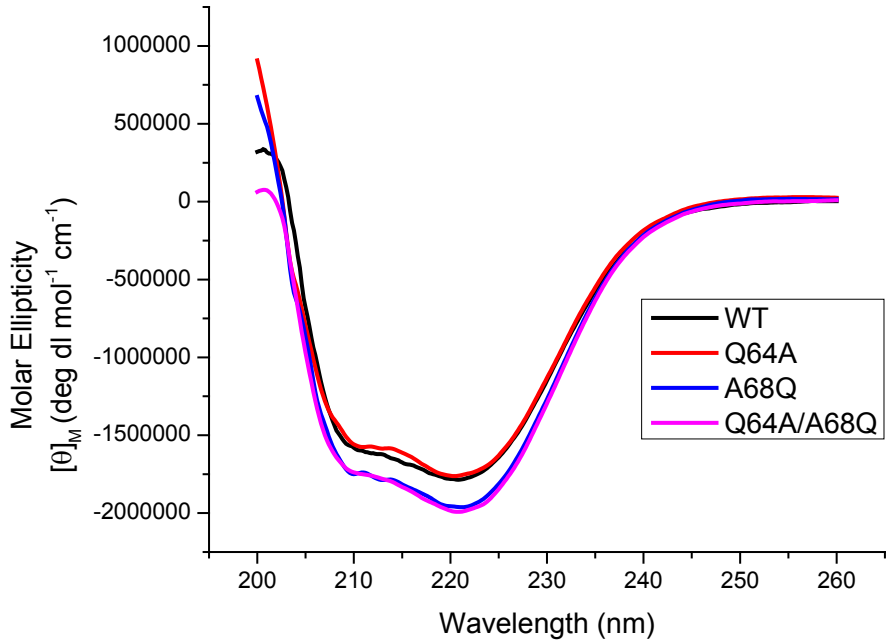

Figure 34 - Secondary Structure Analysis of EntA WT and Variants (5 μM) by Far-UV CD.

3.2.3. Comparison of Thermal Stability of EntA WT and Variants

To measure the thermal stability of EntA WT and variants the thermal denaturation of the protein samples were followed by measuring changes in molar ellipticity at 222 nm using far-UV CD spectroscopy. Ellipticity changes were followed over a temperature range of 20 ^{o}C to 65 ^{o}C. As the temperature increases the α-

helical content, followed at 222 nm, decreases. All proteins exhibited steepest transitions at approximately the same temperature.

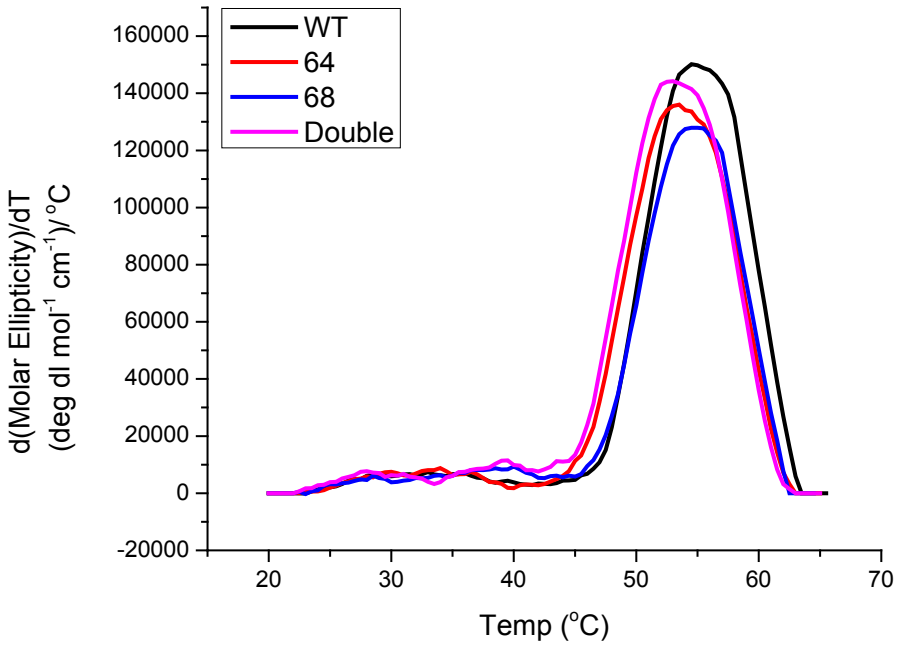

Figure 35 - First Derivative Curve of Thermal Denaturation Data of EntA WT and Variants.

To determine the melting temperature of EntA WT and variants, first derivatives of molar ellipticity changes as a function of temperature were calculated using instrument software, Figure 35. Melting temperatures were determined by peak positions of first-derivative melting curves. The melting temperatures determined by this method are found in Table 5. The original raw data were replotted as Fraction Folded vs. Temperature and presented in Figure 36.

EntA	T_m °C
WT	54.5
Q64A	53.5
A68Q	54.8
Q64A/A68Q	53.0

Table 5 – Summary of Tm Determined from the 1st Derivative Plot of Ellipticity Obtained from Thermal Denaturation Experiments.

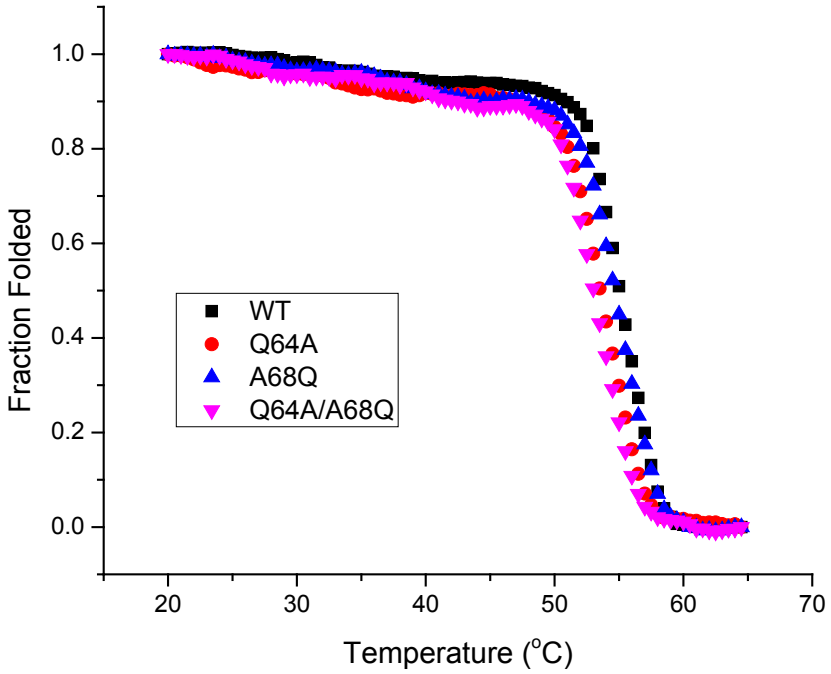

Figure 36 - Thermal Denaturation of EntA WT and Variant Presented as Fraction Folded vs. Temperature

3.2.4. Oligomeric State of EntA WT Compared to EntA Variants by AUC

To determine if site-directed mutagenesis of EntA affected quaternary structure, we employed sedimentation velocity AUC to measure oligomeric states of WT EntA and EntA variant proteins. AUC experiments were conducted at concentrations on the order of that used in our coupled enzyme assay so that we could interpret activity data in the context of protein quaternary structure. The EntA concentration used was 6 μM, since lower protein concentrations would be near the detection limit of the instrument, resulting in inaccuracies. Sedimentation velocity AUC experiments were performed on 6 μM EntA WT and variants. The raw AUC data from every 25th scan of EntA WT is shown in Figure 37.

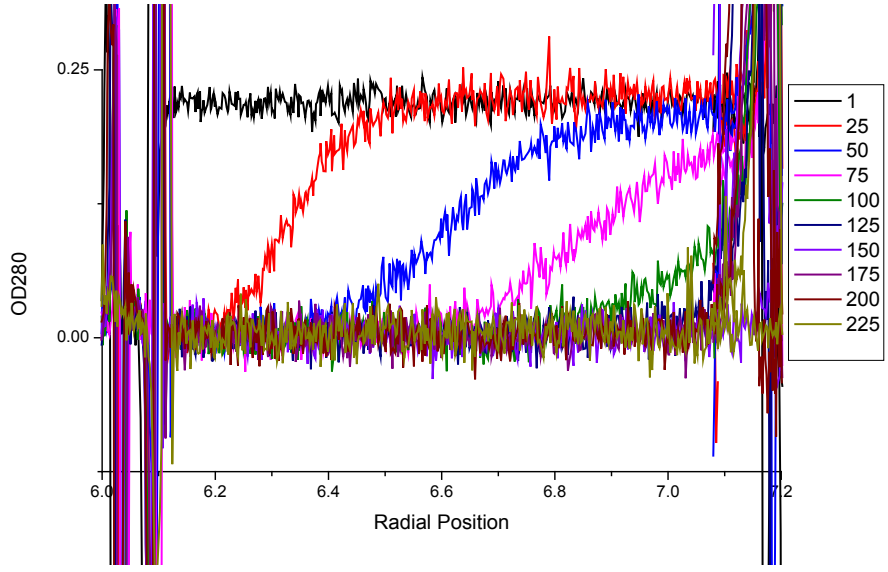

Figure 37 – Raw AUC Data of EntA WT at 6 μM. Every 25th scan is observed in this figure.

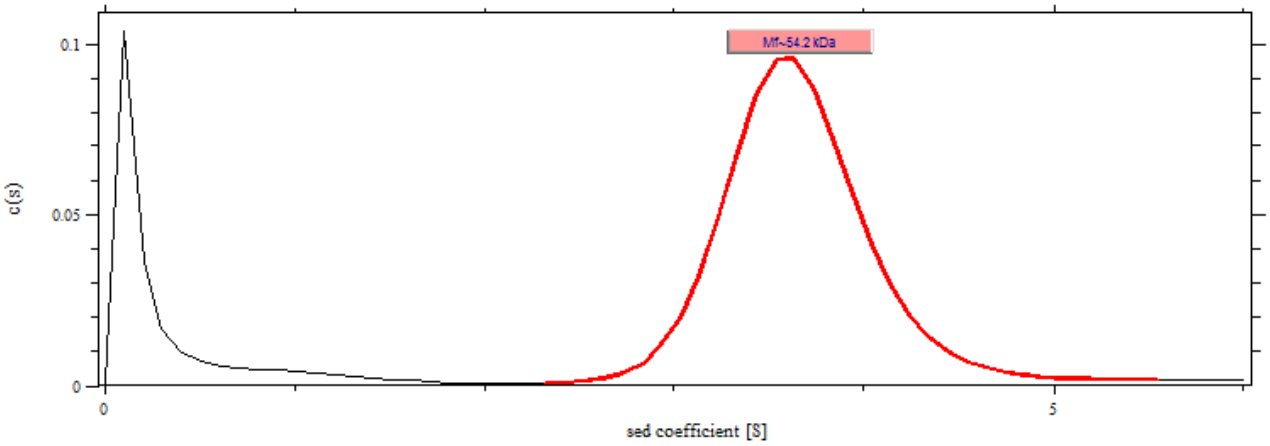

Figure 38 - c(S) Distribution of 6 µM EntA WT.

The AUC analysis was performed using SEDFIT. The raw data were fit to a c(S) continuous distribution model, and the fitted continuous distribution of the model for WT EntA is shown in Figure 38. The sedimentation coefficients, MW and quaternary structures of EntA WT and variant proteins are summarized in Table 6.

EntA	$S_{20,w}$	MW kDa	Quaternary Structure
WT	3.83	54.2	Dimer
Q64A	3.89	55.4	Dimer
A68Q	4.00	50.7	Dimer
Q64A/A68Q	3.91	55.8	Dimer

Table 6 - Summary of AUC Data of EntA WT and Variants.

3.2.5. Determination of Steady-State Kinetic Parameters of EntA WT and Variants

Using a coupled assay similar to that described for EntC in Section 2.17.1, the activity of EntA was followed by a coupled enzyme assay monitoring the production of NADH at 340 nm. The scheme of the assay is presented in Figure 39. In this instance EntA activity was coupled to the activities of EntC and EntB. The coupling enzymes were in ten-fold molar excess of EntA, at a concentration of 10 μM each. The reaction conditions used were 10 μM EntC, 10 μM EntB and 1 μM EntA, 300 μM Chorismate in 50 mM TRIS pH 7.5, 50 mM NaCl, 5 mM $MgCl_2$ with NAD^+ concentrations varying from 0 to 5 mM.

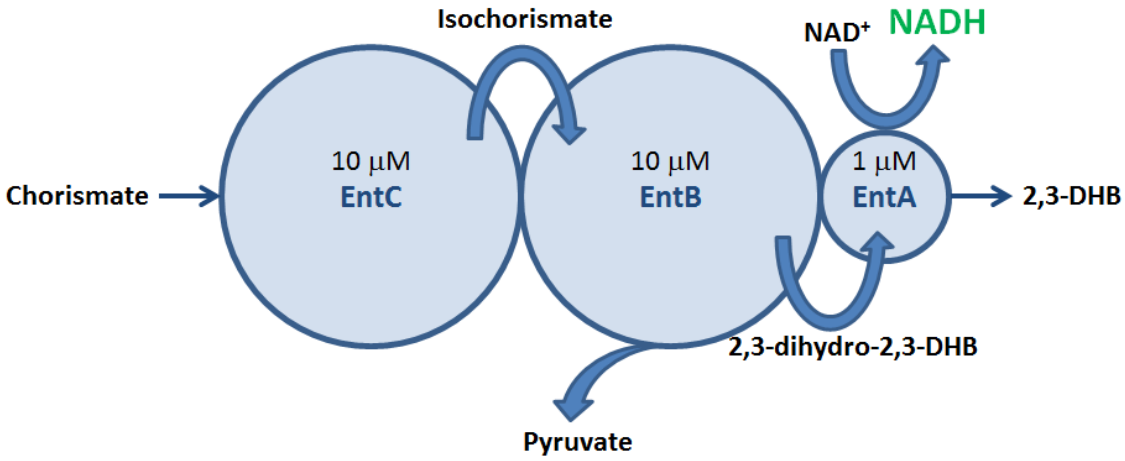

Figure 39 - Scheme of EntA Activity Assay

To validate that the coupled assay is useful for determining steady-state kinetic parameters of WT and variant EntA, it had to be demonstrated that EntA was the limiting enzyme activity being investigated. This was accomplished by measuring the rate of NADH production at three different concentrations of EntA while keeping the remaining components constant (Figure 40). The rates obtained for 0.5, 1 and 2 μM

EntA were plotted against their respective concentrations (Figure 41). We observed that the rate of NADH production responds in a linear fashion to the concentration of EntA, demonstrating that EntA is the limiting component of the assay.

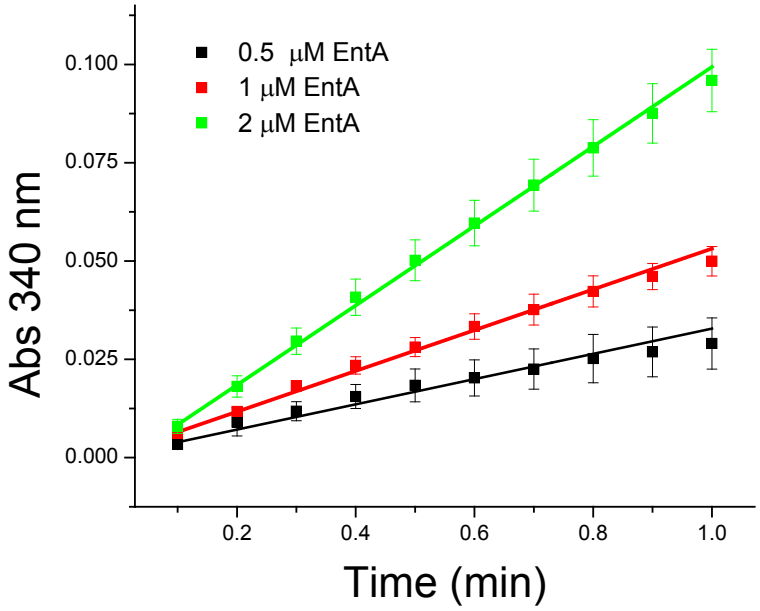

Figure 40 - Validation of EntA Assay. Rates of NADH production at three concentrations of EntA 0.5 μM (Black), 1 μM (Red) and 2 μM (Green)

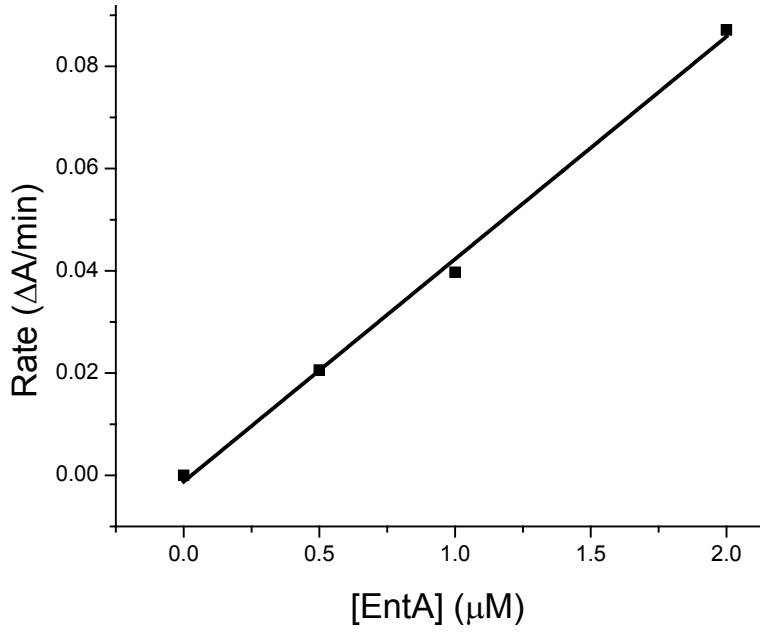

Figure 41 - Validation of EntA Activity Assay. Plot of rates determined for three concentrations of EntA vs. EntA concentration

To determine the steady-state kinetic parameters the initial rates of EntA WT and variants were measured at five concentrations of NAD^+. All rates were expressed as averaged triplicates and standard deviations were plotted as error bars. Similar to what was observed for H6-EntC in our coupled assay, initial rate data fit best to a model describing positive cooperativity (Hill Plot) using OriginPro 8.6. The resulting fit for EntA wild-type is shown in Figures 42.

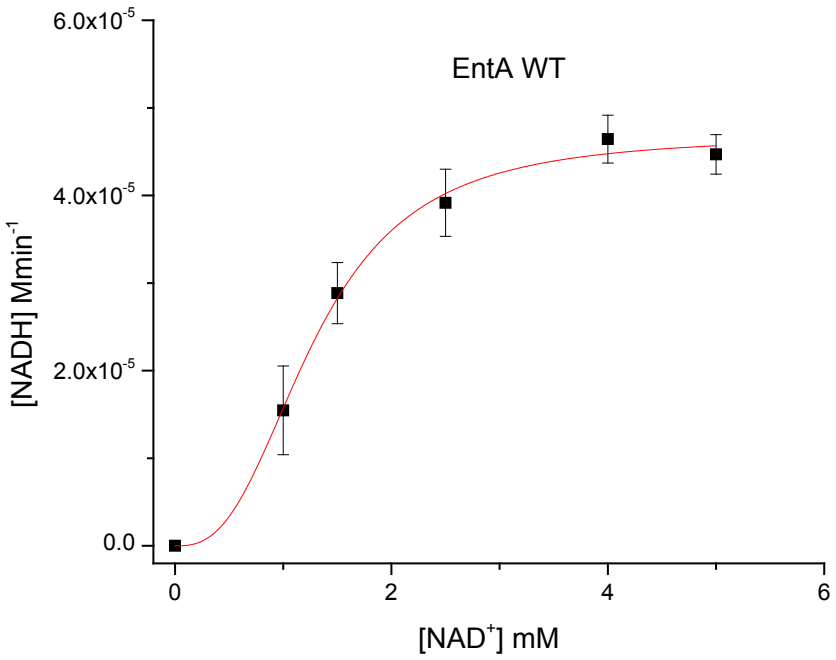

Figure 42 - Steady-State Kinetics Plot for EntA WT. Rate of NADH production vs. NAD^+ concentration

The kinetic parameters obtained are summarized in Table 7. All the K'_m and k'_{cat}/K'_m values for WT and variant EntAs are on the same order of magnitude, indicating that site-directed mutagenesis of EntA at positions 64 and 68 did not significantly affect enzyme activity.

EntA	K'_m μM	k'_{cat} s^{-1}	k'_{cat}/K'_m s^{-1} μM^{-1}
WT	1280 ± 70	0.78 ± 0.03	6.09E-04
Q64A	1090 ± 40	0.43 ± 0.01	3.98E-04
A68Q	1120 ± 40	0.45 ± 0.01	4.00E-04
Q64A/A68Q	1400 ± 140	0.62 ± 0.04	4.39E-04

Table 7 – Steady-State Kinetic Parameters Determined of EntA WT and Variants at pH 7.5 at 37 °C.

3.3. Docking Model of EntE-EntA Interaction

To study the interaction interface of the EntA-EntE complex, automated docking of the two proteins was performed using the published crystal structures of EntE (PDB code: 3RG2) and EntB (PDB code: 2FQ1) and the computer program Autodock 4. The PDB files were prepared for docking by AutoDockTools as were the grid parameter file and the docking parameter file. Parameters optimized for protein-protein docking were used according to section 2.18.

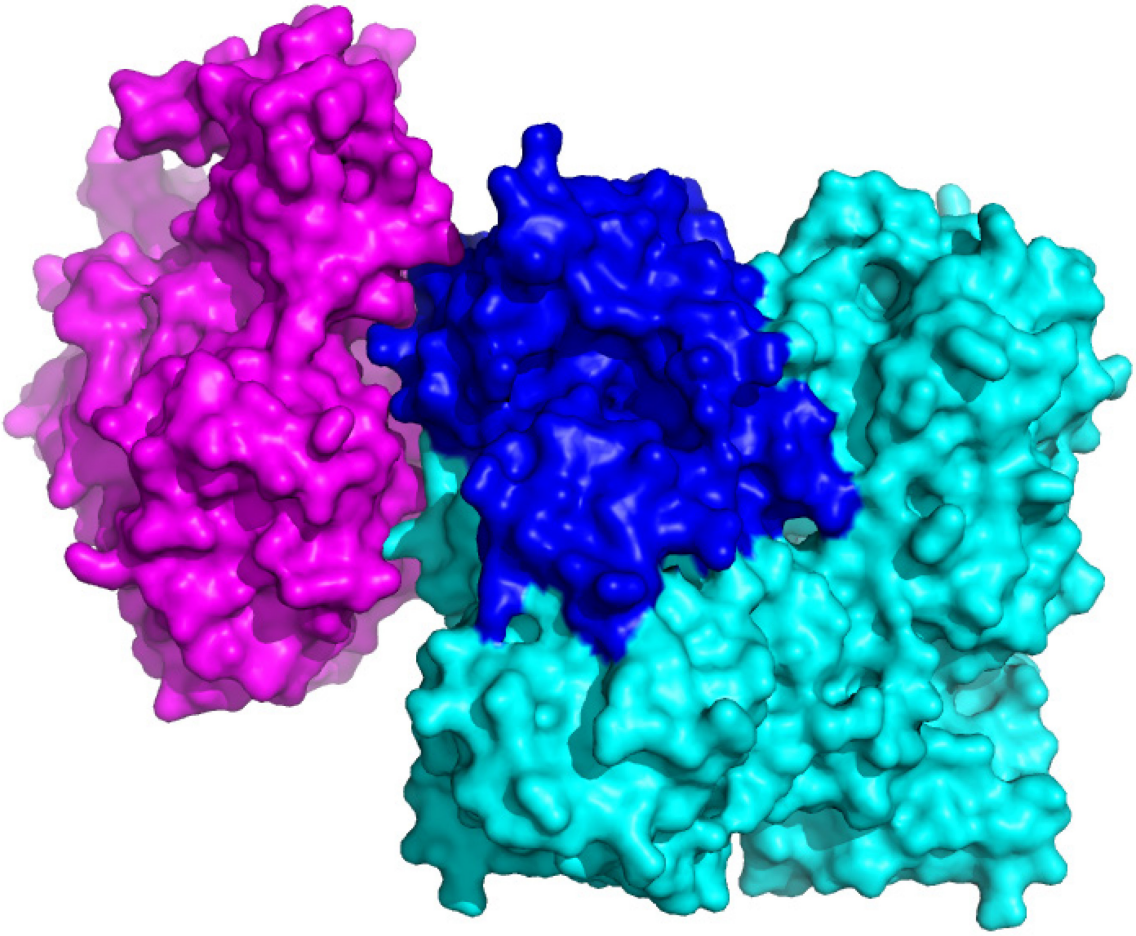

Figure 43 – A Surface Representation of the EntA (Dark Blue: Chain B, Light Blue: Chains A, C, D) Interacting with EntE (Purple). This view of the interaction shows contact not only between EntE and Chain B of EntA but also with Chain D.

The initial docking included flexible residues on the receptor (EntA). However, the structure obtained from this flexible docking was used for a second docking procedure in which all residues were rigid. The resulting docking results are presented in Figure 43. The model of the docked EntA-EntE ensemble revealed that the predicted interaction interface included the same EntE surface residues as found in the experimentally determined EntB-EntE protein interaction interface (Sundlov et al. 2012). Furthermore, the known EntB-interacting surface residues on EntE were found to be proximal to EntA helix 4 that contains Q64, the residue shown by phage display to interact with EntE (Khalil, PhD Thesis 2010). In Figure 44, the EntE protein is colored in purple with EntE residues forming polar contacts with EntA highlighted in pink and EntA residues highlighted in blue (Chain B) and light blue (Chain D). In a similar manner Figure 43 shows the EntA protein highlighted in light blue with only Chain B highlighted in dark blue. The EntE residues predicted by docking to interact with EntA are highlighted in pink as in Figure 44.

The model of the docked ensemble reveals predicted polar contacts between residues of EntE with residues of EntA of both chains B and D. EntE residue Glu 500 is predicted to form a hydrogen bond with Gln 64 of EntA, chain B. EntE residues Arg 491 and Arg 494 can form hydrogen bonds with Glu 49 and the backbone of Gln61 of EntA chain B, respectively.

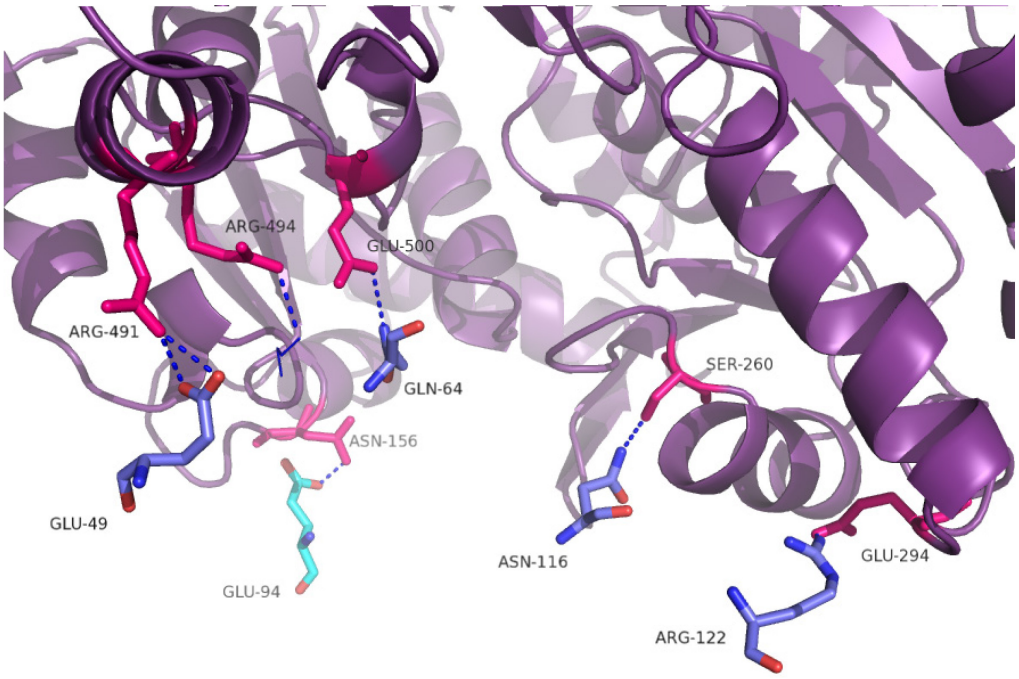

Figure 44 – Interaction Interface on EntE (Purple) that Interacts with EntA Residues (Blue)

Also, Ser 260 of EntE is predicted to form a hydrogen bond with Asn 116 of EntE, while Glu 294 of EntE can form a hydrogen bond with Arg 122 of EntA. Interestingly, Asn 156 is predicted to form a hydrogen bond with Glu 94 of EntA chain D. If the EntA-EntE interaction interface requires contacts with two discrete EntA subunits, then the oligomeric state of EntA would be important for the binding of EntE to EntA. This is consistent with experimental findings reported previously from our lab, showing that EntA affinity for EntE increases when EntA is in the tetrameric form (Khalil & Pawelek 2011).

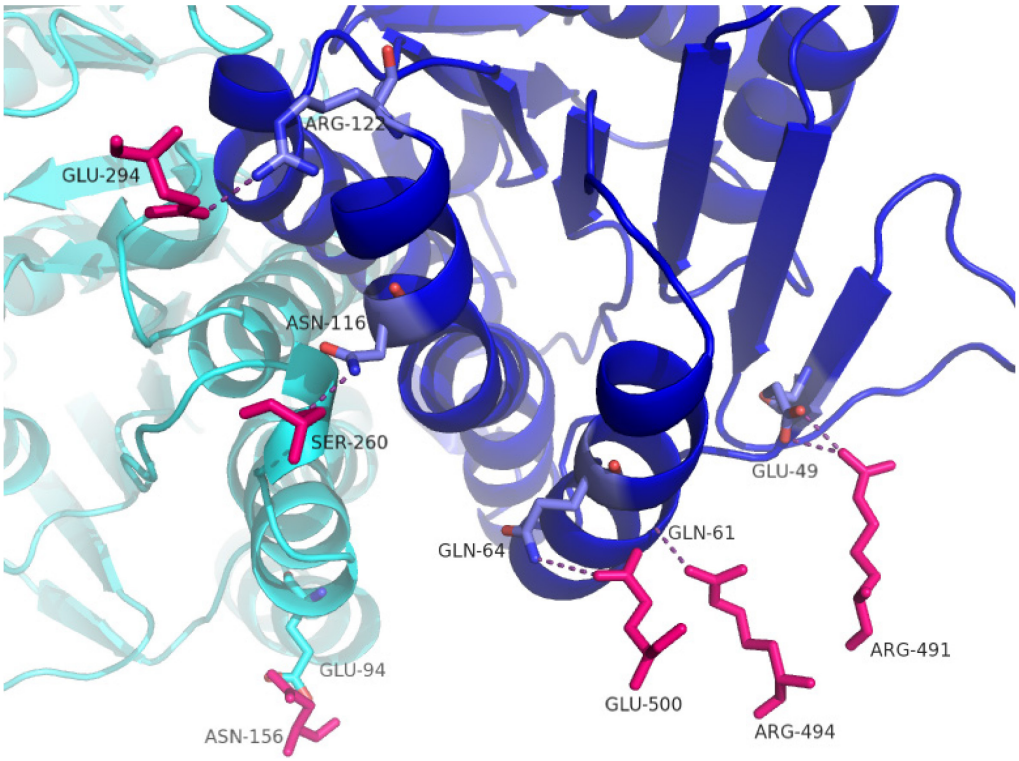

Figure 45 – Interaction Interface of EntA (both shades of blue) that Interacts with EntE Residues (Pink)

4. Discussion

4.1. Structural Characterization of EntC

Recombinant H6-EntC was purified and its solution structure analyzed using far-UV CD, near-UV CD and analytical ultracentrifugation. The secondary structure content of EntC was measured using far-UV circular dichroism. The Far-UV CD spectra collected for EntC, Figure 19, showed characteristic double minima indicative of a strong α-helical content with some β-sheet. Indeed when examining the X-ray crystal structure of EntC, there is a similar mix of α-helix and β-sheet. The binding of the cofactor Mg^{2+} to EntC was monitored by near-UV circular dichroism. Upon addition of the cofactor at saturating levels, changes in peak intensity were observed at 288 nm and 295 nm as well as 267 nm. The peaks at 288 and 295 nm correspond to changes in the local environment of one or more tryptophan chromophores. The peak at 267 nm could correspond to either tryptophan or phenylalanine (Kelly et al. 2005; Pain 2005). Upon examination of the crystal structure it appears there are no aromatic residues within a distance of 8 Å relative to the Mg^{2+} binding site. Therefore, Mg^{2+} binding may induce a conformational shift that leads to a change of environment of one or more aromatic residues. Near-UV CD is a suitable technique to detect such conformational changes since it has been shown that even a small rotation of a tryptophan residue with respect to the protein backbone can be detected by near-UV CD (Pain 2005).

The oligomeric state of EntC was examined using analytical ultracentrifugation. Although EntC had been previously reported to be monomeric, a homologue of EntC, MenF, has been reported to be a dimer (Daruwala et al. 1997). The sedimentation coefficients observed for recombinant H6-EntC in our AUC experiments confirm that it is monomeric in solution and this result is independent of its concentration. This demonstrates that our introduction of additional residues in the form of a hexahistidine tag and intervening spacer region do not result in higher-order aggregation of EntC.

4.2. EntC Binding Studies

4.2.1. Chorismate Binding to EntC

The binding affinity of chorismate to EntC was measured using isothermal titration calorimetry (ITC). ITC directly measures the heat absorbed or released during a binding event. From these measurements, one can determine the stoichiometry, enthalpy and entropy of binding as well as binding affinity. In our ITC experiment the ligand, chorismate, was titrated into the receptor, EntC, and this titration resulted in heat being released. The ITC experiment was performed in the absence of the Mg^{2+} cofactor to avoid enzyme activity in the cell as it can generate large heat changes compared to binding events. The dissociation constant K_D, a measure of how tightly a ligand is bound, was determined to be 336.7 μM for chorismate binding to EntC. When comparing this value to the reported K_m, the K_D is an order of magnitude larger. This difference is likely due to the fact that the ITC

experiment was performed in the absence of Mg^{2+}, an essential cofactor for EntC activity. Also, the K_D determined was above the concentration of EntC in the ITC cell, thus the concentration range used in the experiment was not optimal for fitting of the data to a binding model. To obtain a sigmoidal curve, the constant c (a unitless constant which is equal to the product of the binding constant, macromolecule concentration and stoichiometry) should be between 10-50. The c constant for this experiment was approximately 1. The experiment cannot be repeated with ten-fold higher concentrations of EntC because the concentration of EntC was already very high (above 300 μM). Thus, ITC can only give us an estimate that the K_D of chorismate binding to EntC in the absence of Mg^{2+} is greater than 336 μM. Near-UV CD described in the previous section demonstrated that upon Mg^{2+} addition to EntC there is a local rearrangement of aromatic residues that suggests a conformational change. This conformational change could be necessary to increase the binding affinity to chorismate. This is further supported by our EntC steady-state kinetic assay, which showed that the apparent Km for chorismate (determined in the presence of Mg^{2+}) is approximately 10-fold lower than the K_D obtained by ITC (determined in the absence of Mg^{2+}).

4.2.2. 2,3-DHB Binding to DHB Module Enzymes

To investigate the possibility of feedback inhibition regulating EntC activity fluorescence anisotropy was used to measure the binding of 2,3-DHB to the proteins of the DHB module of enterobactin biosynthesis. If a small fluorophore is free in

solution, it has essentially no fluorescence anisotropy because of its high rotational diffusion coefficient. However, if the fluorophore binds to a large macromolecule such as a protein, its rotational diffusion slows to that of the larger protein and the fluorophore will have different emission in the perpendicular and parallel orientations (Lakowicz 2006). We observed that upon addition of EntC and EntA to a solution containing 15 μM DHB there was no increase in anisotropy, demonstrating that 2,3-DHB does not bind to either of these proteins. This experiment rules out the possibility that 2,3-DHB is a feedback regulator of the first enzyme of the enterobactin biosynthetic pathway. We did find that anisotropy of 2,3-DHB increased in the presence of EntB, consistent the DHB-apo-EntB interaction that our lab previously reported (Khalil 2009). The fluorescence anisotropy data reported here provides supporting evidence that EntB, not EntC, may be a target of regulation *in vivo*. Our experimental data further support a similar conclusion made by Liu et al (1990), who suggested that EntC does not catalyze the first committed step of enterobactin biosynthesis due to its high reversibility.

4.3. EntC Activity

The activity of EntC was measured using a coupled enzyme assay. A coupled enzyme assay was necessary due to the substrate and product of EntC having very similar properties, with the difference between the two being not readily detectable by a spectroscopic or mass-detection assay. The activity of EntC was thus coupled to the activities of EntB and EntA and NAD^+ conversion to NADH by EntA was used to

monitor the progress of the assay. We determined that EntC was the limiting component of the assay because the rate of NADH production responded linearly with EntC concentration. The steady-state kinetic parameters were obtained by measuring the rate of NADH production at various concentrations of substrate chorismate. The data obtained were fit to a Hill plot since it fit best to the experimental data. Hill plots are usually reserved for enzymes who present with positive or negative cooperativity. However, EntC cannot support cooperative binding because it has been demonstrated to be monomeric by AUC (Section 4.1). Nevertheless, the AUC analysis performed was in the absence of ligands and the possibility of substrate-induced oligomerization has not been ruled out. The apparent cooperativity may not reflect an intrinsic property of the EntC-catalyzed reaction, but instead it may reflect a change in EntC activity upon formation of direct interactions with one or more of the coupled enzymes. The apparent kinetic parameters obtained from our coupled assay were found to be on the same order of magnitude of those previously reported for EntC. We therefore concluded that our purified recombinant H6-EntC retained full activity despite the presence of a hexahistidine tag.

4.4. Novel Evidence of an Interaction between EntC and EntB

To detect protein-protein interactions involving EntC, we used a pull-down assay demonstrating that immobilized H6-EntC as bait could specifically bind to a protein that co-migrates with *E. coli* EntB on an SDS-polyacrylamide gel. This band

was pull downed independently of exogenously added 2,3-DHB. This suggests that EntC can form an interaction with EntB *in vitro*, although the identity of the pulled down band will need to be confirmed by mass spectrometry. Further supporting evidence of an EntC-EntB interaction was obtained from Sulfo-SMCC crosslinking (Section 3.1.10). In both mixing activated EntC with pure EntB and vice versa, crosslinked species were observed between 75 and 150 kDa that were not observed in control reactions. Although preliminary, the evidence provided here is the first evidence of a protein-protein interaction between enzymes found within the DHB module. An EntC-EntB interaction would likely facilitate direct channeling of isochorismate to EntB, thus minimizing the possibility of back-conversion of isochorismate to chorismate by EntC.

4.5. Structural Characterization of EntA WT and Variants

In a previous study mutations were introduced to the surface of EntE at residues Q64 and A68 that were shown to interact with EntE by phage display (Khalil, PhD Thesis 2010). It was shown that *entA*-knockout cells transformed with expression constructs harbouring these EntA variants could not grow well in iron-limited medium. Although the growth phenotype was attributed to interference of the EntA-EntE protein interaction *in vivo*, it was not experimentally determined if site-directed mutagenesis of EntA at positions 64 and 68 had an effect on overall fold or enzyme function. To test this, we overexpressed and purified EntA WT and three variants Q64A, A68Q and the double mutant Q64A/A68Q and investigated

their tertiary structures in solution, as well as their enzymatic activities. Far-UV CD spectra and thermal denaturation studies indicated that the mutants Q64A, A68Q and Q64A/A68Q had similar secondary structure contents and melting temperatures. Therefore, mutations at positions 64 and 68 did not affect secondary structure content or overall fold.

EntA WT has been reported to exist in a concentration-dependent equilibrium between dimeric and tetrameric oligomeric states, and it has also been reported that the EntA-EntE interaction occurred with highest affinity when EntA was tetrameric (Khalil & Pawelek 2011). To ensure that the oligomeric state of EntA did not change upon introduction of mutations AUC was used to examine the sedimentation coefficient of WT EntA and variant proteins. The sedimentation coefficients of EntA WT and variants were determined at 6 μM, a concentration similar to that used in our steady-state enzyme activity assays. The $S_{20,w}$ of EntA WT and variants were all found to be similar and the MW values estimated by AUC all correspond to a dimeric oligomeric state. Thus, the mutations at positions 64 and 68 did not alter quaternary structure. The previously reported growth phenotype was therefore not likely due to improper assembly of the EntA variant proteins in the *E. coli* cytoplasm.

4.6. Enzyme Activity of EntA WT and Variants

The activity of EntA WT and variants were compared using a coupled enzyme assay to determine steady-state kinetic parameters. A coupled enzyme assay was used because the substrate of EntA (2,3-dihydro-2,3-dihydroxybenzoate) is not commercially available. The activity of EntA was coupled to the activities of EntB and EntC which will produce 2,3-dihydro-2,3-dihydroxybenzoate from chorismate. Similar to what we observed in our EntC assay, the data obtained for EntA activity best fit to a Hill plot. As with EntC, we currently have insufficient evidence to conclude that positive cooperativity is an intrinsic property of EntA catalysis. Further experiments will need to be performed to investigate this. Regardless, the steady-state kinetic parameters determined for EntA Q64A, A68Q and Q64A/A68Q were all similar those of WT EntA. Therefore, the previously reported growth phenotypes were not due to differences in enzymatic activity between EntA variant proteins and WT EntA.

Taking all of our data together, we can conclude that the growth phenotype was most likely due to a direct disruption of the EntA-EntE protein interaction caused by mutation of key EntA surface residues. Now that we know that the EntA-EntE interaction is necessary for efficient enterobactin biosynthesis *in vivo*, we can proceed with the design of small-molecule inhibitors targeting this interaction. Such an approach would be valuable in the eventual production of antibiotics to specifically target siderophore biosynthesis in pathogens, rendering them bacteriostatic in low-iron environments such as human serum.

4.7. Modelling of the EntA-EntE Complex

To study the protein interaction interface involved in the EntA-EntE interaction, a model of the interaction was generated using automated docking. The model of the EntA-EntE interaction was produced using AutoDock 4.2, with EntA (2FWM) and EntE from the chimeric EntE-EntB complex (3RG2). In the paper reporting the EntE-EntB crystal structure the authors propose a large conformational change that rotates the EntE C-terminal domain 140^{o} (J. A. Sundlov et al. 2012). The authors suggest EntE can adopt an adenylate-forming state as well as a thioesterase-forming state. The EntE found in the EntE-EntB crystal structure was concluded to be in the thioesterase-forming conformation. The authors hypothesize that a conformational change exists in EntE based on what was observed for Acetyl-CoA Synthetase (ACS). ACS was crystallized in two conformations depending on what substrate was bound, adenosine-5'-propylphosphate (adenylate-forming state) or CoA (thioesterase-forming state) (Gulick et al. 2003). However, a homologue to EntE, DhbE of *Bacillus Subtilis*, which has a higher sequence identity to EntE than ACS, was crystallized in the presence of no substrate, 2,3-DHB-AMP and 2,3-DHB and AMP. The crystal structures of these complexes (PDB codes: 1mdf, 1md8 and 1md9) revealed small local rearrangements, but not a large conformational change such as the 140^{o} C-terminal domain rotation proposed for EntE. Since no crystal structure exists for EntE in different substrate-bound states, direct experimental evidence of domain alteration in EntE remains to be reported. Techniques that could reveal such a large conformational change such as near-UV CD, fluorescence and limited

proteolysis have not yet been used to characterize EntE in the presence and absence of substrate. Moreover, both EntA and EntB binding to EntE quench the 2,3-DHB-EntE FRET signal possibly indicating that the EntA and EntB binding site on EntE overlaps (Khalil & Pawelek 2009; Khalil & Pawelek 2011). Such an overlap of interaction surfaces would not be likely if EntE underwent large conformational changes when forming discrete complexes with the two proteins.

The results of our docking EntE in the so-called thioesterase-forming state to tetrameric EntA revealed a binding interface between EntA and EntE that shares key residues on EntE that have been previously reported as being involved in EntE binding to EntB. Most intriguing however is the fact that the key residue on EntE that interacts with EntB, EntE E500, interacts with EntA Q64, which our lab has previously identified by phage display to interact with EntE. The docking model also identifies a predicted hydrogen bond pair between a surface residue on EntE Asn156 and residue Glu194 on the second chain of EntA, chain D. That the interaction between EntE and EntA is predicted to be dependent on contact between two EntA chains is consistent with a previous study showing that the EntA oligomeric state determines the affinity of the EntA-EntE interaction. The docking of EntE to EntA is extremely promising because its reveals a protein-protein interaction interface between the helix 4 of EntA and the EntB-interacting surface of EntE. This suggests that EntA and EntB share the same interaction surface on EntE, which is logical given that both partners would require access to the EntE active site for substrate

channeling. The model of the EntA-EntE complex reported here could be the basis of mutagenesis studies to probe EntE surface residues that interact with EntA.

5. Summary and Future Work

The first of the two major goals of this study was to express and purify EntC and to identify possible protein-protein interactions that occur in the DHB module. The second major goal was to express and purify EntA WT and EntA variants at positions 64 and 68 in order to confirm that mutations at these positions interfere with the EntA-EntE interaction and do not affect overall fold or enzymatic activity.

EntC was purified to near homogeneity and characterized using far-UV CD, near-UV CD and AUC. The kinetic parameters of EntC were determined, and they agreed with previously reported values. AUC needs to be repeated in the presence and absence of ligands to rule out ligand-induced oligomerization. A pull-down assay was then used to identify a preliminary interaction between EntC and EntB. This pull-down assay will need to be repeated and the bands corresponding to what appears to be EntB must be analyzed by mass spectrometry. A crosslinking experiment was performed using the hetero-bifunctional crosslinker sulfo-SMCC and EntC and EntB. Our results indicate that complexes are being formed between the EntB dimer and one or two subunits of EntC. The crosslinking experiments will need to be refined in order to obtain more clearly defined crosslinked species. These species could then be recovered from a gel and identities confirmed by mass spectrometry. In addition, cleavable crosslinkers such as Sulfosuccinimidyl 6-[3'-(2-pyridyldithio)propionamido]hexanoate (Sulfo-LC-SPDP) (Pierce) or 4-

Succinimidyloxycarbonyl-alpha-methyl-alpha(2-pyridyldithio)toluene (SMPT) (Pierce), with similar reactivity to Sulfo-SMCC, can be used to crosslink EntC and EntB. Crosslinked products could then be recovered and chemically reduced prior to peptide mass fingerprinting. On peptides where a crosslinked product was formed there would be a shift in mass associated with the size of the crosslinker. There are also a number of assays that can be used to probe the EntB-EntC interaction *in vivo*. The bacterial two-hybrid assay, for example, could be used to demonstrate an interaction between EntC and EntB fused to respective reporter enzyme activities. Interaction *in vivo* would result in the production of a chromophore in cells grown on appropriate agar-media plates.

The EntA WT and variants were characterized by far-UV CD, thermal denaturation and AUC. All the biophysical results indicate that the mutations to the surface of EntA had no effect on the overall properties of EntA. The enzyme steady-state kinetic parameters were determined for WT and variants and all values were found to be on the same order of magnitude. The observed cooperativity could be studied using ITC to determine if two NAD^+ binding sites exist on EntA with different binding affinities. These results indicate that the mutations do not disturb the integrity of the enzyme but rather the poor growth observed in the growth phenotype assay is mostly likely due to the disruption of the protein-protein interaction between EntE and EntA. A similar approach can be used to probe EntE variants in which EntA-interacting residues on the surface of EntE have been

substituted. Taken together, this rigorous approach would confirm that disruption of the EntA-EntE interaction by mutagenesis was not due to confounding artifacts such as protein misfolding.

In order to identify such EntA-interacting residues on the surface of EntE, we generated a model of the protein-protein interaction between EntE and EntA using AutoDock 4.2. The protein-protein interaction interface of the modeled interaction demonstrated a common interface on EntE for EntA and EntB binding. As discussed above, this model needs to be confirmed by mutagenesis studies on the surface of EntE that disrupt the EntA-EntE interaction. The aforementioned bacterial-two-hybrid could be used to detect the protein-protein interaction between EntE and EntB as well as between EntE and EntA. This system would be ideal to test the residues on EntE that disrupt the proposed common interaction interface for EntB and EntA.

Also, the domain alteration of EntE proposed by Drake and colleagues and later Sundlov and colleagues could be experimentally tested by a number of methods. A limited proteolysis experiment can be performed on EntE in the presence of various substrates and the cleavage pattern can be analyzed. If the cleavage pattern of EntE in the presence of various substrates is identical to each other then it is likely that no conformational alteration exists. Alternatively, different cleavage patterns would confirm substrate-dependent domain alternation in solution. Furthermore, near-UV CD difference spectroscopy could be used to

measure changes in the local environment of protein chromophores in the presence and absence of EntE ligands.

6. References

Abergel, R.J. et al., 2009. Enzymatic hydrolysis of trilactone siderophores: where chiral recognition occurs in enterobactin and bacillibactin iron transport. *Journal of the American Chemical Society*, 131(35), pp.12682–92.

Abergel, R.J. et al., 2006. Microbial evasion of the immune system: structural modifications of enterobactin impair siderocalin recognition. *Journal of the American Chemical Society*, 128(34), pp.10998–9.

Abergel, R.J. et al., 2008. The siderocalin/enterobactin interaction: a link between mammalian immunity and bacterial iron transport. *Journal of the American Chemical Society*, 130(34), pp.11524–34.

An, S. et al., 2010. Reversible Compartmentalization of de Novo Purine Biosynthetic Complexes in Living Cells. *Science*, 103(2008).

Atkin, C.L. et al., 1973. Iron and Free Radical in Ribonucleotide Reductase. EXCHANGE OF IRON AND MOSSBAUER SPECTROSCOPY OF THE PROTEIN B2 SUBUNIT OF THE ESCHERICHIA COLI ENZYME. *J. Biol. Chem.*, 248(21), pp.7464–7472.

Bagg, A. & Neilands, J B, 1987. Molecular mechanism of regulation of siderophore-mediated iron assimilation. *Microbiological reviews*, 51(4), pp.509–18.

Balbo, A. & Schuck, Peter, 2005. Analytical Ultracentrifugation in the Study of Protein Self- association and Heterogeneous Protein-Protein Interactions. In E. Golemis & P. D. Adams, eds. *Protein-Protein Interactions: A Molecular Cloning Manual*. Cold Spring Harbor.

Ballouche, M., Cornelis, P. & Baysse, C., 2009. Iron metabolism: a promising target for antibacterial strategies. *Recent patents on anti-infective drug discovery*, 4(3), pp.190–205.

Bleuel, C. et al., 2005. TolC Is Involved in Enterobactin Efflux across the Outer Membrane of Escherichia coli. *Society*, 187(19), pp.6701–6707.

Bäumler, A.J. et al., 1996. Identification of a new iron regulated locus of Salmonella typhi. *Gene*, 183(1-2), pp.207–213.

Candiano, G. et al., 2004. Blue silver: a very sensitive colloidal Coomassie G-250 staining for proteome analysis. *Electrophoresis*, 25(9), pp.1327–1333.

Cartron, M.L. et al., 2006. Feo--transport of ferrous iron into bacteria. *Biometals : an international journal on the role of metal ions in biology, biochemistry, and medicine*, 19(2), pp.143–57.

Caza, M., Lépine, F. & Dozois, C.M., 2011. Secretion, but not overall synthesis, of catecholate siderophores contributes to virulence of extraintestinal pathogenic Escherichia coli. *Molecular microbiology*, 80(1), pp.266–82.

Chenault, S.S. & Earhart, C. F., 1992. Identification of hydrophobic proteins FepD and FepG of the Escherichia coli ferrienterobactin permease. *Journal of General Microbiology*, 138(10), pp.2167–2171.

Crosa, J.H., Mey, A.R. & Payne, S.M., 2004. *Iron transport in bacteria*, ASM Press.

Daar, S. & Pathare, A.V., 2006. Combined therapy with desferrioxamine and deferiprone in beta thalassemia major patients with transfusion iron overload. *Annals of Hematology*, 85(5), p.315.

Dahm, C. et al., 1998. The role of isochorismate hydroxymutase genes entC and menF in enterobactin and menaquinone biosynthesis in Escherichia coli. *Biochimica et biophysica acta*, 1425(2), pp.377–86.

Daruwala, R. et al., 1997. Menaquinone (vitamin K2) biosynthesis: overexpression, purification, and characterization of a new isochorismate synthase from Escherichia coli. *Journal of bacteriology*, 179(10), pp.3133–8.

Dean, D.R., Bolin, J.T. & Zheng, L., 1993. Nitrogenase metalloclusters: structures, organization, and synthesis. *Journal of bacteriology*, 175(21), pp.6737–44.

Drake, E.J., Nicolai, D.A. & Gulick, A.M., 2006. Structure of the EntB multidomain nonribosomal peptide synthetase and functional analysis of its interaction with the EntE adenylation domain. *Chemistry & biology*, 13(4), pp.409–19.

Earhart, Charles F, 2004. Iron Uptake Via the Enterobactin System. In J. H. Crosa, A. R. Mey, & S. M. Payne, eds. *Iron Transport in Bacteria*. ASM Press.

Fischbach, M. a et al., 2006. How pathogenic bacteria evade mammalian sabotage in the battle for iron. *Nature chemical biology*, 2(3), pp.132–8.

Fontecave, M., Covs, J. & Pierre, J., 1994. Ferric reductases or flavin reductases ? , 71994, pp.3–8.

French, G.L., 2010. The continuing crisis in antibiotic resistance. *International journal of antimicrobial agents*, 36 Suppl 3, pp.S3–7.

Furrer, J.L. et al., 2002. Export of the siderophore enterobactin in Escherichia coli: involvement of a 43 kDa membrane exporter. *Molecular Microbiology*, 44(5), pp.1225–1234.

Garénaux, A., Caza, M. & Dozois, C.M., 2011. The Ins and Outs of siderophore mediated iron uptake by extra-intestinal pathogenic Escherichia coli. *Veterinary microbiology*, 153(1-2), pp.89–98.

Gehring, a M. et al., 1998. Iron acquisition in plague: modular logic in enzymatic biogenesis of yersiniabactin by Yersinia pestis. *Chemistry & biology*, 5(10), pp.573–86.

Gehring, A.M., Bradley, K. a & Walsh, C T, 1997. Enterobactin biosynthesis in Escherichia coli: isochorismate lyase (EntB) is a bifunctional enzyme that is phosphopantetheinylated by EntD and then acylated by EntE using ATP and 2,3-dihydroxybenzoate. *Biochemistry*, 36(28), pp.8495–503.

Gulick, A.M., 2009. Conformational dynamics in the Acyl-CoA synthetases, adenylation domains of non-ribosomal peptide synthetases, and firefly luciferase. *ACS chemical biology*, 4(10), pp.811–27.

Gulick, A.M. et al., 2003. The 1.75 A crystal structure of acetyl-CoA synthetase bound to adenosine-5'-propylphosphate and coenzyme A. *Biochemistry*, 42(10), pp.2866–73.

Harris, W.R. et al., 1979. Coordination chemistry of microbial iron transport compounds. 19. Stability constants and electrochemical behavior of ferric enterobactin and model complexes. *Journal of the American Chemical Society*, 101(20), pp.6097–6104.

Hayes, D. B., Laue, T., and Philo, J.S., 1995. *Sednterp: Sedimentation Interpretation Program*, Thousand Oaks, CA: Alliance Protein Laboratories.

Izadi-Pruneyre, N. et al., 2006. The heme transfer from the soluble HasA hemophore to its membrane-bound receptor HasR is driven by protein-protein interaction from a high to a lower affinity binding site. *The Journal of biological chemistry*, 281(35), pp.25541–50.

Katz, A.R. et al., 2012. Neisseria gonorrhoeae with high-level resistance to azithromycin: case report of the first isolate identified in the United States. *Clinical infectious diseases : an official publication of the Infectious Diseases Society of America*, 54(6), pp.841–3.

Kelly, S.M., Jess, T.J. & Price, N.C., 2005. How to study proteins by circular dichroism. *Biochimica et biophysica acta*, 1751(2), pp.119–39.

Kerbarh, O. et al., 2005. Salicylate biosynthesis: overexpression, purification, and characterization of Irp9, a bifunctional salicylate synthase from Yersinia enterocolitica. *Journal of bacteriology*, 187(15), pp.5061–6.

Khalil, S., 2010. *Studies of the Protein Interaction Network Required for Enterobactin Biosynthesis in Escherichia coli*. Concordia University.

Khalil, S. & Pawelek, P.D., 2011. Enzymatic adenylation of 2,3-dihydroxybenzoate is enhanced by a protein-protein interaction between Escherichia coli 2,3-dihydro-2,3-dihydroxybenzoate dehydrogenase (EntA) and 2,3-dihydroxybenzoate-AMP ligase (EntE). *Biochemistry*, 50(4), pp.533–45.

Khalil, S. & Pawelek, P.D., 2009. Ligand-Induced Conformational Rearrangements Promote Interaction between the Escherichia coli Enterobactin Biosynthetic Proteins EntE and EntB. *Journal of Molecular Biology*, 393(3), pp.658–671.

Kiley, P.J. & Beinert, H., 2003. The role of Fe–S proteins in sensing and regulation in bacteria. *Current Opinion in Microbiology*, 6(2), pp.181–185.

Kitagawa, M. et al., 2005. Complete set of ORF clones of Escherichia coli ASKA library (a complete set of E. coli K-12 ORF archive): unique resources for biological research. *DNA research : an international journal for rapid publication of reports on genes and genomes*, 12(5), pp.291–9.

Kozlowski, M.C. et al., 1995. Chorismate-utilizing enzymes isochorismate synthase, anthranilate synthase, and p-aminobenzoate synthase: mechanistic insight through inhibitor design. *Journal of the American Chemical Society*, 117(8), pp.2128–2140.

Lai, J.R. et al., 2006. A protein interaction surface in nonribosomal peptide synthesis mapped by combinatorial mutagenesis and selection. *Proceedings of the National Academy of Sciences of the United States of America*, 103(14), pp.5314–9.

Lakowicz, J.R., 2006. *Principles of Fluorescence Spectroscopy* 3rd editio., Springer New York.

Leduc, D., Bouveret, E. & Battesti, A., 2007. The hotdog thioesterase EntH (YbdB) plays a role in vivo in optimal enterobactin biosynthesis by interacting with the ArCP domain of EntB. *Journal of bacteriology*, 189(19), pp.7112–26.

Lin, H. et al., 2005. In vitro characterization of salmochelin and enterobactin trilactone hydrolases IroD, IroE, and Fes. *Journal of the American Chemical Society*, 127(31), pp.11075–11084.

Liu, J et al., 1990. Overexpression, purification, and characterization of isochorismate synthase (EntC), the first enzyme involved in the biosynthesis of enterobactin from chorismate. *Biochemistry*, 29(6), pp.1417–25.

López-Goñi, I., Moriyón, I. & Neilands, J B, 1992a. Identification of 2,3-dihydroxybenzoic acid as a Brucella abortus siderophore. *Infection and immunity*, 60(11), pp.4496–503.

López-Goñi, I., Moriyón, I. & Neilands, J B, 1992b. Identification of 2,3-dihydroxybenzoic acid as a Brucella abortus siderophore. *Infection and immunity*, 60(11), pp.4496–503.

May, J.J. et al., 2002. Crystal structure of DhbE, an archetype for aryl acid activating domains of modular nonribosomal peptide synthetases. *Proceedings of the National Academy of Sciences of the United States of America*, 99(19), pp.12120–5.

Meiwes, J., 1990. Isolation and characterization of staphyloferrin A, a compound with siderophore activity from Staphylococcus hyicus DSM 20459. *FEMS Microbiology Letters*, 67(1-2), pp.201–205.

Meyer, F.M. et al., 2011. Physical interactions between tricarboxylic acid cycle enzymes in Bacillus subtilis: evidence for a metabolon. *Metabolic engineering*, 13(1), pp.18–27.

Miethke, M., Hou, J. & Marahiel, M.A., 2011. The siderophore-interacting protein YqjH acts as a ferric reductase in different iron assimilation pathways of Escherichia coli. *Biochemistry*, 50(50), pp.10951–64.

Miethke, M. & Marahiel, M.A., 2007. Siderophore-based iron acquisition and pathogen control. *Microbiology and molecular biology reviews : MMBR*, 71(3), pp.413–51.

Miller, R.E. & Stadtman, E.R., 1972. Glutamate synthase from Escherichia coli. An iron-sulfide flavoprotein. *The Journal of biological chemistry*, 247(22), pp.7407–19.

Moore, C.H. et al., 1995. Identification of alcaligin as the siderophore produced by Bordetella pertussis and B . bronchiseptica . Identification of Alcaligin as the Siderophore Produced by Bordetella pertussis and B . bronchiseptica. , 177(4).

Morris, G.M. et al., 2010. AutoDock Version 4.2. , pp.1–49.

NEB, 2012. Transformation Protocol. Available at: http://www.neb.com/nebecomm/products/protocol3.asp [Accessed July 17, 2012].

Noinaj, N. et al., 2012. Structural basis for iron piracy by pathogenic Neisseria. *Nature*.

Noto, J.M. & Cornelissen, C.N., 2008. Identification of TbpA residues required for transferrin-iron utilization by Neisseria gonorrhoeae. *Infection and immunity*, 76(5), pp.1960–9.

O'Brien, I.G. & Gibson, F., 1970. The structure of enterochelin and related 2,3-dihydroxy-N-benzoyne conjugates from Eschericha Coli. *Biochimica et Biophysica Acta (BBA) - General Subjects*, 215(2), pp.393–402.

Pain, R., 2005. Determining the CD spectrum of a protein. *Current protocols in protein science editorial board John E Coligan et al*, Chapter 7(Cd), p.Unit 7.6.

Pollack, J.R. & Neilands, J.B., 1970. Enterobactin, an iron transport compound from. *Biochemical and Biophysical Research Communications*, 38(5), pp.989–992.

Quadri, L.E. et al., 1998. Identification of a Mycobacterium tuberculosis gene cluster encoding the biosynthetic enzymes for assembly of the virulence-conferring siderophore mycobactin. *Chemistry & biology*, 5(11), pp.631–45.

Raymond, K.N., Dertz, E. a & Kim, S.S., 2003. Enterobactin: an archetype for microbial iron transport. *Proceedings of the National Academy of Sciences of the United States of America*, 100(7), pp.3584–8.

Rusnak, F, Faraci, W.S. & Walsh, C T, 1989. Subcloning, expression, and purification of the enterobactin biosynthetic enzyme 2,3-dihydroxybenzoate-AMP ligase: demonstration of enzyme-bound (2,3-dihydroxybenzoyl)adenylate product. *Biochemistry*, 28(17), pp.6827–35.

Sambrook, J. & Russel, D.W., 2001. *Molecular Cloning: A Laboratory Manual* 3rd ed., Cold Spring Harbor, N.Y.: Cold Spring Harbor Laboratory Press.

Sandy, M. & Butler, A., 2009. Microbial iron acquisition: marine and terrestrial siderophores. *Chemical reviews*, 109(10), pp.4580–95.

Sanner, M.F., 1999. Python: A Programming Language for Software Integration and Development. *J. Mol. Graphics Mod.*, 17, pp.57–61.

Schrodinger LLC, 2010. The PyMOL Molecular Graphics System, Version 1.3r1.

Schuck, P, 2000. Size-distribution analysis of macromolecules by sedimentation velocity ultracentrifugation and lamm equation modeling. *Biophysical Journal*, 78(3), pp.1606–1619.

Sinz, A., 2006. Chemical cross-linking and mass spectrometry to map three-dimensional protein structures and protein-protein interactions. *Mass spectrometry reviews*, 25(4), pp.663–82.

Sridharan, S. et al., 2010. Crystal structure of Escherichia coli enterobactin-specific isochorismate synthase (EntC) bound to its reaction product isochorismate: implications for the enzyme mechanism and differential activity of chorismate-utilizing enzymes. *Journal of molecular biology*, 397(1), pp.290–300.

Studier, F.W., 2006. NIH Public Access. , 41(1), pp.207–234.

Sundlov, J. a et al., 2006. Determination of the crystal structure of EntA, a 2,3-dihydro-2,3-dihydroxybenzoic acid dehydrogenase from Escherichia coli. *Acta crystallographica. Section D, Biological crystallography*, 62(Pt 7), pp.734–40.

Sundlov, J.A. et al., 2012. Structural and Functional Investigation of the Intermolecular Interaction between NRPS Adenylation and Carrier Protein Domains. *Chemistry & biology*, 19(2), pp.188–98.

Touati, D., 2000. Iron and Oxidative Stress in Bacteria 1. *Archives of biochemistry and biophysics*, 373(1), pp.1–6.

Walsh, C. et al., 1990. Molecular studies on enzymes in chorismate metabolism and the enterobactin biosynthetic pathway. *Chemical Reviews*, 90(7), pp.1105–1129.

Williamson, M.P. & Sutcliffe, M.J., 2010. Protein-protein interactions. *Biochemical Society transactions*, 38(4), pp.875–8.

Zhu, M. et al., 2005. Functions of the siderophore esterases IroD and IroE in iron-salmochelin utilization. *Microbiology (Reading, England)*, 151(Pt 7), pp.2363–72.

Abergel, R.J. et al., 2009. Enzymatic hydrolysis of trilactone siderophores: where chiral recognition occurs in enterobactin and bacillibactin iron transport. *Journal of the American Chemical Society*, 131(35), pp.12682–92.

Abergel, R.J. et al., 2006. Microbial evasion of the immune system: structural modifications of enterobactin impair siderocalin recognition. *Journal of the American Chemical Society*, 128(34), pp.10998–9.

Abergel, R.J. et al., 2008. The siderocalin/enterobactin interaction: a link between mammalian immunity and bacterial iron transport. *Journal of the American Chemical Society*, 130(34), pp.11524–34.

An, S. et al., 2010. Reversible Compartmentalization of de Novo Purine Biosynthetic Complexes in Living Cells. *Science*, 103(2008).

Atkin, C.L. et al., 1973. Iron and Free Radical in Ribonucleotide Reductase. EXCHANGE OF IRON AND MOSSBAUER SPECTROSCOPY OF THE PROTEIN B2 SUBUNIT OF THE ESCHERICHIA COLI ENZYME. *J. Biol. Chem.*, 248(21), pp.7464–7472.

Bagg, A. & Neilands, J B, 1987. Molecular mechanism of regulation of siderophore-mediated iron assimilation. *Microbiological reviews*, 51(4), pp.509–18.

Balbo, A. & Schuck, Peter, 2005. Analytical Ultracentrifugation in the Study of Protein Self- association and Heterogeneous Protein-Protein Interactions. In E. Golemis & P. D. Adams, eds. *Protein-Protein Interactions: A Molecular Cloning Manual*. Cold Spring Harbor.

Ballouche, M., Cornelis, P. & Baysse, C., 2009. Iron metabolism: a promising target for antibacterial strategies. *Recent patents on anti-infective drug discovery*, 4(3), pp.190–205.

Bleuel, C. et al., 2005. TolC Is Involved in Enterobactin Efflux across the Outer Membrane of Escherichia coli. *Society*, 187(19), pp.6701–6707.

Bäumler, A.J. et al., 1996. Identification of a new iron regulated locus of Salmonella typhi. *Gene*, 183(1-2), pp.207–213.

Candiano, G. et al., 2004. Blue silver: a very sensitive colloidal Coomassie G-250 staining for proteome analysis. *Electrophoresis*, 25(9), pp.1327–1333.

Cartron, M.L. et al., 2006. Feo--transport of ferrous iron into bacteria. *Biometals : an international journal on the role of metal ions in biology, biochemistry, and medicine*, 19(2), pp.143–57.

Caza, M., Lépine, F. & Dozois, C.M., 2011. Secretion, but not overall synthesis, of catecholate siderophores contributes to virulence of extraintestinal pathogenic Escherichia coli. *Molecular microbiology*, 80(1), pp.266–82.

Chenault, S.S. & Earhart, C. F., 1992. Identification of hydrophobic proteins FepD and FepG of the Escherichia coli ferrienterobactin permease. *Journal of General Microbiology*, 138(10), pp.2167–2171.

Crosa, J.H., Mey, A.R. & Payne, S.M., 2004. *Iron transport in bacteria*, ASM Press.

Daar, S. & Pathare, A.V., 2006. Combined therapy with desferrioxamine and deferiprone in beta thalassemia major patients with transfusion iron overload. *Annals of Hematology*, 85(5), p.315.

Dahm, C. et al., 1998. The role of isochorismate hydroxymutase genes entC and menF in enterobactin and menaquinone biosynthesis in Escherichia coli. *Biochimica et biophysica acta*, 1425(2), pp.377–86.

Daruwala, R. et al., 1997. Menaquinone (vitamin K2) biosynthesis: overexpression, purification, and characterization of a new isochorismate synthase from Escherichia coli. *Journal of bacteriology*, 179(10), pp.3133–8.

Dean, D.R., Bolin, J.T. & Zheng, L., 1993. Nitrogenase metalloclusters: structures, organization, and synthesis. *Journal of bacteriology*, 175(21), pp.6737–44.

Drake, E.J., Nicolai, D.A. & Gulick, A.M., 2006. Structure of the EntB multidomain nonribosomal peptide synthetase and functional analysis of its interaction with the EntE adenylation domain. *Chemistry & biology*, 13(4), pp.409–19.

Earhart, Charles F, 2004. Iron Uptake Via the Enterobactin System. In J. H. Crosa, A. R. Mey, & S. M. Payne, eds. *Iron Transport in Bacteria*. ASM Press.

Fischbach, M. a et al., 2006. How pathogenic bacteria evade mammalian sabotage in the battle for iron. *Nature chemical biology*, 2(3), pp.132–8.

Fontecave, M., Covs, J. & Pierre, J., 1994. Ferric reductases or flavin reductases ? , 71994, pp.3–8.

French, G.L., 2010. The continuing crisis in antibiotic resistance. *International journal of antimicrobial agents*, 36 Suppl 3, pp.S3–7.

Furrer, J.L. et al., 2002. Export of the siderophore enterobactin in Escherichia coli: involvement of a 43 kDa membrane exporter. *Molecular Microbiology*, 44(5), pp.1225–1234.

Garénaux, A., Caza, M. & Dozois, C.M., 2011. The Ins and Outs of siderophore mediated iron uptake by extra-intestinal pathogenic Escherichia coli. *Veterinary microbiology*, 153(1-2), pp.89–98.

Gehring, a M. et al., 1998. Iron acquisition in plague: modular logic in enzymatic biogenesis of yersiniabactin by Yersinia pestis. *Chemistry & biology*, 5(10), pp.573–86.

Gehring, A.M., Bradley, K. a & Walsh, C T, 1997. Enterobactin biosynthesis in Escherichia coli: isochorismate lyase (EntB) is a bifunctional enzyme that is phosphopantetheinylated by EntD and then acylated by EntE using ATP and 2,3-dihydroxybenzoate. *Biochemistry*, 36(28), pp.8495–503.

Gulick, A.M., 2009. Conformational dynamics in the Acyl-CoA synthetases, adenylation domains of non-ribosomal peptide synthetases, and firefly luciferase. *ACS chemical biology*, 4(10), pp.811–27.

Gulick, A.M. et al., 2003. The 1.75 A crystal structure of acetyl-CoA synthetase bound to adenosine-5'-propylphosphate and coenzyme A. *Biochemistry*, 42(10), pp.2866–73.

Harris, W.R. et al., 1979. Coordination chemistry of microbial iron transport compounds. 19. Stability constants and electrochemical behavior of ferric enterobactin and model complexes. *Journal of the American Chemical Society*, 101(20), pp.6097–6104.

Hayes, D. B., Laue, T., and Philo, J.S., 1995. *Sednterp: Sedimentation Interpretation Program*, Thousand Oaks, CA: Alliance Protein Laboratories.

Izadi-Pruneyre, N. et al., 2006. The heme transfer from the soluble HasA hemophore to its membrane-bound receptor HasR is driven by protein-protein interaction from a high to a lower affinity binding site. *The Journal of biological chemistry*, 281(35), pp.25541–50.

Katz, A.R. et al., 2012. Neisseria gonorrhoeae with high-level resistance to azithromycin: case report of the first isolate identified in the United States. *Clinical infectious diseases : an official publication of the Infectious Diseases Society of America*, 54(6), pp.841–3.

Kelly, S.M., Jess, T.J. & Price, N.C., 2005. How to study proteins by circular dichroism. *Biochimica et biophysica acta*, 1751(2), pp.119–39.

Kerbarh, O. et al., 2005. Salicylate biosynthesis: overexpression, purification, and characterization of Irp9, a bifunctional salicylate synthase from Yersinia enterocolitica. *Journal of bacteriology*, 187(15), pp.5061–6.

Khalil, S., 2010. *Studies of the Protein Interaction Network Required for Enterobactin Biosynthesis in Escherichia coli*. Concordia University.

Khalil, S. & Pawelek, P.D., 2011. Enzymatic adenylation of 2,3-dihydroxybenzoate is enhanced by a protein-protein interaction between Escherichia coli 2,3-dihydro-2,3-dihydroxybenzoate dehydrogenase (EntA) and 2,3-dihydroxybenzoate-AMP ligase (EntE). *Biochemistry*, 50(4), pp.533–45.

Khalil, S. & Pawelek, P.D., 2009. Ligand-Induced Conformational Rearrangements Promote Interaction between the Escherichia coli Enterobactin Biosynthetic Proteins EntE and EntB. *Journal of Molecular Biology*, 393(3), pp.658–671.

Kiley, P.J. & Beinert, H., 2003. The role of Fe–S proteins in sensing and regulation in bacteria. *Current Opinion in Microbiology*, 6(2), pp.181–185.

Kitagawa, M. et al., 2005. Complete set of ORF clones of Escherichia coli ASKA library (a complete set of E. coli K-12 ORF archive): unique resources for biological research. *DNA research : an international journal for rapid publication of reports on genes and genomes*, 12(5), pp.291–9.

Kozlowski, M.C. et al., 1995. Chorismate-utilizing enzymes isochorismate synthase, anthranilate synthase, and p-aminobenzoate synthase: mechanistic insight through inhibitor design. *Journal of the American Chemical Society*, 117(8), pp.2128–2140.

Lai, J.R. et al., 2006. A protein interaction surface in nonribosomal peptide synthesis mapped by combinatorial mutagenesis and selection. *Proceedings of the National Academy of Sciences of the United States of America*, 103(14), pp.5314–9.

Lakowicz, J.R., 2006. *Principles of Fluorescence Spectroscopy* 3rd editio., Springer New York.

Leduc, D., Bouveret, E. & Battesti, A., 2007. The hotdog thioesterase EntH (YbdB) plays a role in vivo in optimal enterobactin biosynthesis by interacting with the ArCP domain of EntB. *Journal of bacteriology*, 189(19), pp.7112–26.

Lin, H. et al., 2005. In vitro characterization of salmochelin and enterobactin trilactone hydrolases IroD, IroE, and Fes. *Journal of the American Chemical Society*, 127(31), pp.11075–11084.

Liu, J et al., 1990. Overexpression, purification, and characterization of isochorismate synthase (EntC), the first enzyme involved in the biosynthesis of enterobactin from chorismate. *Biochemistry*, 29(6), pp.1417–25.

López-Goñi, I., Moriyón, I. & Neilands, J B, 1992a. Identification of 2,3-dihydroxybenzoic acid as a Brucella abortus siderophore. *Infection and immunity*, 60(11), pp.4496–503.

López-Goñi, I., Moriyón, I. & Neilands, J B, 1992b. Identification of 2,3-dihydroxybenzoic acid as a Brucella abortus siderophore. *Infection and immunity*, 60(11), pp.4496–503.

May, J.J. et al., 2002. Crystal structure of DhbE, an archetype for aryl acid activating domains of modular nonribosomal peptide synthetases. *Proceedings of the National Academy of Sciences of the United States of America*, 99(19), pp.12120–5.

Meiwes, J., 1990. Isolation and characterization of staphyloferrin A, a compound with siderophore activity from Staphylococcus hyicus DSM 20459. *FEMS Microbiology Letters*, 67(1-2), pp.201–205.

Meyer, F.M. et al., 2011. Physical interactions between tricarboxylic acid cycle enzymes in Bacillus subtilis: evidence for a metabolon. *Metabolic engineering*, 13(1), pp.18–27.

Miethke, M., Hou, J. & Marahiel, M.A., 2011. The siderophore-interacting protein YqjH acts as a ferric reductase in different iron assimilation pathways of Escherichia coli. *Biochemistry*, 50(50), pp.10951–64.

Miethke, M. & Marahiel, M.A., 2007. Siderophore-based iron acquisition and pathogen control. *Microbiology and molecular biology reviews : MMBR*, 71(3), pp.413–51.

Miller, R.E. & Stadtman, E.R., 1972. Glutamate synthase from Escherichia coli. An iron-sulfide flavoprotein. *The Journal of biological chemistry*, 247(22), pp.7407–19.

Moore, C.H. et al., 1995. Identification of alcaligin as the siderophore produced by Bordetella pertussis and B . bronchiseptica . Identification of Alcaligin as the Siderophore Produced by Bordetella pertussis and B . bronchiseptica. , 177(4).

Morris, G.M. et al., 2010. AutoDock Version 4.2. , pp.1–49.

NEB, 2012. Transformation Protocol. Available at: http://www.neb.com/nebecomm/products/protocol3.asp [Accessed July 17, 2012].

Noinaj, N. et al., 2012. Structural basis for iron piracy by pathogenic Neisseria. *Nature*.

Noto, J.M. & Cornelissen, C.N., 2008. Identification of TbpA residues required for transferrin-iron utilization by Neisseria gonorrhoeae. *Infection and immunity*, 76(5), pp.1960–9.

O'Brien, I.G. & Gibson, F., 1970. The structure of enterochelin and related 2,3-dihydroxy-N-benzoyne conjugates from Eschericha Coli. *Biochimica et Biophysica Acta (BBA) - General Subjects*, 215(2), pp.393–402.

Pain, R., 2005. Determining the CD spectrum of a protein. *Current protocols in protein science editorial board John E Coligan et al*, Chapter 7(Cd), p.Unit 7.6.

Pollack, J.R. & Neilands, J.B., 1970. Enterobactin, an iron transport compound from. *Biochemical and Biophysical Research Communications*, 38(5), pp.989–992.

Quadri, L.E. et al., 1998. Identification of a Mycobacterium tuberculosis gene cluster encoding the biosynthetic enzymes for assembly of the virulence-conferring siderophore mycobactin. *Chemistry & biology*, 5(11), pp.631–45.

Raymond, K.N., Dertz, E. a & Kim, S.S., 2003. Enterobactin: an archetype for microbial iron transport. *Proceedings of the National Academy of Sciences of the United States of America*, 100(7), pp.3584–8.

Rusnak, F, Faraci, W.S. & Walsh, C T, 1989. Subcloning, expression, and purification of the enterobactin biosynthetic enzyme 2,3-dihydroxybenzoate-AMP ligase: demonstration of enzyme-bound (2,3-dihydroxybenzoyl)adenylate product. *Biochemistry*, 28(17), pp.6827–35.

Sambrook, J. & Russel, D.W., 2001. *Molecular Cloning: A Laboratory Manual* 3rd ed., Cold Spring Harbor, N.Y.: Cold Spring Harbor Laboratory Press.

Sandy, M. & Butler, A., 2009. Microbial iron acquisition: marine and terrestrial siderophores. *Chemical reviews*, 109(10), pp.4580–95.

Sanner, M.F., 1999. Python: A Programming Language for Software Integration and Development. *J. Mol. Graphics Mod.*, 17, pp.57–61.

Schrodinger LLC, 2010. The PyMOL Molecular Graphics System, Version 1.3r1.

Schuck, P, 2000. Size-distribution analysis of macromolecules by sedimentation velocity ultracentrifugation and lamm equation modeling. *Biophysical Journal*, 78(3), pp.1606–1619.

Sinz, A., 2006. Chemical cross-linking and mass spectrometry to map three-dimensional protein structures and protein-protein interactions. *Mass spectrometry reviews*, 25(4), pp.663–82.

Sridharan, S. et al., 2010. Crystal structure of Escherichia coli enterobactin-specific isochorismate synthase (EntC) bound to its reaction product isochorismate: implications for the enzyme mechanism and differential activity of chorismate-utilizing enzymes. *Journal of molecular biology*, 397(1), pp.290–300.

Studier, F.W., 2006. NIH Public Access. , 41(1), pp.207–234.

Sundlov, J. a et al., 2006. Determination of the crystal structure of EntA, a 2,3-dihydro-2,3-dihydroxybenzoic acid dehydrogenase from Escherichia coli. *Acta crystallographica. Section D, Biological crystallography*, 62(Pt 7), pp.734–40.

Sundlov, J.A. et al., 2012. Structural and Functional Investigation of the Intermolecular Interaction between NRPS Adenylation and Carrier Protein Domains. *Chemistry & biology*, 19(2), pp.188–98.

Touati, D., 2000. Iron and Oxidative Stress in Bacteria 1. *Archives of biochemistry and biophysics*, 373(1), pp.1–6.

Walsh, C. et al., 1990. Molecular studies on enzymes in chorismate metabolism and the enterobactin biosynthetic pathway. *Chemical Reviews*, 90(7), pp.1105–1129.

Williamson, M.P. & Sutcliffe, M.J., 2010. Protein-protein interactions. *Biochemical Society transactions*, 38(4), pp.875–8.

Zhu, M. et al., 2005. Functions of the siderophore esterases IroD and IroE in iron-salmochelin utilization. *Microbiology (Reading, England)*, 151(Pt 7), pp.2363–72.

Abergel, R.J. et al., 2009. Enzymatic hydrolysis of trilactone siderophores: where chiral recognition occurs in enterobactin and bacillibactin iron transport. *Journal of the American Chemical Society*, 131(35), pp.12682–92.

Abergel, R.J. et al., 2006. Microbial evasion of the immune system: structural modifications of enterobactin impair siderocalin recognition. *Journal of the American Chemical Society*, 128(34), pp.10998–9.

Abergel, R.J. et al., 2008. The siderocalin/enterobactin interaction: a link between mammalian immunity and bacterial iron transport. *Journal of the American Chemical Society*, 130(34), pp.11524–34.

An, S. et al., 2010. Reversible Compartmentalization of de Novo Purine Biosynthetic Complexes in Living Cells. *Science*, 103(2008).

Atkin, C.L. et al., 1973. Iron and Free Radical in Ribonucleotide Reductase. EXCHANGE OF IRON AND MOSSBAUER SPECTROSCOPY OF THE PROTEIN B2 SUBUNIT OF THE ESCHERICHIA COLI ENZYME. *J. Biol. Chem.*, 248(21), pp.7464–7472.

Bagg, A. & Neilands, J B, 1987. Molecular mechanism of regulation of siderophore-mediated iron assimilation. *Microbiological reviews*, 51(4), pp.509–18.

Balbo, A. & Schuck, Peter, 2005. Analytical Ultracentrifugation in the Study of Protein Self- association and Heterogeneous Protein-Protein Interactions. In E. Golemis & P. D. Adams, eds. *Protein-Protein Interactions: A Molecular Cloning Manual*. Cold Spring Harbor.

Ballouche, M., Cornelis, P. & Baysse, C., 2009. Iron metabolism: a promising target for antibacterial strategies. *Recent patents on anti-infective drug discovery*, 4(3), pp.190–205.

Bleuel, C. et al., 2005. TolC Is Involved in Enterobactin Efflux across the Outer Membrane of Escherichia coli. *Society*, 187(19), pp.6701–6707.

Bäumler, A.J. et al., 1996. Identification of a new iron regulated locus of Salmonella typhi. *Gene*, 183(1-2), pp.207–213.

Candiano, G. et al., 2004. Blue silver: a very sensitive colloidal Coomassie G-250 staining for proteome analysis. *Electrophoresis*, 25(9), pp.1327–1333.

Cartron, M.L. et al., 2006. Feo--transport of ferrous iron into bacteria. *Biometals : an international journal on the role of metal ions in biology, biochemistry, and medicine*, 19(2), pp.143–57.

Caza, M., Lépine, F. & Dozois, C.M., 2011. Secretion, but not overall synthesis, of catecholate siderophores contributes to virulence of extraintestinal pathogenic Escherichia coli. *Molecular microbiology*, 80(1), pp.266–82.

Chenault, S.S. & Earhart, C. F., 1992. Identification of hydrophobic proteins FepD and FepG of the Escherichia coli ferrienterobactin permease. *Journal of General Microbiology*, 138(10), pp.2167–2171.

Crosa, J.H., Mey, A.R. & Payne, S.M., 2004. *Iron transport in bacteria*, ASM Press.

Daar, S. & Pathare, A.V., 2006. Combined therapy with desferrioxamine and deferiprone in beta thalassemia major patients with transfusion iron overload. *Annals of Hematology*, 85(5), p.315.

Dahm, C. et al., 1998. The role of isochorismate hydroxymutase genes entC and menF in enterobactin and menaquinone biosynthesis in Escherichia coli. *Biochimica et biophysica acta*, 1425(2), pp.377–86.

Daruwala, R. et al., 1997. Menaquinone (vitamin K2) biosynthesis: overexpression, purification, and characterization of a new isochorismate synthase from Escherichia coli. *Journal of bacteriology*, 179(10), pp.3133–8.

Dean, D.R., Bolin, J.T. & Zheng, L., 1993. Nitrogenase metalloclusters: structures, organization, and synthesis. *Journal of bacteriology*, 175(21), pp.6737–44.

Drake, E.J., Nicolai, D.A. & Gulick, A.M., 2006. Structure of the EntB multidomain nonribosomal peptide synthetase and functional analysis of its interaction with the EntE adenylation domain. *Chemistry & biology*, 13(4), pp.409–19.

Earhart, Charles F, 2004. Iron Uptake Via the Enterobactin System. In J. H. Crosa, A. R. Mey, & S. M. Payne, eds. *Iron Transport in Bacteria*. ASM Press.

Fischbach, M. a et al., 2006. How pathogenic bacteria evade mammalian sabotage in the battle for iron. *Nature chemical biology*, 2(3), pp.132–8.

Fontecave, M., Covs, J. & Pierre, J., 1994. Ferric reductases or flavin reductases ? , 71994, pp.3–8.

French, G.L., 2010. The continuing crisis in antibiotic resistance. *International journal of antimicrobial agents*, 36 Suppl 3, pp.S3–7.

Furrer, J.L. et al., 2002. Export of the siderophore enterobactin in Escherichia coli: involvement of a 43 kDa membrane exporter. *Molecular Microbiology*, 44(5), pp.1225–1234.

Garénaux, A., Caza, M. & Dozois, C.M., 2011. The Ins and Outs of siderophore mediated iron uptake by extra-intestinal pathogenic Escherichia coli. *Veterinary microbiology*, 153(1-2), pp.89–98.

Gehring, a M. et al., 1998. Iron acquisition in plague: modular logic in enzymatic biogenesis of yersiniabactin by Yersinia pestis. *Chemistry & biology*, 5(10), pp.573–86.

Gehring, A.M., Bradley, K. a & Walsh, C T, 1997. Enterobactin biosynthesis in Escherichia coli: isochorismate lyase (EntB) is a bifunctional enzyme that is phosphopantetheinylated by EntD and then acylated by EntE using ATP and 2,3-dihydroxybenzoate. *Biochemistry*, 36(28), pp.8495–503.

Gulick, A.M., 2009. Conformational dynamics in the Acyl-CoA synthetases, adenylation domains of non-ribosomal peptide synthetases, and firefly luciferase. *ACS chemical biology*, 4(10), pp.811–27.

Gulick, A.M. et al., 2003. The 1.75 A crystal structure of acetyl-CoA synthetase bound to adenosine-5'-propylphosphate and coenzyme A. *Biochemistry*, 42(10), pp.2866–73.

Harris, W.R. et al., 1979. Coordination chemistry of microbial iron transport compounds. 19. Stability constants and electrochemical behavior of ferric enterobactin and model complexes. *Journal of the American Chemical Society*, 101(20), pp.6097–6104.

Hayes, D. B., Laue, T., and Philo, J.S., 1995. *Sednterp: Sedimentation Interpretation Program*, Thousand Oaks, CA: Alliance Protein Laboratories.

Izadi-Pruneyre, N. et al., 2006. The heme transfer from the soluble HasA hemophore to its membrane-bound receptor HasR is driven by protein-protein interaction from a high to a lower affinity binding site. *The Journal of biological chemistry*, 281(35), pp.25541–50.

Katz, A.R. et al., 2012. Neisseria gonorrhoeae with high-level resistance to azithromycin: case report of the first isolate identified in the United States. *Clinical infectious diseases : an official publication of the Infectious Diseases Society of America*, 54(6), pp.841–3.

Kelly, S.M., Jess, T.J. & Price, N.C., 2005. How to study proteins by circular dichroism. *Biochimica et biophysica acta*, 1751(2), pp.119–39.

Kerbarh, O. et al., 2005. Salicylate biosynthesis: overexpression, purification, and characterization of Irp9, a bifunctional salicylate synthase from Yersinia enterocolitica. *Journal of bacteriology*, 187(15), pp.5061–6.

Khalil, S., 2010. *Studies of the Protein Interaction Network Required for Enterobactin Biosynthesis in Escherichia coli*. Concordia University.

Khalil, S. & Pawelek, P.D., 2011. Enzymatic adenylation of 2,3-dihydroxybenzoate is enhanced by a protein-protein interaction between Escherichia coli 2,3-dihydro-2,3-dihydroxybenzoate dehydrogenase (EntA) and 2,3-dihydroxybenzoate-AMP ligase (EntE). *Biochemistry*, 50(4), pp.533–45.

Khalil, S. & Pawelek, P.D., 2009. Ligand-Induced Conformational Rearrangements Promote Interaction between the Escherichia coli Enterobactin Biosynthetic Proteins EntE and EntB. *Journal of Molecular Biology*, 393(3), pp.658–671.

Kiley, P.J. & Beinert, H., 2003. The role of Fe–S proteins in sensing and regulation in bacteria. *Current Opinion in Microbiology*, 6(2), pp.181–185.

Kitagawa, M. et al., 2005. Complete set of ORF clones of Escherichia coli ASKA library (a complete set of E. coli K-12 ORF archive): unique resources for biological research. *DNA research : an international journal for rapid publication of reports on genes and genomes*, 12(5), pp.291–9.

Kozlowski, M.C. et al., 1995. Chorismate-utilizing enzymes isochorismate synthase, anthranilate synthase, and p-aminobenzoate synthase: mechanistic insight through inhibitor design. *Journal of the American Chemical Society*, 117(8), pp.2128–2140.

Lai, J.R. et al., 2006. A protein interaction surface in nonribosomal peptide synthesis mapped by combinatorial mutagenesis and selection. *Proceedings of the National Academy of Sciences of the United States of America*, 103(14), pp.5314–9.

Lakowicz, J.R., 2006. *Principles of Fluorescence Spectroscopy* 3rd editio., Springer New York.

Leduc, D., Bouveret, E. & Battesti, A., 2007. The hotdog thioesterase EntH (YbdB) plays a role in vivo in optimal enterobactin biosynthesis by interacting with the ArCP domain of EntB. *Journal of bacteriology*, 189(19), pp.7112–26.

Lin, H. et al., 2005. In vitro characterization of salmochelin and enterobactin trilactone hydrolases IroD, IroE, and Fes. *Journal of the American Chemical Society*, 127(31), pp.11075–11084.

Liu, J et al., 1990. Overexpression, purification, and characterization of isochorismate synthase (EntC), the first enzyme involved in the biosynthesis of enterobactin from chorismate. *Biochemistry*, 29(6), pp.1417–25.

López-Goñi, I., Moriyón, I. & Neilands, J B, 1992a. Identification of 2,3-dihydroxybenzoic acid as a Brucella abortus siderophore. *Infection and immunity*, 60(11), pp.4496–503.

López-Goñi, I., Moriyón, I. & Neilands, J B, 1992b. Identification of 2,3-dihydroxybenzoic acid as a Brucella abortus siderophore. *Infection and immunity*, 60(11), pp.4496–503.

May, J.J. et al., 2002. Crystal structure of DhbE, an archetype for aryl acid activating domains of modular nonribosomal peptide synthetases. *Proceedings of the National Academy of Sciences of the United States of America*, 99(19), pp.12120–5.

Meiwes, J., 1990. Isolation and characterization of staphyloferrin A, a compound with siderophore activity from Staphylococcus hyicus DSM 20459. *FEMS Microbiology Letters*, 67(1-2), pp.201–205.

Meyer, F.M. et al., 2011. Physical interactions between tricarboxylic acid cycle enzymes in Bacillus subtilis: evidence for a metabolon. *Metabolic engineering*, 13(1), pp.18–27.

Miethke, M., Hou, J. & Marahiel, M.A., 2011. The siderophore-interacting protein YqjH acts as a ferric reductase in different iron assimilation pathways of Escherichia coli. *Biochemistry*, 50(50), pp.10951–64.

Miethke, M. & Marahiel, M.A., 2007. Siderophore-based iron acquisition and pathogen control. *Microbiology and molecular biology reviews : MMBR*, 71(3), pp.413–51.

Miller, R.E. & Stadtman, E.R., 1972. Glutamate synthase from Escherichia coli. An iron-sulfide flavoprotein. *The Journal of biological chemistry*, 247(22), pp.7407–19.

Moore, C.H. et al., 1995. Identification of alcaligin as the siderophore produced by Bordetella pertussis and B . bronchiseptica . Identification of Alcaligin as the Siderophore Produced by Bordetella pertussis and B . bronchiseptica. , 177(4).

Morris, G.M. et al., 2010. AutoDock Version 4.2. , pp.1–49.

NEB, 2012. Transformation Protocol. Available at: http://www.neb.com/nebecomm/products/protocol3.asp [Accessed July 17, 2012].

Noinaj, N. et al., 2012. Structural basis for iron piracy by pathogenic Neisseria. *Nature*.

Noto, J.M. & Cornelissen, C.N., 2008. Identification of TbpA residues required for transferrin-iron utilization by Neisseria gonorrhoeae. *Infection and immunity*, 76(5), pp.1960–9.

O'Brien, I.G. & Gibson, F., 1970. The structure of enterochelin and related 2,3-dihydroxy-N-benzoyne conjugates from Eschericha Coli. *Biochimica et Biophysica Acta (BBA) - General Subjects*, 215(2), pp.393–402.

Pain, R., 2005. Determining the CD spectrum of a protein. *Current protocols in protein science editorial board John E Coligan et al*, Chapter 7(Cd), p.Unit 7.6.

Pollack, J.R. & Neilands, J.B., 1970. Enterobactin, an iron transport compound from. *Biochemical and Biophysical Research Communications*, 38(5), pp.989–992.

Quadri, L.E. et al., 1998. Identification of a Mycobacterium tuberculosis gene cluster encoding the biosynthetic enzymes for assembly of the virulence-conferring siderophore mycobactin. *Chemistry & biology*, 5(11), pp.631–45.

Raymond, K.N., Dertz, E. a & Kim, S.S., 2003. Enterobactin: an archetype for microbial iron transport. *Proceedings of the National Academy of Sciences of the United States of America*, 100(7), pp.3584–8.

Rusnak, F, Faraci, W.S. & Walsh, C T, 1989. Subcloning, expression, and purification of the enterobactin biosynthetic enzyme 2,3-dihydroxybenzoate-AMP ligase: demonstration of enzyme-bound (2,3-dihydroxybenzoyl)adenylate product. *Biochemistry*, 28(17), pp.6827–35.

Sambrook, J. & Russel, D.W., 2001. *Molecular Cloning: A Laboratory Manual* 3rd ed., Cold Spring Harbor, N.Y.: Cold Spring Harbor Laboratory Press.

Sandy, M. & Butler, A., 2009. Microbial iron acquisition: marine and terrestrial siderophores. *Chemical reviews*, 109(10), pp.4580–95.

Sanner, M.F., 1999. Python: A Programming Language for Software Integration and Development. *J. Mol. Graphics Mod.*, 17, pp.57–61.

Schrodinger LLC, 2010. The PyMOL Molecular Graphics System, Version 1.3r1.

Schuck, P, 2000. Size-distribution analysis of macromolecules by sedimentation velocity ultracentrifugation and lamm equation modeling. *Biophysical Journal*, 78(3), pp.1606–1619.

Sinz, A., 2006. Chemical cross-linking and mass spectrometry to map three-dimensional protein structures and protein-protein interactions. *Mass spectrometry reviews*, 25(4), pp.663–82.

Sridharan, S. et al., 2010. Crystal structure of Escherichia coli enterobactin-specific isochorismate synthase (EntC) bound to its reaction product isochorismate: implications for the enzyme mechanism and differential activity of chorismate-utilizing enzymes. *Journal of molecular biology*, 397(1), pp.290–300.

Studier, F.W., 2006. NIH Public Access. , 41(1), pp.207–234.

Sundlov, J. a et al., 2006. Determination of the crystal structure of EntA, a 2,3-dihydro-2,3-dihydroxybenzoic acid dehydrogenase from Escherichia coli. *Acta crystallographica. Section D, Biological crystallography*, 62(Pt 7), pp.734–40.

Sundlov, J.A. et al., 2012. Structural and Functional Investigation of the Intermolecular Interaction between NRPS Adenylation and Carrier Protein Domains. *Chemistry & biology*, 19(2), pp.188–98.

Touati, D., 2000. Iron and Oxidative Stress in Bacteria 1. *Archives of biochemistry and biophysics*, 373(1), pp.1–6.

Walsh, C. et al., 1990. Molecular studies on enzymes in chorismate metabolism and the enterobactin biosynthetic pathway. *Chemical Reviews*, 90(7), pp.1105–1129.

Williamson, M.P. & Sutcliffe, M.J., 2010. Protein-protein interactions. *Biochemical Society transactions*, 38(4), pp.875–8.

Zhu, M. et al., 2005. Functions of the siderophore esterases IroD and IroE in iron-salmochelin utilization. *Microbiology (Reading, England)*, 151(Pt 7), pp.2363–72.